CRANFIELD UNIVERSITY

**ENRICO PANDIN**

# MODELLING OF ENGINE PERFORMANCE DURING ICE PARTICLES INGESTION

SCHOOL OF AEROSPACE TRANSPORT AND MANUFACTURING

PhD THESIS

CRANFIELD UNIVERSITY

SCHOOL OF AEROSPACE TRANSPORT AND MANUFACTURING

PhD THESIS

Academic Year 2016-2019

ENRICO PANDIN

# Modelling of engine performance during ice particles ingestion

Supervisor: Dr. P. Laskaridis, Prof. V. Pachidis

May 2020

This thesis is submitted in fulfillment of the requirements for the degree of Doctor of Philosophy

# Executive Summary

A turbofan engine flying through adverse weather conditions will experience a change in its performance. One of the most common examples of these hostile conditions is the case of ice crystals ingestion. Identifying these performance variations would lead to a detection strategy, that could be used to inform the pilots about the flying conditions, enhancing their decision making capability. In order to be able to understand which are the key features of the engine behaviour during ice ingestion, it is necessary to model and simulate such phenomenon.
In literature there are some examples of engine and compressor performance modelling during ice ingestion, but they are either incapable of producing transient or full engine simulations, or impose very strict assumptions to the particles behaviour. The objective of this PhD is to develop a gas turbine performance model for the simulation of engine performance during ice particles ingestion and analyse the engine behaviour in those conditions, to identify its key characteristics.
The method was generated by coupling an engine simulation tool internally available at Cranfield UTC and a newly developed code capable of modelling the ice particles evolution. The engine simulation tool splits the engine core into a compression side, modelled using 1D Euler equations with source terms to account for the influence of bleeds, compressors and combustion chamber, and an expansion side, modelled via quasi steady state matching. The ice particles code adopts a Lagrangian approach, introducing a certain amount of ice particles at defined time steps and modelling their behaviour until they completely evaporate in the engine. The influence of the particles on the engine performance is taken into account by source terms in the Euler equations and a new mass equation has been added to model the water vapour that is being introduced into the main flow. The model takes into consideration also the possibility of ice particles accretion on the compressor stator vanes.
The results have been compared with in-flight data, showing promising results in capturing the expected trends in shaft rotational speed as well as pressure and temperature at the high pressure compressor outlet.

# Acknowledgements

Working on an aerospace project such as the one I am about to finish with this thesis, and cooperating with one of the main players in the aerospace industry such as Rolls-Royce, has always been one of my biggest dreams. At the end of this three-year journey, I would like to thank all the people who made it possible and who helped me achieve this prestigious goal.

First of all I would like to thank my first supervisor, Panagiotis Laskaridis, for his help and support during this project. He was always extremely helpful and willing to listen to my suggestions for the continuation of the project as well as to accomodate, when possible, my personal needs. I am also grateful to my second supervisor, Vassilios Pachidis, and the people in Rolls-Royce who started this project and believed in me in the first place: Ben Eastman and Paul Harris, without them I would have not been granted this huge opportunity.

I would like also to thank Rolls-Royce as a whole for sponsoring my scholarship. Moreover, the support and suggestions provided by people like Peter Beecroft and Geoff Jones were invaluable, and I am thankful for all their help.

I am proud of having been part of the UTC, where I have met some of the most hard working and motivating people of my career. In particular, I would like to thank Alvise, Mauro, Giovanni and Matteo for the time we have spent together and the many conversations we had. Thank also to Inigo and Serena for the fun times we had together and for having been two great housemates.

I would like to thank my family, which has always supported me and my choices, I hope all their efforts paid off, and I hope I made them proud.

Finally, I want to thank Francesa, my girlfriend,who has been able to overcome the challenge of a long distance relationship, and nevertheless has always been there for me, even when it was not easy. Thank you very much, I love you.

# Contents

# List of Figures

# List of Tables

# List of Symbols and Acronyms

## Symbols

| | | |
|---|---|---|
| $\alpha$ | Particles impact angle | [degrees] |
| $\gamma$ | Fluid specific heats ratio, Stagger angle | [−], [degrees] |
| $\gamma_1$ | Surface tension | $[Nm]$ |
| $\delta$ | Ice thickness | $[m]$ |
| $\epsilon$ | Energy of molecular interaction | $[m^2kg/s]$ |
| $\eta$ | Efficiency | |
| $\mu$ | Dynamic viscosity | $[Pas]$ |
| $\rho$ | Density | $[kg/m^3]$ |
| $\sigma$ | Collision diameter | [Å] |
| $\tau$ | Torque | $[Nm]$ |
| $\omega$ | Rotational speed, Total ice mass flow | $[rad/s]$ $[kg/s]$ |
| $\dot{\omega}$ | Source term for combustion results and unburnt fuel | |
| $A$ | Area | $[m^2]$ |
| $C$, $C_x$ | Courant number | |
| $C_D$ | Drag coefficient | |
| $C_p$ | Heat capacity | $[J/kgK]$ |
| $D_\ni$ | Ice/water to air diffusivity | $[s]$ |
| $E$ | Flow total internal energy | $[J]$ |
| $F$ | Momentum source term, Axial force, Flux matrix | $[J/m]$, $[N]$, [−] |
| $G$ | Source terms matrix | |
| $H$ | Enthalpy source term, Flow total enthalpy | $[J]$ |
| $I$ | Polar moment of inertia | $[kgm^2]$ |
| $L_m$ | Latent heat of fusion | $[J/kg]$ |
| $L_{vi}$ | Latent heat of sublimation | $[J/kg]$ |
| $L_{vw}$ | Latent heat of evaporation | $[J/kg]$ |
| $M$ | Molecular mass | $[g/mol]$ |

| | | |
|---|---|---|
| $N$ | Total number of elements, Shaft roational speed | $[-]$, $[rpm]$ |
| $NRT$ | Corrected rotational speed | $[rpm/K^{0.5}]$ |
| $Pr$ | Prandtl Number | |
| $Q$ | Heat source term, Heat absorbed | $[J/m]$, $[J]$ |
| $R$ | Ideal gas constant | $[J/kgK]$ |
| $Re$ | Reynolds number | |
| $RH$ | Relative humidity | |
| $S$ | Artificial viscosity, Source term | |
| $S_c$ | Schmidt number | |
| $SW$ | Shaft work | $[J/m]$ |
| $U$ | Conservative variables matrix | |
| $W$ | Mass source term, Area source matrix | $[kg/m \cdot s]$,$[-]$ |
| $WRTP$ | Corrected mass flow | $[WK^{0.5}/Pa]$ |
| $Y$ | Mass fraction | |
| $a$ | Local speed of sound | $[m/s]$ |
| $corr$ | Correction factor | |
| $dmv_1$ | Evaporated mass | $[kg]$ |
| $dmv_2$ | Vaporised mass | $[kg]$ |
| $dmw$ | Melted mass | $[kg]$ |
| $e$ | Static internal energy | $[J]$ |
| $h$ | Static enthalpy, Heat transfer coefficient | $[J]$, $[W/m^2K]$ |
| $h_m$ | Mass transfer coefficient | [m/s] |
| $k$ | Boltzmann constant, Thermal conductivity | $[m^2kg/sK$, $W/mK]$ |
| $m$ | Mass | $[kg]$ |
| $\dot{m}$ | Mass flow | $[kg/s]$ |
| $n$ | Particles density | $[1/m^3]$ |
| $p$ | Pressure | $[Pa]$ |
| $q$ | Mixing ratio | |
| $r$ | Radius | $[m]$ |
| $s$ | Source term prior to differentiation | |
| $t$ | Time | $[s]$ |
| $u$ | Flow velocity | $[m/s]$ |
| $u_{ap}$ | Particles apparent velocity | $[m/s]$ |
| $u_i$ | Impact velocity | $[m/s]$ |
| $x$ | Axial position | $[m]$ |

# Subscripts

| | |
|---|---|
| $B$ | Bleeds |
| $D$ | Drag |
| $F$ | Fuel flow |
| $FNB$ | Unburnt fuel |
| $N$ | Final element of any given goup of elements, NRT |
| $SP$ | Combustion results |
| $W$ | WRTP |
| $c$ | Compressor |
| $calc$ | Calculated |
| $comb$ | Combustor |
| $comp$ | Compressor |
| $crit$ | Critical |
| $e$ | Energy |
| $ext$ | External |
| $i$ | Element's axial index, Ice, Current stage |
| $m$ | Mean, Mass |
| $map$ | Map |
| $max$ | Maximum |
| $mo$ | Momentum |
| $p$ | Particles |
| $ps$ | Saturated conditions at particles temperature |
| $s$ | Static, Saturated |
| $t$ | Total, Turbine |
| $v$ | Vapour |
| $vap$ | Vaporisation |
| $vs$ | Saturated conditions at vapour/air temperature |
| $w$ | Water |

# Superscripts and accents

| | |
|---|---|
| $*$ | Pure substance |
| $N"_p$ | Number of particles after ice accretion |
| $\bar{U}$ | First step values |
| $\bar{\bar{U}}$ | Second step values |
| $\bar{d}'$ | Average diameter after the breakup event |
| $n$ | Current time step |
| $n+1$ | Next time step |

# Acronyms and abbreviations

| | |
|---|---|
| DI | Disruption Index |
| DOD | Domestic Object Damage |
| ECDM | Enhanced Cockpit Decision Making |
| FOD | Foreign Object Damage |
| HPC | High Pressure Compressor |
| LPC | Low Pressure Compressor |
| N1 | Fan rotational speed |
| N2A.1 | Intermediate pressure shaft nondimensional rotational speed, engine 1 |
| NGVs | Nozze Guide Vanes |
| N3A.1 | High pressure shaft nondimensional rotational speed, engine 1 |
| PR | Pressure ratio |
| PS3.1 | High pressure compressor outlet static pressure, engine 1 |
| PT3 | High pressure compressor outlet total pressure |
| SAS | Secondary Air System |
| SLD | Supercooled Liquid Droplets |
| T3.1 | High pressure compressor outlet temperature, engine 1 |
| TR | Temprature ratio |
| TT3 | High pressure compressor outlet total temperature |
| TT45 | High pressure turbine outlet temperature |
| UER | Unplanned Engine Removal |
| UTC | University Technology Center |
| WEST | Whole Engine Simulation Tool |

# Chapter 1

# Introduction

In this introduction, four main topics will be discussed. First of all, the aim and objectives of the project will be listed, followed by the exposition of its novelty and contribution to knowledge. These introductory aspects will be followed by an explanation of the background of this project and how it came to be, to finish with a brief outline of the thesis organisation.

## 1.1 Project aim and objectives

The aim of this project was to investigate the behaviour of a whole engine under ice crystals ingestion conditions.
In particular, the focus was to understand some specific behaviours of shaft rotational speeds and high pressure compressor outlet pressure and temperature which, from the observation of some in-flight data, seemed to be two peculiar characteristics of this phenomenon.
In order to do it, a series of objectives has been defined, as a guide for the different phases of the project:

- review the technical and scientific literature on the problem
- analyse the different phenomena interacting and develop a methodology to take them into account
- develop a gas turbine performance model following the aforementioned methodology

- search if the simulation results confirmed the rotational speed, temperature and pressure behaviours of in-flight data

## 1.2 Novelty and contribution to knowledge

The method developed for this project presents two main aspects of novelty:

- It is a novel modelling method capable of carrying out a transient simulation of both an isolated compressor or a full engine during ice ingestion conditions that can be applied to any engine architecture
- It represents the first time an independent Euler mass equation for water vapour was introduced in a similar method

In the literature three main methods to model compressor and engine performance during ice ingestion can be found. However, they all lack some key characteristics compared to the one presented in this thesis. While these aspects will be explored in much more detail in the next chapter, it is worth anticipating here some key points. One one side, some methods present in literature are in fact capable of modelling the performance of a whole engine and can be applied to any engine architecture[1, 2, 3, 4, 5], however, those are not capable of modelling the engine transient behaviour. On the other side, one model that is able to simulate the engine transient behaviour, imposes such strict conditions on the ice particles evolution that it is only applicable to the specific engine architecture that it was developed for[6, 7]. Finally, a promising method that did not impose restrictive limitations on the particles behaviour and was capable of performing transient simulations has only been implemented in isolated compressor simulations at constant speed[8, 9, 10, 11, 12, 13].
The main contribution of this project is that this is the first research analysing the general engine behaviour during ice ingestion.
In fact, previous studies on full engine behaviour have all been focused on the specific event of engine rollback during ice ingestion, and in reproducing it in a simulation[1, 2, 4, 5, 6, 7, 14, 15].
Thanks to the various simulations run during this project, it was possible to understand the intricacies of the ice ingestion phenomenon. It was possible for example to understand how the particles ingestion causes a variation in shaft rotational speed,

by causing an imbalance between the compression and expansion side torque of the shaft. This imbalance is due to a combination of the mass and energy effects that the particles have on the fluid flow, by adding mass flow in the form of vapour and absorbing energy in the form of heat. During the project various simulations were performed also to understand the influence that different air inlet conditions and particles properties have on the engine performance. This allowed to improve our knowledge of the event, showing for example that a lower air and particles inlet temperature reduces the effects of ice ingestion.
Finally, an important aspect to take into consideration is the huge potential for future research that the development of this new method has opened, and that will be explored in the conclusions of this thesis. Without the modelling methodology presented here, the contribution that these future projects will have could not be possible.

## 1.3 Project background

This research is part of a larger project started by Rolls-Royce aimed at finding new ways to improve the pilots decision-making capabilities by giving them more and better information about the engine, named Enhanced Cockpit Decision Making (ECDM).
The idea behind this project was that if the pilots were aware of the health conditions of the engine during in-flight events, they might be able to avoid potential mistakes, make better decisions and, in doing so, minimize the disruptive effects of such events. Even though this research is only part of the ECDM project, it is appropriate to present the work that has been done within this project before the scope of this PhD was determined, as it was crucial in determining the aim and objectives of the final research, and because it highlights well the potential value of it.

### 1.3.1 ECDM project

Given the extremely complex and broad nature of the project, an overall strategy was devised, which can be summarised in Figure 1.1.
The first steps of the project were to identify the main stakeholders for the project, consider different scenarios for its applicability, identify the potential functions of an ECDM system and categorize the events that might benefit from such a system.

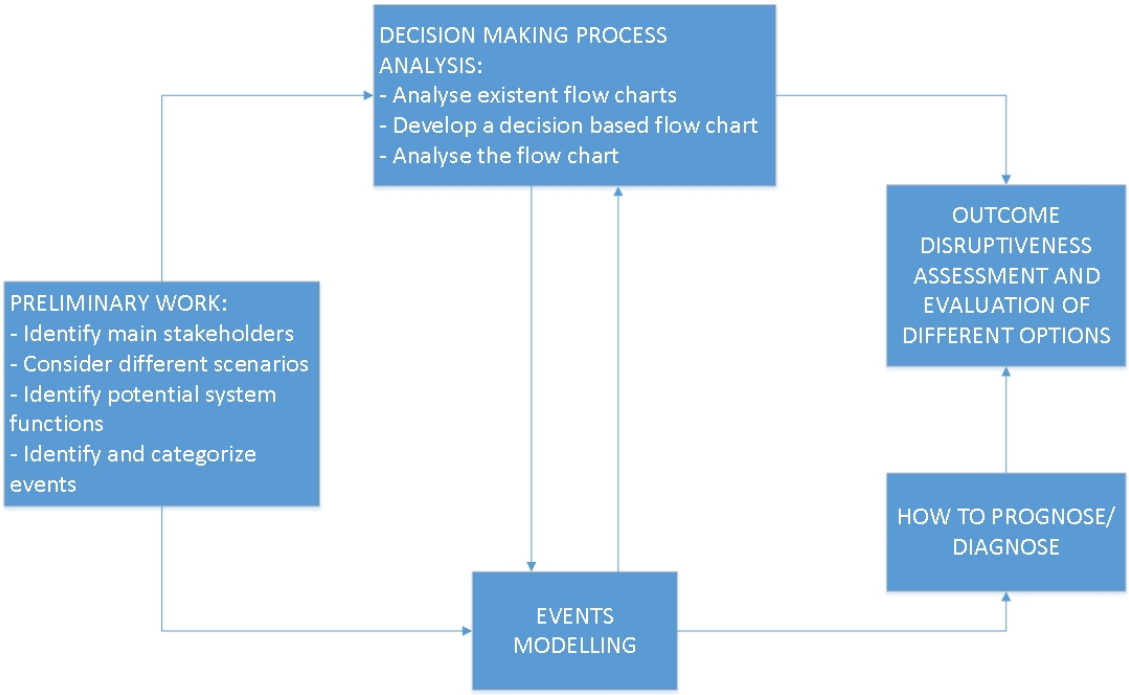


Figure 1.1: ECDM project overall strategy

After this, one or more events would be analysed at a time, at first analysing the decision making process of the pilots during these events. This would set focus for the events modelling effort, which is where this research lies within the main project strategy, which would in turn suggest changes to the decisional process and new ways to eventually diagnose or even prognose certain events. Finally, there would be an assessment of how the new diagnostic systems and the better decisions made by the pilots assisted by the ECDM system could reduce the disruptiveness of the selected events in the future.

### Preliminary work

The final and most important phase of the preliminary work was to devise a categorisation method for in-flight events. This categorisation method is shown in Table 1.1. The classification is based on the effect that the events have on the engine operability, and it defines four main categories. The first two include recoverable events, either self recoverable by the engine itself or requiring action from the pilot, such as an engine religth. The third category, defined as ECDM operability, includes those events where, even though the engine has incurred in some kind of actual damage, it would still be operable at certain power sets. The reason for the name of this category is that now an engine with any kind of damage would most likely be shut

| Minimise economic damage | | Mission Completion | Crew and passengers safety |
|---|---|---|---|
| Self recoverable | Recoverable with action | ECDM operability | Engine out of order |
| Ice ingestion | Engine flame out | FOD/DOD blade | Engine fire |
| stall/surge | Ice ingestion | damage | Engine seizure |
| Ash ingestion | stall/surge | Blade missing | FOD/DOD blade |
| stall/surge | Ash ingestion | Fatigue blade | damage |
| Lightning strike | stall/surge | damage | Blade missing |
| surge | Lightning strike | Bearing damage | Fatigue blade |
| Tip rub surge | surge | | damage |
| | Tip rub surge | | Bearing damage |
| | | | Shaft failure |
| | | | Fan blade off |

Table 1.1: ECDM events categorisation

down. With the possibility to inform the pilot about the safe operative settings that the engine could operate at, its operability would now be directed by the ECDM system. Finally, the last category includes those events where a catastrophic failure causes the engine to be completely unusable. It is worth noting that many events appear in more than one category, this would depend on the severity of the event itself and its effects on the engine.

On top of this classification, which is more pilot centered, a second one was realised, alos reported in Table 1.1, where the focus is the main objective that the ECDM system should pursue in the aim of reducing the event disruptiveness. For example, the first two categories of the pilot based classification would be grouped together, as the main objective in both cases would be to minimise the economic damage resulting from the bad management of an essentially healthy engine. In the case of the third class, the focus would be to assure the completion of the mission, without turnbacks, diversions or delays, even with one damaged engine. Finally, for the last category of the pilots centered classification, the objective would be to preserve the safety of the crew and passengers in case of a catastrophic event.

It appears clear that the events that would benefit the most from an ECDM system are those in the first and third categories. On one side, there is the issue that pilots might overestimate the severity of an actually innocuous malfunction, causing unnecessary engine relights followed by overhauls on ground. In case of ECDM operability, it is obvious the added value that there would be in being able to keep running an engine, even at a lower power set, and being able to complete the mission.

Being this the first research effort related to the ECDM project, it was decided

to not delve into the heavily safety-related cases of the enhanced operability category. Instead, the focus has been set on self recoverable events where the pilots might take unrequired actions. In particular, it has been decided to investigate the decision making process in case of self recoverable surges.

### 1.3.2 Decision making process analysis

The second phase of the work that has been done in preparation for the research effort that is described in this thesis included the analysis of existing aircraft checklists in case of surge and their comparison against malfunction reports[16] and conversations with Rolls-Royce experts and pilots.
What came out of this analysis is that, even though pilots do have checklists to follow in case of surge, they often overestimate the gravity of simple, self recoverable surges, due to the startling effect of the surge loud noise and the rightful concern for the passengers safety. A tree chart was developed, highlighting all the possible decision points where the pilot could step out of the checklist, and cause additional, unwanted disruptions. The result of this analysis can be seen in Figure 1.2. In the chart, the out of checklist decision points are highlighted in purple, and the ending points are coloured in green, yellow or red depending on the disruption level. The number in parenthesis is the Disruption Index, DI. It was taken from Rolls-Royce tables, it assesses the level of disruption of each different outcome, and its values have been normalised, for confidentiality reasons, with the maximum reached in this scenario. Also, the abbreviation UER stands for Unplanned Engine Removal.
The preferable course of action, highlighed in green in the figure, is to not act at all, as with the surge being self recoverable the engine is perfectly safe and can keep operating without any problem.
The biggest question was then how to provide the pilots the information they need to correctly assess the situation and not overestimate the severity of the event taking place. From conversations with human factor experts and pilots, the main concerns about this topic were the absence of any signal that could reduce the startling effect that comes with the loud noise of an engine surge, and lack of characterization of different surges, that often lead the pilots to consider the worst possible scenario.
Given the wide variety of possible surge causes, it was decided to proceed in a progressive manner and address and characterise them one at a time, which meant that an additional event selection was needed. The exact event taken into consideration was ice particles ingestion.

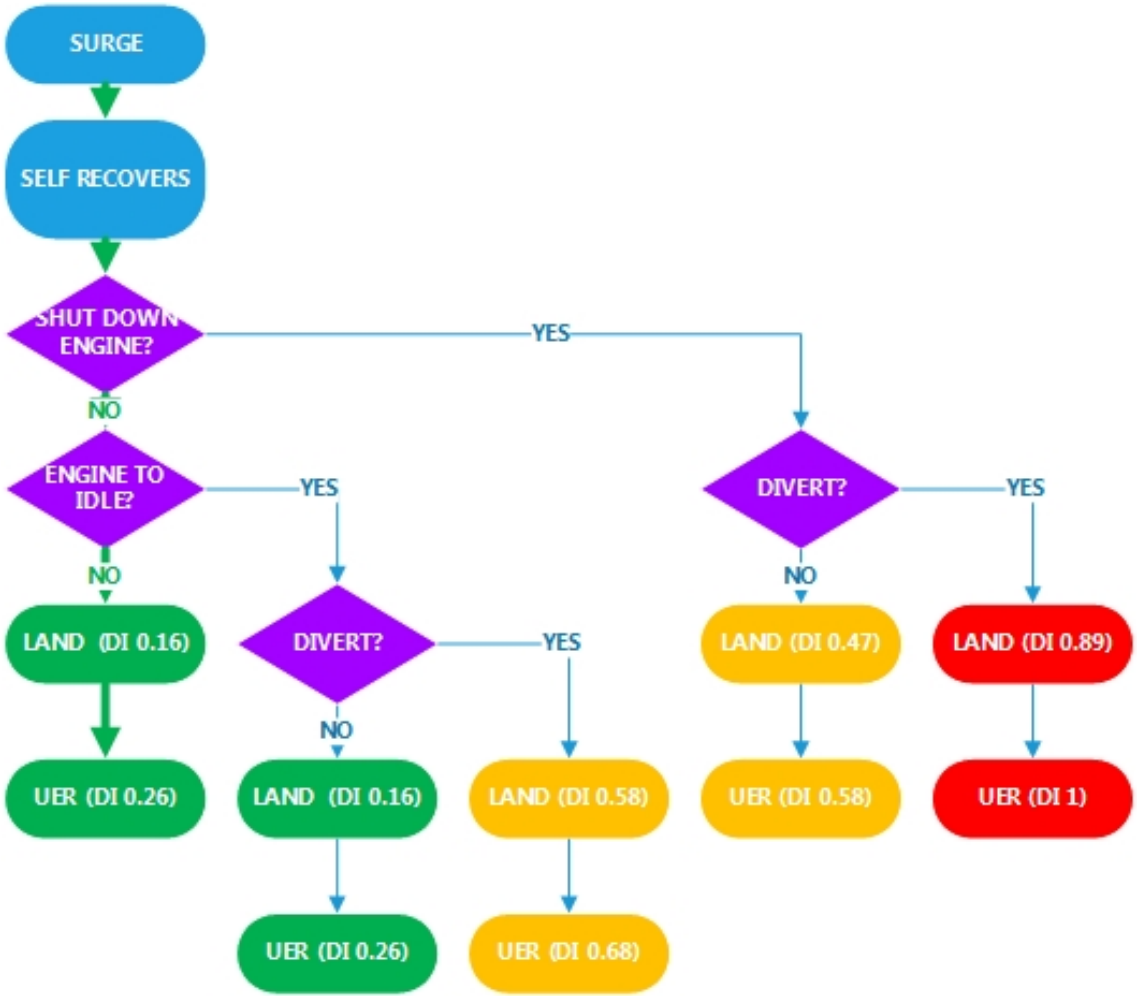


Figure 1.2: Decision making process tree chart in case of self recoverable surge

### 1.3.3 Ice ingestion selection and simulation effort rationale

Ice particles ingestion takes place when an aircraft flies throught a cloud with dispersed ice crystals in it, which end up being ingested by the engines. This could also lead to the particles partially melting and then sticking to the stationary parts of the compression system. This process is defined as engine icing, which differs from normal icing, that normally takes place on fan blades and wings leading edges, as in that case we are in presence of supercooled water droplets, that need an accreting surface to solidify.

The conditions for the formation of ice crystals are generally met in the outflow region of large thunderstorms, called anvil[17]. Even though pilots generally prefer to fly around thunderstorms, due to weather or air traffic restrictions, they are sometimes forced to fly through them.

Ice particles ingestion is a phenomenon that has gained importance over the last

decades[18]. It can cause various malfunctions spreading from surge to engine rollback. All these events are generally self recoverable, in the case of surge, or easily recoverable, in case of rollback, with an engine relight. However, the sudden noise of an engine surge or the loss of power without any anticipation could lead the pilot to misjudge the situation and overreact, causing an unnecessary disruption in the operations and economical costs to the company.
All these potential problems could be reduced by a system able to identify the behaviour of the engine in ice ingestion conditions and communicate it to the pilot. In this way, pilots situation awareness would be increased, and they would not be surprised if any event occurred, being ready to manage it in the best way possible. Such system could be a data-based model able to recognise the behavioural pattern of engines in ice particles ingestion conditions.
A data-based model is an algorithm that, after a process called training, is able to recognise patterns and behave accordingly. The training process is probably the most crucial aspect of a good data based model. During this phase, a great amount of data are used to set the parameters that will allow the algorithm to operate.
The main problem arising when trying to apply data based models to engine events and malfunctions, is that they are so rare that there are not nearly enough data to perform a data based model training. Even though the focus would be to only characterize the engine behaviour during ice ingestion, those data are collected and analysed only when an event does in fact occur, initiating an investigation that lead to the conclusion that the engine was flying in ice particles ingestion conditions.
Hence, it is necessary to develop an engine performance model capable of simulating a whole engine under ice crystals ingestion conditions. This would improve our knowledge of this phenomenon, and allow us to generate enough data to train a data based model capable of recognize the engine behaviour in these conditions in real time and communicate it to the pilots. In this way, they would be aware of the possibilities of minor malfunctions of the propulsive system, and would be able to manage them correctly, improving their decision making capabilities, and minimising possible disruptions that could arise from a mismanaged event.
Where the in-flight data are useful are in assessing the validity of the engine model. In particular Rolls-Royce provided a set of data about ice ingestion related surges that highlighted how, apparently, in the moments immediately ahead of the event, in all ice ingestion related cases there was a convergence of intermediate and high pressure shaft rotational speeds, and a divergence of high pressure compressor outlet temperature and pressure.
The objective of the following modelling effort is then to reproduce the two main

features that were just presented. However, given the fact that in these data many parameters were not known, such as ice ingestion rate, particles size, particles temperature, humidity or control system schedules, it will not be possible to quantitatively compare the simulation results with the in-flight data.

## 1.4 Thesis structure

The structure of the thesis follows the completion of the objectives that were outlined in the previous section.
After this initial introduction, the literature on the subject of ice particles ingestion will be reviewed in Chapter 2, concentrating in particular on the studies that were most useful in the following development of the new model.
Subsequently, Chapter 3 will present a quick exposition of the main challenges posed by modelling such a complex phenomenon and an explanation of the methodology adopted to solve them, followed by the description of the actual model developed in Chapter 4.
The results of this modelling effort will then be discussed in Chapter 5, with them being split into isolated compressor, single shaft and whole engine results.
Finally, in Chapter 6 the conclusions of this project will be drawn, and its possible future developments will be discussed.

# Chapter 2

# Ice Particles Ingestion Background and Literature Review

In this chapter, after a brief introduction of the topic of ice particles ingestion and ice particles accretion, and how it is different from normal aircraft ice accretion, we will analyse the state of the art of the research on ice particles ingestion modelling.

## 2.1 Ice particles ingestion background

Atmospheric ice particles can either be small single ice crystals with the average dimensions of a few $\mu m$, or aggregates of multiple ice crystals, that can reach dimensions of a few millimiters[19, 20]. The conditions for their formation are generally met in the outflow region of vast convective systems, such as the thunderstorm anvils[18, 21]. The anvil region of a thunderstorm, named after its characteristic shape, is the region above 8 $km$ where the cold water spreads[17]. Even though anvil clouds are most common in tropical thuderstorms, they can be found all over the world[17, 18, 21, 22].
Even though a study from Lawson et al. pointed out the potential effects of ice particles on engines[17], until the last two decades they were believed to be a benign phenomenon for turbofan and turbojet propulsion systems[18], as they would bounce off the engine internal surfaces, without causing significant damage. On the other side, the main concern for aircrafts related to cold weather and icing conditions were the supercooled liquid droplets (SLD)[23].

The SLDs are water droplets that are still in liquid form at temperatures lower than


Figure 2.1: Anvil cloud over Europe[24]

273.15 $K$, and can be found in the atmosphere at altitudes that range from 7000 to 22000 feet[23], which correspond to roughly 2100 and 6700 $m$. These SLDs tend to freeze and accrete upon hitting the external surfaces of an aircraft, such as wings, engine nacelles and fan blades[23]. Once the ice starts to form on these surfaces, it can have a detrimental effect on their aerodynamic characteristics as well as, in the case of fan blades, shed and cause foreign object damage to the engine internal parts.

This idea changed at the beginning of the twenty first century. Starting from the last decade of the twentieth century, a series of engine icing events took place at altitudes above 22000 feet, where SLDs can not be found[18]. In 2003 for the first time the connection was made between the presence of high quantity of ice particles and these events[22], dated 2003 is also the first experimental campaign that included the possibility of icing caused by mixed phase and glaciated clouds[25]. The first study specifically on the topic of ice ingestion was then published in 2006[18].

The fact that the interest in ice particles ingestion is relatively new, is most likely the main reason for the low number of studies on the subject, which have, however, started to substantially increase after 2011 and 2012[1, 8, 43].

When these ice particles are ingested into the engine, a mutual influence starts to take place between them and the main flow field[26], the air surrounding them starts

to be accelerated, compressed and heated up by the engine compression system. As a result of these phenomena the particles start to evaporate and their temperature starts to increase, until they eventually melt, to rise again once they have completely become water droplets. These phenomena by themselves induce changes in the compressor performance[8] and could potentially cause stability problems such as compressor surges[9]. With the ice particles being transported forward by the accelerated fluid flow, they also induce a drag effect as a reaction.
As the ice particles hit a compressor rotating surface, such as the rotor blades, they are succeptible to breakage[27].
Additionally, once the particles start to melt, becoming mixed phase particles, under certain conditions of melt ratio, total water content in the air and air wet bulb temperature, the particles can start accreting on the static surfaces of the engine[28, 29, 30, 31, 32, 33]. The ice formations, modifying the stator vanes shape, can easily induce a degradation of the stator aerodynamic performance[28]. Moreover, by restricting the passage area, the accreted ice could cause some more serious effects such as an uncommanded engine rollback, which means that there is a decrease in engine delivered power without any action from the pilot or the engine controller[34, 35, 36].
As already mentioned, the first paper to specifically study ice ingestion was published in 2006 by Mason et al.[18]. In this study, analyzing data coming from in-flight event reports and two test flights with instrumentend aircrafts, they analysed in particular the environment in which ice particles ingestion events, and specifically ice particles accretion events, might take place, and identified the most important challenges for the aerospace industry and research moving forward.
The main challenges for the aerospace industry that they identified were:

- the avoidance of areas with dense presence of ice particles
- the improvement of engine ice particles accretion tolerance
- atmospheric characterization of ice particles
- development of new testing facilities for ice particles ingestion, and in particular ice particles accretion
- development of modelling methods for ice particles ingestion and accretion

Given the topic of this thesis, this literature review will analyse the body of knowledge concerning the improvements in ice particles ingestion and accretion modelling methods.

## 2.2 Ice particles ingestion and accretion modelling methods

There are various high fidelity methods capable of modelling the phenomenon of icing on the aircraft external surfaces, which is caused by supercooled liquid droplets. Two of the most important icing codes are McGill University FENSAP-ICE[37, 38] and NASA LEWICE3D[39].
In 2007 FENSAP-ICE was modified to allow for the simulation of internal geometries and mixed phase particles[40], and the resulting tool was later validated against both the experimental results obtained in 1979 by Lozowski[41] on a cylinder and in 2003 by Al-Khalil on a NACA 0012 profile[25, 41, 42]. These changes allowed FENSAP-ICE to simulate the engine ingestion of partly glaciated water droplets. The results obtained with this method highlighted how higher concentrations of ice particles can be found at the exit of the compressor stages, where pressure increases and velocity decreases. These findings suggest that the components that are potentially most vulnerable to ice particles accretion are the compressor stator vanes.
On the other side, NASA started to adapt LEWICE3D to ice and mixed phase particles ingestion in 2012[43] with the implementation of the previously developed particles trajectory and phase change model GlennICE[44]. By coupling LEWICE3D with GlennHT[45, 46], an internal flow solver which would calculate the flow conditions within the compressor and pass them on to LEWICE3D, Bidwell, Rigby and colleagues were capable of analysing the low pressure compressor of an engine that would have later been used in a series of experimental campaigns at the Propulsion Systems Laboratory[35, 36, 47, 48]. The method successfully predicted the the possibility to have or not ice accretion in various conditions[36, 49].
Additionally, NASA has also worked on their 2-D code LEWICE[50]. In 2015 Wright and colleagues[51] modified the aforementioned code by adding a break-up model that took into account the experimental findings by Hauk et al.[52] for what concerns the particles impact behaviour, Palacios et al.[53] for the particles trajectory after the break-up, and Currie et al.[54] for the assessment of whether the particles would bounce or impinge upon contact with the compressor surfaces.
Finally, it is worth mentioning that also ONERA[55], the Turkish Aerospace Industries Flight Sciences Department in cooperation with the Middle East Techincal University[56], and Oxford University in cooperation with Rolls-Royce[57], have all developed their own 2-D and/or 3-D ice particles ingestion and ice accretion codes. While all these high fidelity tools are extremely valuable for understanding the detailed behaviour of the ice particles as they travel through the compressor, as well

as the mechanisms for ice accretion and its effects on compressor aerodynamics, they are not well suited for more systemic analyses. These methods, in fact, are not capable of performing whole engine simulations, where it could be possible to investigate the effects that the ingestion of ice particles has on the overall engine performance and behaviour.
Given that the overall engine behaviour is in fact the main focus of this research effort, we will now concentrate our analysis on the 0/1-D models.
In fact, these more simple models allow to more easily simulate the interactions between different subsystems and components, given their lower computational demands, which is something that would not be feasible with more complex and refined tools.
The main contributor in this area are NASA and General Electric, which followed two slightly different approaches.

### 2.2.1 NASA modelling approach

NASA tried different methods over the years to model the ice particles ingestion in the engine with a systemic approach, always focusing however on the mechanisms and effects of ice particles accretion.
In their first iteration, they adopted a combination of a 0-D, a 1-D and a 2-D code. In a study published by Jorgenson and colleagues[1] a mix of NPSS (Numerical Propulsion System Simulation), COMDES and the 2-D version of GlennICE was used to determine which conditions, over a determined flight envelope, could present risk of ice accretion within the compressor of a two spool turbofan engine.
NPSS is an object oriented software developed by NASA[58, 59, 60]. This software, given a set of maps for the different components of the engine, is able to simulate the performance of the engine and the thermodynamic values of the flow at the inlet and outlet of each component at different ambient conditions and throttle settings.
On the other side, COMDES is a 1-D, mean line compressor flow code[61]. The software can be used both for the preliminary design[62] of a new compressor or for the analysis of the off-design performance of an existing one. In this second case, the software calculates the compressor performance using as inputs the rotor blade angles for both leading and trailing edges at hub, mean and tip radius, and the flow inlet conditions.
With this method, NPSS would determine the low pressure compressor (LPC) inlet conditions and shaft rotational speed, together with the performance of all the other engine components. The LPC performance, on the other hand, are calculated

by COMDES, as well as the blade-row to blade-row flow characteristics, which are passed on to GlennICE. Finally, this last code would determine the particles evolution and assess the possibility of ice accretion. This methodology is displayed in Figure 2.2

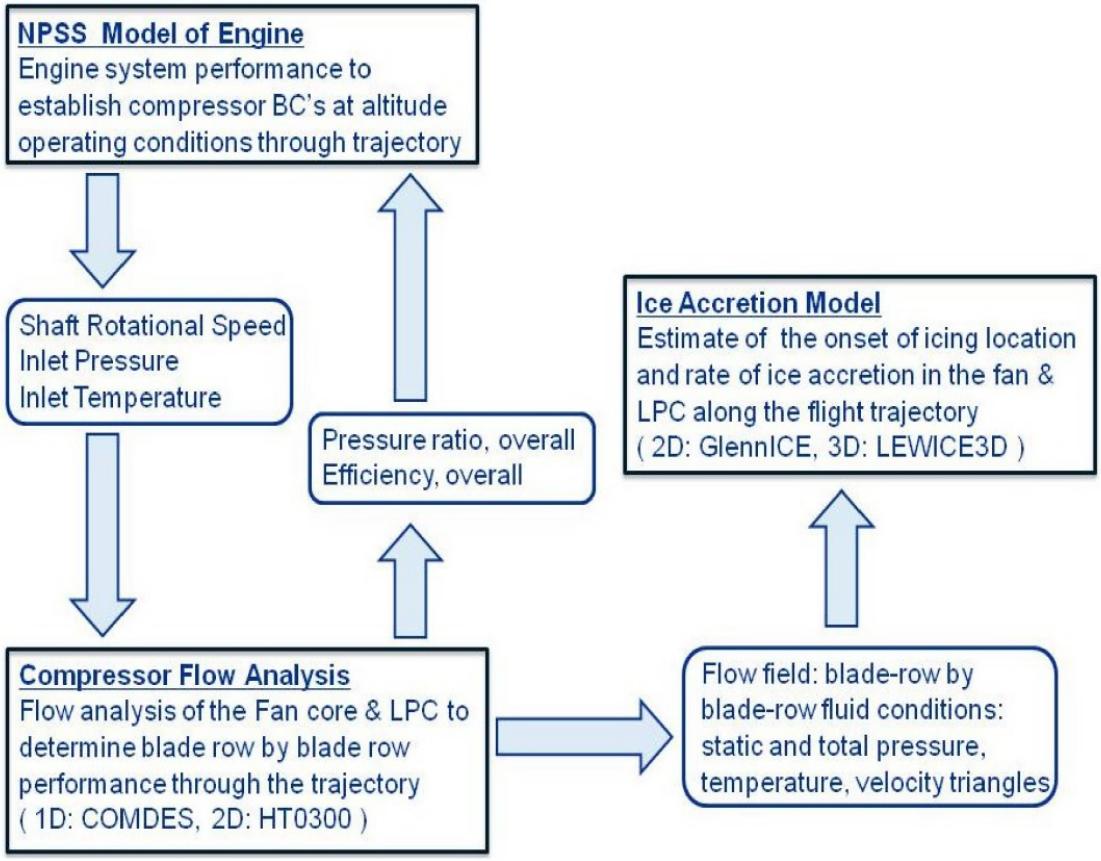


Figure 2.2: Jorgenson et al. modelling methodology[1]

During the first phase of the study, Jorgenson and colleagues ran the NPSS-COMDES code in steady state at different locations over a typical flight envelope to identify possible ice accretion conditions. They assumed that there would be ice accretion on stator vanes with static temperature between 509 and 515 degrees Rankine, based on some previous laboratory test results[28], and introduced there a blockage factor to simulate the effect of ice accretion on the LPC compressor characteristics.
In the second half of the study, they confirmed the locations of potential ice accretion with the use of GlennICE, which takes into account also other parameters such as temperature and relative humidity.
While the approach taken by Jorgenson and colleagues was a good starting point and presented good preliminary results, some of which also in agreement with some experimental work, it considered only the influence that the fluid flow has on the particles, and not how the ice crystals influence the flow as their temperature rises,

they change state and evaporate. Also for what concerns the ice accretion, the only influence that it has on the flow, according to this model, is the induced blockage. Finally, the study does not take into consideration the transient behaviour of the engine, which will be modelled in a fairly different way in the follow-up study[14], but only the changes in the compressor characteristics.
The aforementioned follow-up study by May et al.[14] represents the first attempt by NASA to simulate the transient behaviour of an engine during ice accretion, and in particular to simulate the occurence of an ice accretion induced engine rollback. In this study, they used C-MAPSS40k, a publicly available MATLAB/Simulink code that models a generic 40.000 lbf thrust double spool high bypass turbofan engine, including an engine controller. They also generated some component blocked maps for the LPC using COMDES, and progressively transitioned from the standard maps to the blocked ones, to simulate the build up of ice. This method, however simple, gave good results, allowing them to reproduce the behaviour of an engine rollback.
In the following years, the modelling method proposed by Jorgenson et al. was improved in several ways:

- The NPSS-COMDES code was modified by adding GASPLUS, a code capable of calculating the fluid properties of a air/water vapour mixture. NPSS has also been replaced in some studies by a code directly provided by the manufacturer of the engine they were testing and/or modelling[2, 3, 4, 5]
- A new particles code was developed: MELT, a 1-D code with equations taken from LEWICE2D[50], capable of calculating the evolution of the particles as they proceed through the LPC
- The enthalpy necessary for the particles evolution was subtracted from the main flow in COMDES at the gap between rotor and stator and through the stator vanes

The main implication of these changes was that the method now did take into consideration the mass and enthalpy effects of the particles on the fluid flow, leaving out only the potential effects on the flow momentum. There was also athe addition of the capability to calculate wet bulb temperature, $T_{wb}$, and the melt ratio, the ratio between the mass of liquid water and solid ice, that were found to be crucial parameters for the onset of ice accretion[29]. The ice accretion blockage then was modelled as a reduced spacing in COMDES, and was a function of time and ice accretion growth rate, which has been preliminarly estimated by Struk et al.[30].

The NPSS set-up for this new modelling method is shown in Figure 2.3, while the relations between the different codes are displayed in Figure 2.4.

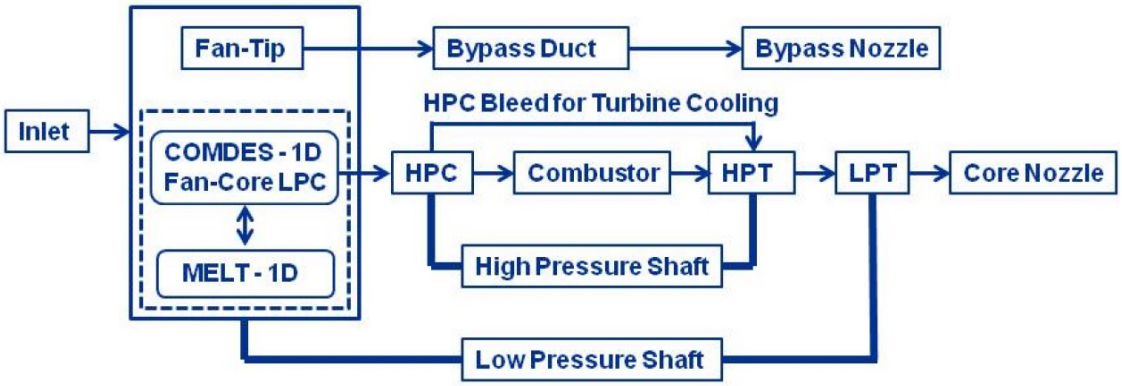


Figure 2.3: Veres et al. NPSS set-up[63]

This methodology was first implemented by Veres and colleagues in 2012[63] with the main focus of assessing the probability of ice accretion.
In a 2013 study[2], this methodology successfully reproduced ice accretion in the same cases where it was detected during some test runs that replicated flying conditions. In addition, it predicted ice accretion for some additional altitudes and flying conditions, which were then confirmed by additional tests. Moreover, one of the main findings of this study was the confirmation that no ice accretion event presented a 0 melt ratio, meaning that ice accretion is possible only if the ice crystals are partially melted.
In a following study[3] this method helped understanding the differences in wet bulb temperature and melt ratio between cases that during the experimental tests showed an imminent (fast) icing event, a gradual (slow) icing event, or no icing event at all. By introducing proper degradation factors, in 2016 it was possible to reach a good agreement between experimental data and NPSS computational results for a full rollback event of a Honeywell turbofan commercial engine[4]. The comparison between test data and NPSS results can be seen in Figure 2.5, where N1 is the fan speed, N2 the core speed, WF the fuel flow rate, PT3 and TT3 the core compressor exit pressure and temperature respectively, and finally TT45 is the high pressure turbine exit temperature.

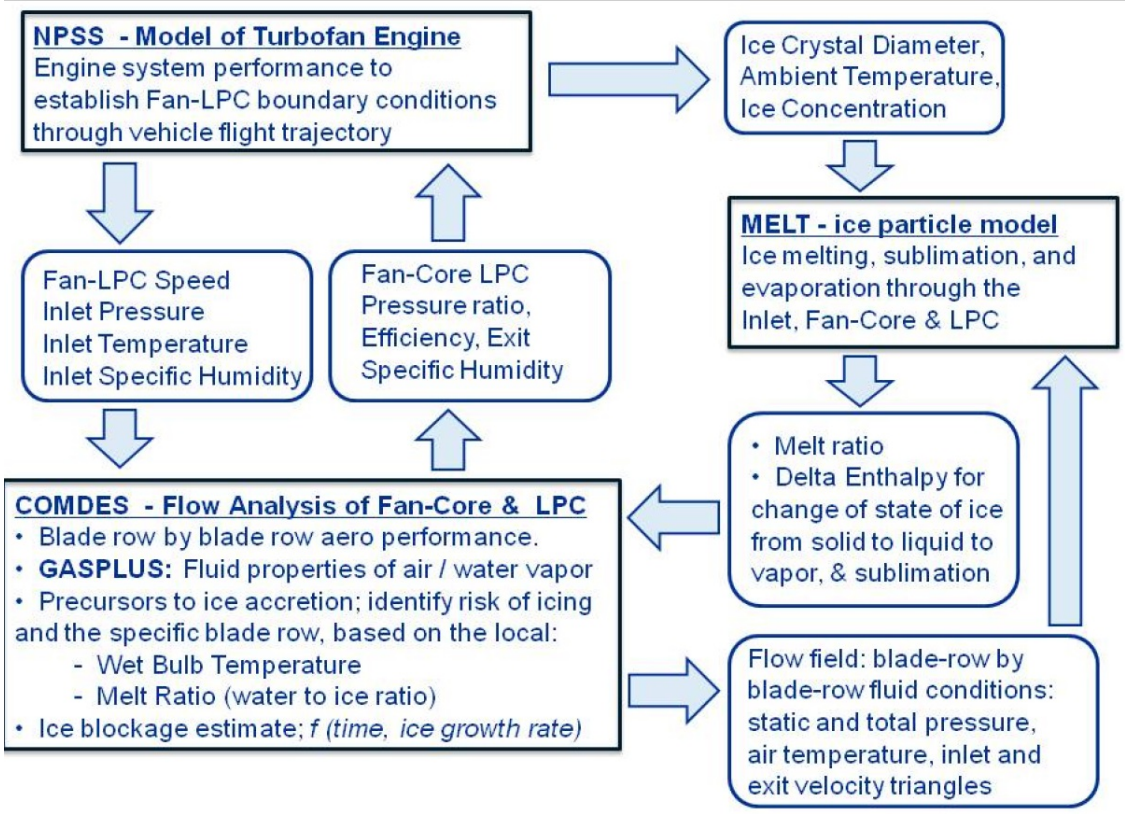


Figure 2.4: Veres et al. modelling methodology[63]

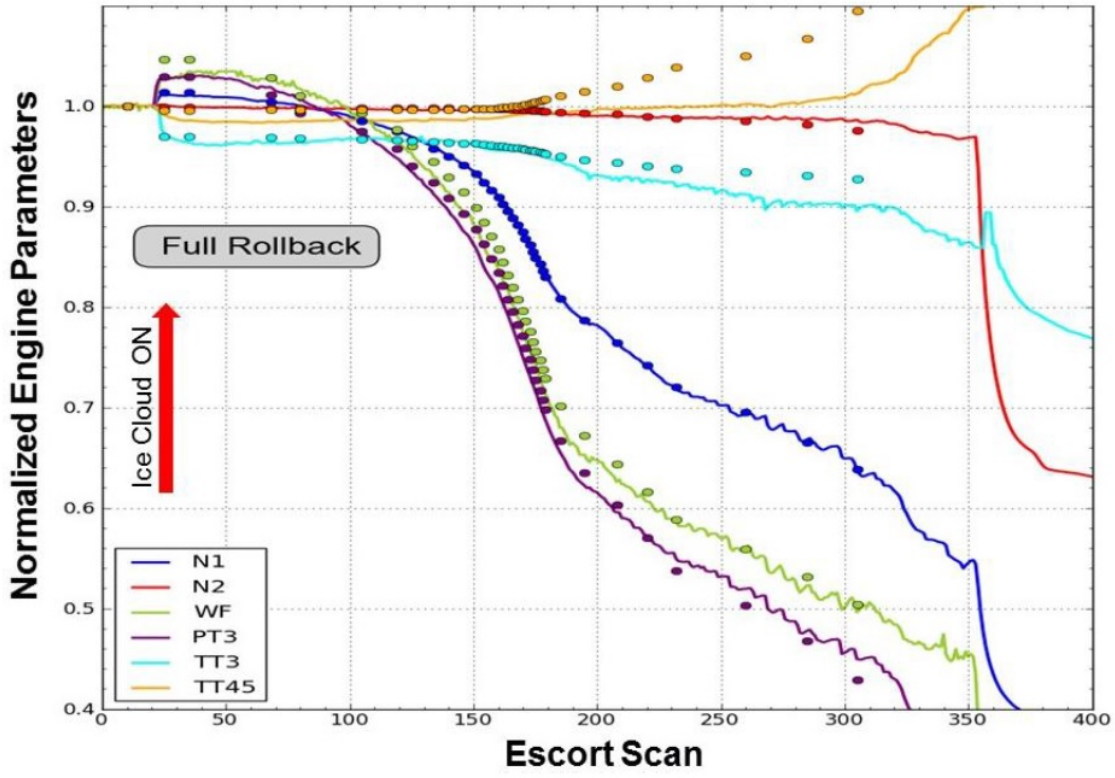


Figure 2.5: NPSS calculated performance results (dots) and test data (solid curve)[4]

Additionally, by calculating with COMDES the level of blockage required to have the same level of degradation introduced in NPSS, they were able to obtain an estimation of the blockage growth rate with varying wet bulb temperature and ice-water to air ratio (IWAR), which have been found to be the most important parameters for determining the ice growth rate.
Using the same method, these findings were then expanded and refined in a 2017 paper by the same authors, whose results will be discussed later in this thesis.[5].
While this second approach does introduce the thermodynamic effects that the particles have on the flow with their evaporation, temperature rise and phase change, this method still is not capable of performing transient simulations, but it rather produces single operative points. Moreover, it lacks a particle break-up modelling capability and does not take into consideration the effect that the particles have on the flow momentum.
The last approach to be described here took by NASA is the most simple to be listed in this review. In this method, the engine is modelled using only NPSS, with the simulation set-up that can be observed in Figure 2.6[6]. In the model, scalar correction terms for pressure ratio and efficiency are applied to the LPC maps in order to take into consideration the deterioration effect of ice accretion. The enthalpy required to raise the particles temperature to 273.15 K and subsequently completely melt them is calculated and extracted at the end of the LPC. On the other side, the HPC is divided stage by stage, and the enthalpy necessary to convert the resulting water droplets into vapour and raise its temperature to the HPC exit temperature is extracted between each stage. Finally, a correction parameter is applied to the HPC required power to take into account the effect of the non-adiabatic compression process.
By appropriately setting the degradation factors, this method produced similar results to the previous one in modelling ice accretion induced rollbacks in two different occasions[6, 15].
What really differentiates this approach from the previous two, however, is that in a 2017 study Simon and colleagues derived from this a modelling method in T-MATS capable of performing dynamic and transient simulations[7]. T-MATS (Toolbox for the Modeling and Analysis of Thermodynamic Systems) is a NASA-developed MATBLAB/Simulink code[64]. Simon et al. model transferred the same NPSS simulation set-up of Jorgenson et al.[6] to T-MATS, adopting also the same assumptions for enthalpy extraction and deterioration factors.
In order to transform the Jorgenson method[6] into a dynamic model, they merged it with the maps stacking methodology already applied by May[14]. In this method, as

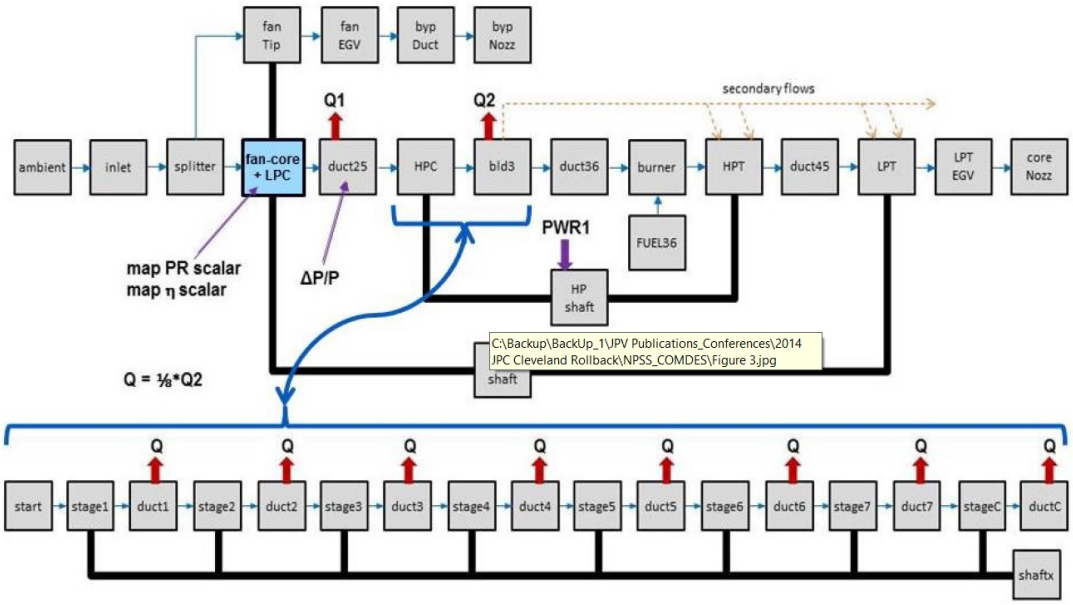


Figure 2.6: Jorgenson et al. NPSS set-up[6]

already described, a series of progressively blocked maps is produced using COMDES, using a method proposed by Jorgenson in 2011[1], and the operative map utilized by the solver is progressively changed as the blockage level increases. Moreover, Simon et al.[7] utilised new experimental data obtained from NASA PSL test facility[35, 36] to calibrate their input data, such as the particles density. The model also had the possibility to control fuel flow, bleeds and auxiliary power extraction actuators, and these controls could be operated both in open or closed loop. This method produced results with very good agreement with engine test data for ice accretion induced roll-backs for what concerns engine system level behaviour, and it was set to be used to formulate new ice accretion detection techniques in future studies.

This last approach, while being able to perform transient and dynamic simulations, does not take into consideration the physics behind the particles evolution, relying on the assumptions made about their melting in the LPC and evaporating in the HPC. While it did bring good results, it is not clear if these assumptions would reveal to be as reliable when simulating engines with a different architecture.

We will now discuss the modelling approach adopted by General Electric, before closing this literature review section with some final remarks.

### 2.2.2 General Electric modelling approach

From 2012 General Electric started a research effort with the aim to model the effects of ice ingestion on a compressor, in cooperation with the Georgia Institute of Technology. In their first publication, they laid down what would be the main method they would use to model this phenomenon[8]. The base of their approach is a quasi 1-D Euler solver that calculated the main flow characteristics, and that was validated in a following paper[65]. In parallel, a dedicated code would calculate

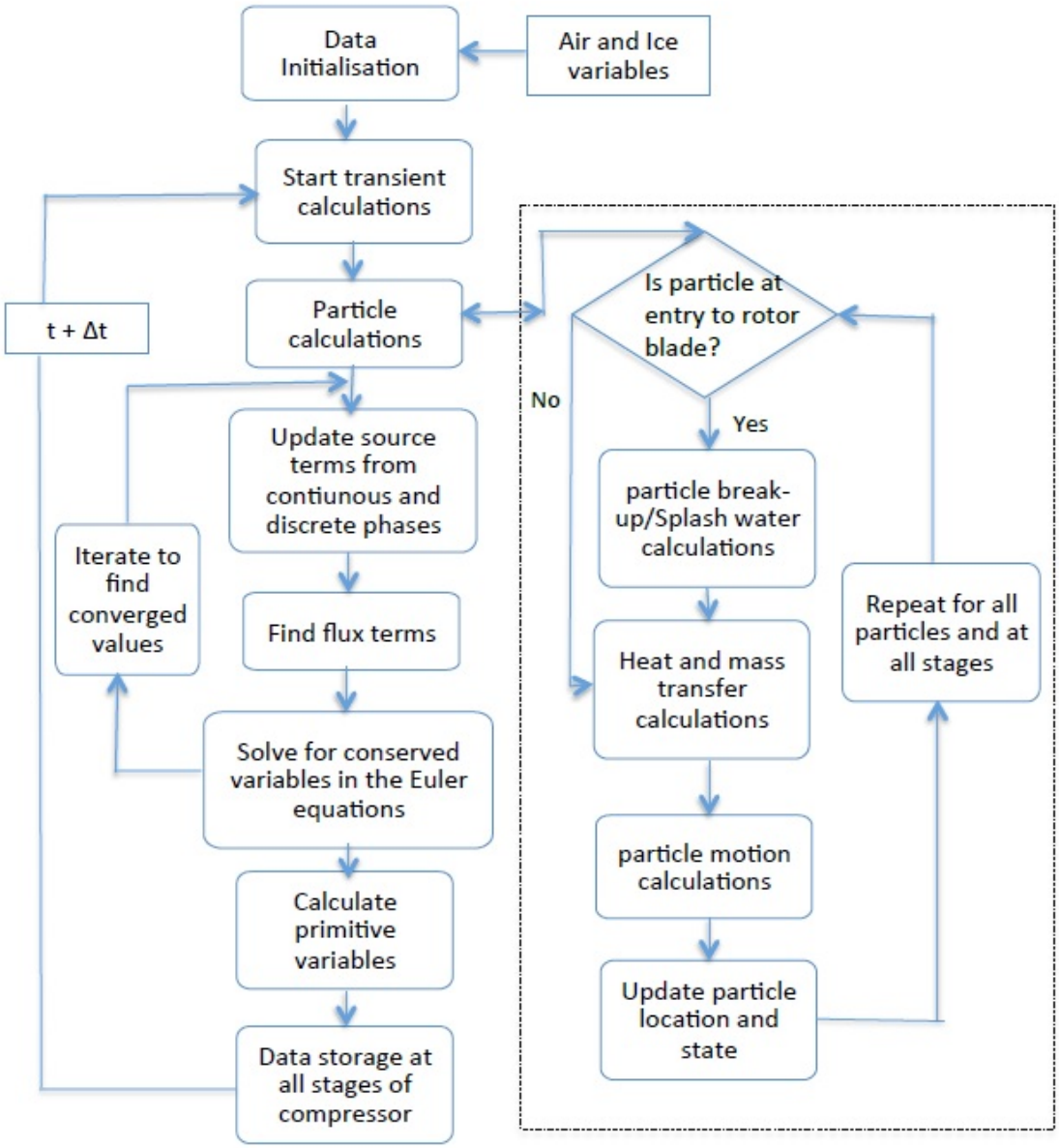


Figure 2.7: Kundu et al. numerical scheme[8]

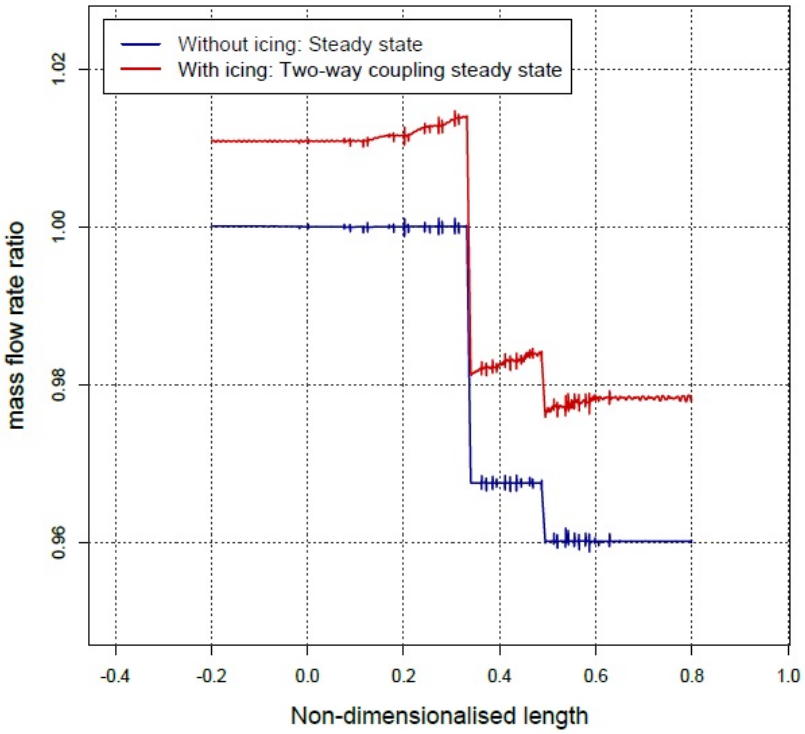


Figure 2.8: Kundu et al. results for mass flow[8]

the evolution of each single particle ingested by the compressor, whose diameter is determined using a probability curve around a mean value. The particles were assumed to be spherical and to be dragged forward by the flow, which means that they had an influence also on the momentum equation, not only on the mass and energy ones. The enthalpy exchange between the particles and the flow was considered to take place only at the stators, while the particles passing through the rotors were broken up, and the water droplets splashed. The break-up model is an inportant novelty compared to the previous approaches considered. The influence of the particles on the flow was accounted for with the introduction of source terms into the Euler equations. Finally, instead of having a second mass equation, they opted to introduce a species balancing equation in the form of[8]:

$$\frac{\partial \rho A q}{\partial t} + \frac{\partial \left(\rho A q\right) u}{\partial x} = \frac{\partial \dot{m}_{wv}}{\partial x} \tag{2.1}$$

Where $\rho$ is the flow density, $A$ the passage area, $q$ the humidity ratio, defined as the ratio of mass of water vapour over mass of dry air, $t$ is time, $u$ is the flow velocity and $\dot{m}_{wv}$ the particles evaporation/sublimation rate. The method numerical scheme

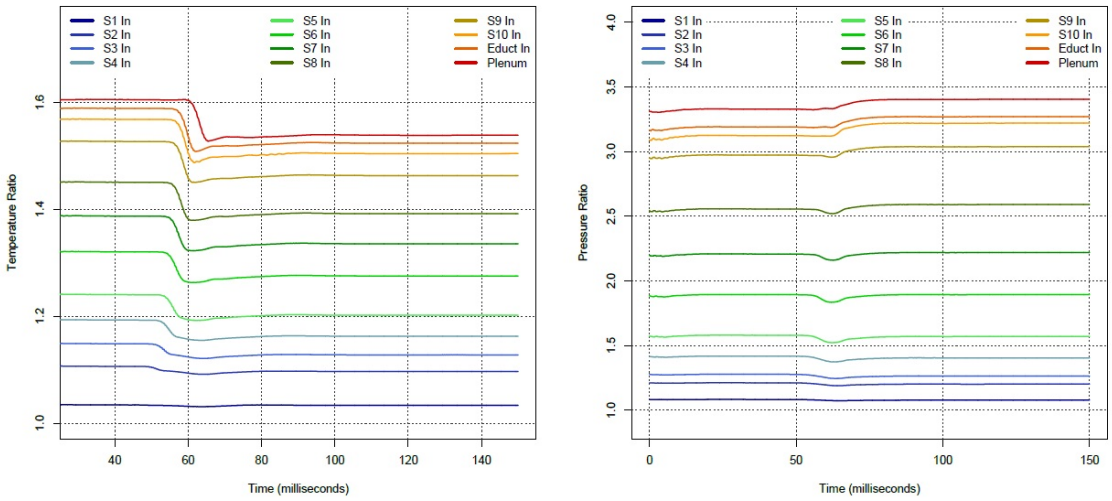


Figure 2.9: Kundu et al. results for temperature and pressure ratio[8]

can be observed in Figure 2.7.

Using this approach, Kundu and colleagues simulated a ten stages compressor at constant rotating speed, and found that the introduction of ice particles causes a series of changes in the operative conditions of the compressor. The first of these changes was the increase in overall mass flow, with a further increase throughout the compressor due to the evaporation of water particles, that can be seen in Figure 2.8. It is worth noting that the fluctuations visible in this figure are due to the numerical error of the solving scheme, and were greatly reduced by Kundu in subsequent refinements of the method[11].

Additionally, in Figure 2.9 can be observed how temperature and pressure ratio behave differently along the different stages.

All these effects combined together cause the initial stages operative points to move away from the surge line, while the operative points of the last stages move towards it[8].

Using this method, they also showed how the ingestion of ice crystals could trigger a compressor surge[9]. Considering the research done by NASA on ice accretion induced engine rollbacks, this finding highlights the importance of understanding the engine behaviour during ice ingestion and its effects.

After a study analysing the influence and importance of different particles and flow parameters on the compressor behaviour in modelling the ice shedding phenomenon[10], a new study by General Electric highlighted how a compressor might actually sustain more easily, under a thermodynamic point of view, a moderate amount of ice ingestion for a prolonged period of time, rather than the abrupt introduction of a big amount of ice, even though for just a brief moment[12].

Finally, the last research published by the GE working group was a comparison between different strategies for particles break-up and droplets splashing[13].
This modelling approach does account for the particles influence on all the aspects of the fluid flow (mass, momentum and energy), includes the particles break-up and droplets splashing, and is able to perform transient simulations. However, it has never been applied to a full engine, and does not account for possible ice accretion within the compressor. Moreover, it most likely requires a high computational power and/or computational time, as it models the evolution of each ice particle separately.

### 2.2.3 Final remarks

Figure 2.10 is an overview of the different ice ingestion model presented in this literature review, showing their characteristics, their pros and cons.

| Study | Mass | Momentum | Energy | Break-Up | Ice Accretion | Transient | Whole Engine | Engine Specific |
|---|---|---|---|---|---|---|---|---|
| Jorgenson 2011 | No | No | No | No | Yes | No | Yes | No |
| May 2011 | No | No | No | No | Yes | Yes | Yes | No |
| Veres 2012, 2013, 2014, 2016, 2017 | Yes | No | Yes | No | Yes | No | Yes | No |
| Jorgenson 2014, Veres 2015, Simon 2017 | Yes | No | Yes | No | Yes | Yes | Yes | Yes |
| Kundu 2012, 2014, Saxena 2015, 2017 | Yes | Yes | Yes | Yes | No | Yes | No | No |
| Pandin 2019 | Yes | Yes | Yes | Yes | Yes | Yes | Yes | No |

Figure 2.10: Overview of ice ingestion models characersitics

The first models proposed by NASA were preliminary attempts to assess the effects that ice particles, and in particular ice particles accretion, have on engine performance[1, 14]. In doing so, they considered only the effects that the main flow has on the particles, and the blockage effect that the particles accretion has on the engine performance. This approach, however simple, gave promising results, and induced NASA in going forward in their modelling effort.
In its second wave of studies, NASA took into consideration also the effects that ice particles have on the engine flow mass and energy, with the introduction of water vapour and subtraction of enthalpy resulting from the particles evolution. This approach has produced excellent results, improving the understanding of the mechanisms of ice particles accretion[49], which was the main target that NASA was

pursuing, and these findings are and will be of paramount importance for anyone who aims at appropriately model the phenomenon of engine ice ingestion including the possibility of ice crystals accretion.

Additionally, NASA carried out a study that could be seen as the first study to analyse the engine system behaviour in case of ice ingestion[7]. The model they used, however, is arguably very specific to the engine it was applied to, given the assumptions that were made about the particles evolution. These assumptions were however understandable, considering that the main focus of the study was the modelling of the single case of ice ingestion and ice accretion induced engine rollback on a specific engine, rather than the general engine behaviour during ice crystals ingestion conditions.

On the other side, the General Electric and Georgia Institute of Technology working group has proposed an interesting methodology for modelling ice ingestion that necessitates of less assumptions about the particles behaviour, hence it can be applied to a wide range of engine architectures. However, they only used this model to analyse an isolated compressor, and did not consider ice accretion. Moreover, the methodology could result to be very demanding under the computational point of view, as it models the particles one by one.

In conclusion, it appears that at the moment there are no models in literature capable of simulating the overall transient behaviour of an engine subject to ice ingestion that include the influence of the particles on the flow mass, momentum and energy, that can take into account for ice accretion, and that are not constrained by critical assumptions regarding the crystals evolution. The method presented in this study tries to accomplish the target to put all these characteristics together, as it can be seen in the last row of Figure 2.10, and in doing so tried to couple together the best of both NASA and General Electric approaches. Moreover, no studies have been found that investigated the general behaviour of the entire engine in these conditions, without focusing on one specific type of event.

# Chapter 3

# Methodology

The aim of realising a simulation tool capable of modelling the behaviour of a whole engine in ice ingestion conditions presented many challenges due to the big number of concurrent phenomena that such scenario implies.

These different phenomena can be summarised as follows:

- the performance of the engine compression system
- the performance of the combustor
- the performance of the expansion system
- the shaft behaviour
- the particles behaviour
- the process of particles breaking up upon encountering the compressor blades
- the eventual process of ice accretion on the compressor stator vanes
- the behaviour of the accreted ice

Each of these main phenomena is extremely complex, and they all are intertwined and influence each other:

- the compressor performance influences the behaviour of the combustor

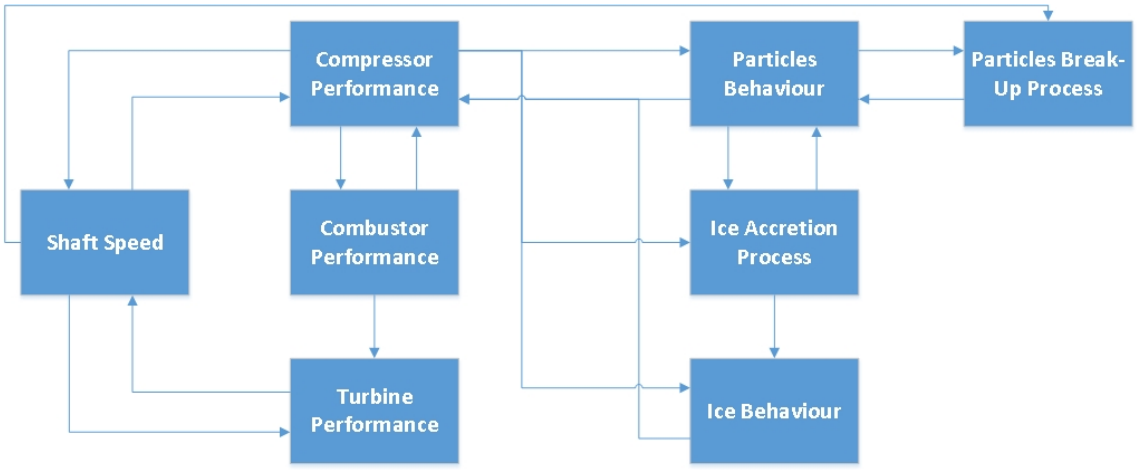


Figure 3.1: Correlations between simulated phenomena

- there is a mutual inluence between the combustor and the compression system, while the former unilaterally affects the turbine, as in most cases the first row of NGVs is choked

- both the turbine power output and compressor power requirement define the shaft rotational speed, which in turn influences the performance of both of them

- the particles behaviour is affected by the main flow conditions, which are defined by the compressor performance, and in turn it affects the compression system with the mass, momentum and energy exchanges that it implies

- the particles break-up is dependant on the particles velocity, size, and on the compressor blades velocity, and it results in a reduction on particles size and an increment of their number

- the process of ice accretion is regulated by a mixture of ambient conditions, defined by the compressor performance, and particles characteristics. This process obiviously influences the amount of ice that passes from the particles form to the accreted, static one

- the static ice behaviour is influenced by ambient conditions and by the amount of ice that is accreting at every moment and, in a similar manner to the particles behavior, influences the compressor with the mass and heat exchanges that it implies

The aformentioned relations can be visually portrayed in figure 3.1.

Now that the very complex nature of the problem has been highlighted, it is also possible to notice a way to simplify it. For example, it is pretty clear that it is possible to divide the blocks in Figure 3.1 in two groups, with those on the left representing the engine, and those on the right representing the ice, both particles and static.
This observation determined the choise to split the overall modelling of ice particles ingestion into two main problems: the modelling of the engine behaviour, which is calculated by a tool already present within Cranfield UTC, and the modelling of ice particles and accreted ice, which is carried out by a new model that was developed for this thesis.
Moreover, among the engine subsystems perfomance blocks, only the compressor one influences and is in turn directly influenced back by the phenomena on the right side of the picture. Of course, all the systems feel the effects of the ingestion of ice particles, such as the introduction of water vapour or the temperature drop, but the ice is directly acting only on the compressor, which then carries these effects over to the other components.
Following the fact that only the engine compressors do have a direct interaction with the ice particles and the accreted ice, the project was divided into three main phases and a series of sub-steps, which can be observed in Figure 3.2, with the light blue boxes highlighting the coding steps, and the dark blue ones indicating the steps where the work was constituted by running simulations and analysing their results.
The first phase began with the development of the code modelling the particles behaviour, which was tested by simulating the particles evolution as they enter a duct with a fixed set-up of air velocity, pressure and temperature. The results of these simulations will not be reported in this thesis as they were carried out merely to check for evident mistakes in the particles code. After this, the parts of the method that allow the compression system and the particles to interact were coded. The effects of particles evaporation on the compressor flow mass, momentum and energy are taken into account with dedicated source terms to the flow solving equations, as it will be explained in detail in the next chapter. On the other side, the interaction between compressor blades and particles determines the necessity of a break-up model, and a splashing model for water droplets, which were implemented at this stage. Finally, the introduction of water vapour introduces some changes in the thermodynamic properties of the compression system working fluid, which is not pure air anymore. The coding of these changes was carried out during this phase, which concluded with a series of simulations of an isolated compressor at fixed rotational speed, followed by a plenum. The results of these and the following

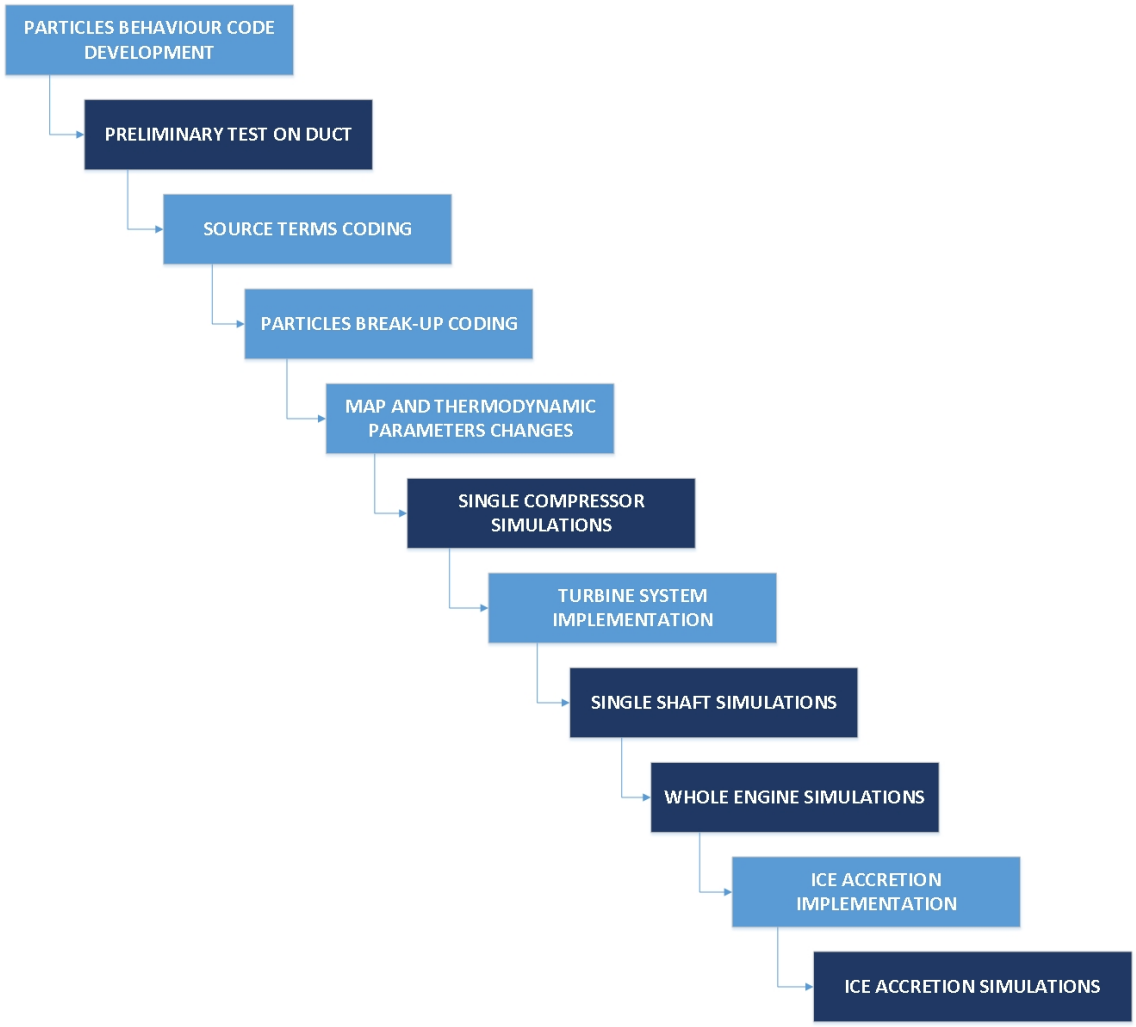


Figure 3.2: Project work flow

simulations are reported in

Chapter 5 of this thesis.

For the second phase of the project, the addition of the expansion side to the simulations required the implementation in the expansion side part of the engine performance code of the aforementioned changes to the flow thermodynamic properties of the working fluid. This operation was then followed by single shaft simulations. Once the code was capable of smoothly running with both the compression and the expansion sides of the engine implemented, the whole engine simulations were carried out, and their results analysed.

Finally, the capability to detect and model the eventual particles ice accretion was implemented into the particles modelling code, and a series of simulations was carried out to test this new capability.

The remaining of this chapter will be dedicated at analysing how the elements listed

in Figure 3.2 were implemented and interacted between each other during the three mentioned phases.

## 3.1 First phase

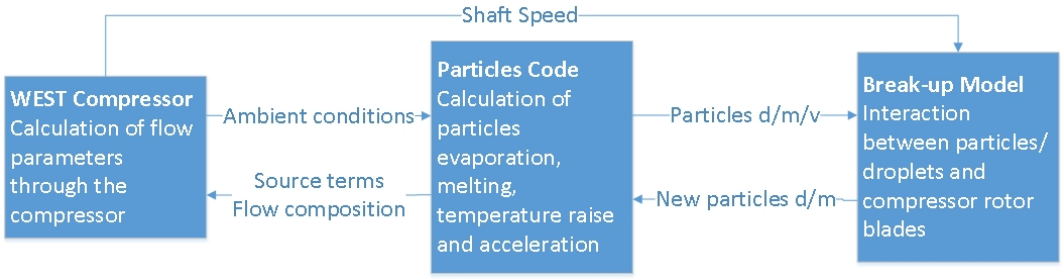


Figure 3.3: Isolated compressor simulations modelling methodology

At the time this project was being defined, a new tool was being developed internally by the UTC. WEST (Whole Engine Simulation Tool) is a Matlab code capable of performing whole engine unsteady simulations, which was first meant for simulating shaft failure overspeed events, and to be applied in the preliminary design phase of an engine [66].

WEST, which will be the subject of the first section of the next chapter, in particular models the flow of air in the compressor using quasi 1-D Euler equations with source terms. This characteristics makes it very suitable for simulating many different phenomena within the compressor. In the case of ice ingestion, for example, where the aerodynamic effects can be considered negligible, it is possible to model the influence that the ice has on the flow that is being compressed by adding the appropriate source terms to the Euler equations. This made WEST the chosen baseline for this simulation effort.

Hence, while WEST simulates the compressor, and more precisely the behaviour of the air flowing through the compressor, it is not able to simulate the behaviour of particles or static ice. It has been the main work of this project to build some additional routines into WEST in order to be able to perform a full ice ingestion simulation.

In order to do so, the flow is split in two phases, a continuous one, constituted by the air and water vapour, which is modelled by WEST, and a discrete phase, formed by the ice particles and accreted ice, which are modelled using a Lagrangian approach. The particles are followed as they enter the compressor, melt and evaporate, so that their evolution will define the values for the source terms to be applied to the con-

tinuous phase. The behaviour of both the particles and the accreted ice is regulated by basic mechanical and thermodynamic equations[67], so that the calculation does not need any iterative process. This approach is similar to the one already utilised by Kundu[8]. The influence of the particles on the main flow is accounted for by the aforementioned source terms, but also by the modification of the flow composition, that induces a series of changes in the flow thermodynamic properties. A particles break-up model and a water doplets splashing model were also implemented. These models were taken from the literature[13].
Figure 3.3 shows how WEST and the ice modelling formulation interact with each other.
On one hand, the WEST calculated flow conditions serve as ambient conditions for the particles calculation. On the other, the evolution of the particles themselves determines the magnitude of the source terms for the Euler equations and the amount of water vapour that will change the flow composition. On the right side of the figure is then possible to appreciate how the particles break-up model, by taking into account particles diameter, mass and velocity and shaft speed, which is fixed in these simulations, calculates the interaction between particles and rotor blades determining the new mass and diatemer of the formers.

## 3.2 Second phase

In order to perform single and multiple shaft simulations, it was necessary to add the combustion chamber and the WEST turbine system simulation code, allowing the shaft rotational speed to change responding to the varying operating conditions of the components. This new set-up is shown in Figure 3.4. In the figure, all the blocks and connective links present from phase one and lacking the description do not serve any additional purpose compared to Figure 3.3
As it will be clarified in the next chapter, the combustion chamber in WEST is still modelled using quasi 1-D Euler equations, and is actually considered one subcomponent in the overall compression system subroutine. This means that its introduction did not require any additional coding.
The WEST turbine modelling tool, on the other side, is a separate subroutine. Using the flow conditions coming from the combustion chamber as inlet conditions and the ambient pressure as an outlet condition, it uses an iterative method, which will be discussed in the modelling chapter, to identify the flow conditions at the inlet and outlet of each turbine that is being modelled, as well as the final nozzle. As

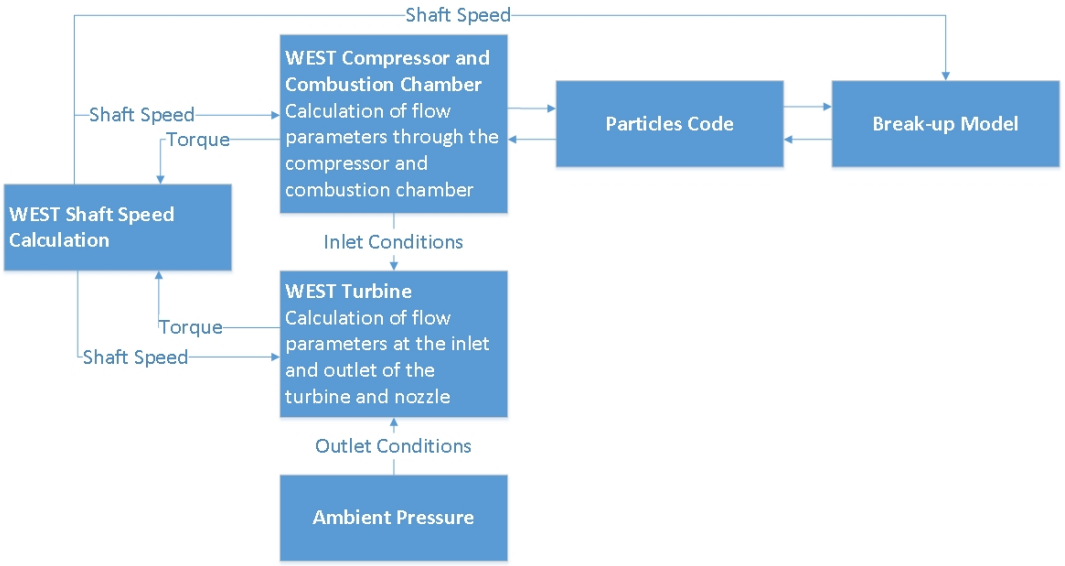


Figure 3.4: Single and multiple shaft simulations modelling methodology

it has already been mentioned, the ice particles completely evaporate within the engine compression system, which means that they do not have any direct influence on the turbines. However, the changes in flow composition determined by the introduction of water vapour are carried past the combustion chamber. This means that the turbines code had to be modified in order to account for these flow composition changes.

Finally, considering the balance of the opposite torque coming from the compressor and the turbine, a third WEST subroutine calculates the variation of shaft rotational speed in time. In these simulations, this unsteady rotational speed is considered for the particles break-up and droplets splashing calculations.

There is no methodological difference between single and multiple shaft simulations, since the presence of one or more shafts is implemented into WEST by introducing one or more subcomponents into the compression and expansion subroutines respectively. For this reason they were both included into the second phase.

## 3.3 Third phase

The focus of the last phase of the project was the addition of the capability to simulate ice accretion to the modelling method. Figure 3.5 shows how the new subroutines necessary for this feature interact with the already existent method, like in the previous section, the blocks and links lacking any description serve the same purpose as in Figure 3.4.

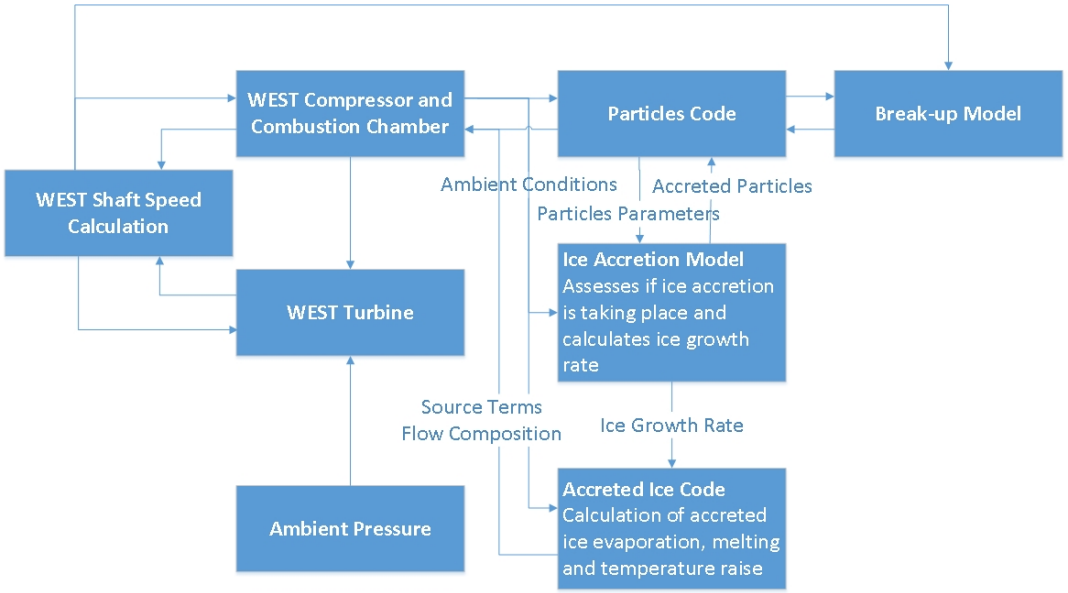


Figure 3.5: Ice accretion simulations modelling methodology

The main features added during this phase are the ice accretion model and a code capable of modelling the behaviour of the accreted ice. It is assumed that the ice accretion process can take place only at the compressor stator vanes.
The ice accretion code assesses for each compressor stator vane if the conditions for ice accretion are met. It does so comparing ambient conditions and particles parameters, coming from WEST and the particles code respectively, and the requirements for ice accretion that were found by NASA[49]. Using those same findings, the model also calculates the ice growth rate, and the number of particles that need to accrete. These particles are subtracted from the particles code, and go to increase the mass of accreted ice.
The accreted ice code, on the other side, serves a very similar purpose as the particles code. Using the flow data coming from WEST as ambient conditions, and considering the mass that accretes at every time step calculated by the ice accretion code, it models the evolution of the accreted ice using the same basic thermodynamic equations that the particles code adopted. The influence of the accreted ice on the main flow is then accounted for by source terms, formulated very similarly to those used for the particles, and by the change in flow composition induced by the ice and water evaporation. All these processes will be discussed in more detail in the dedicated section of the next chapter and in Appendix B.

## 3.4 Overall simulation strategy

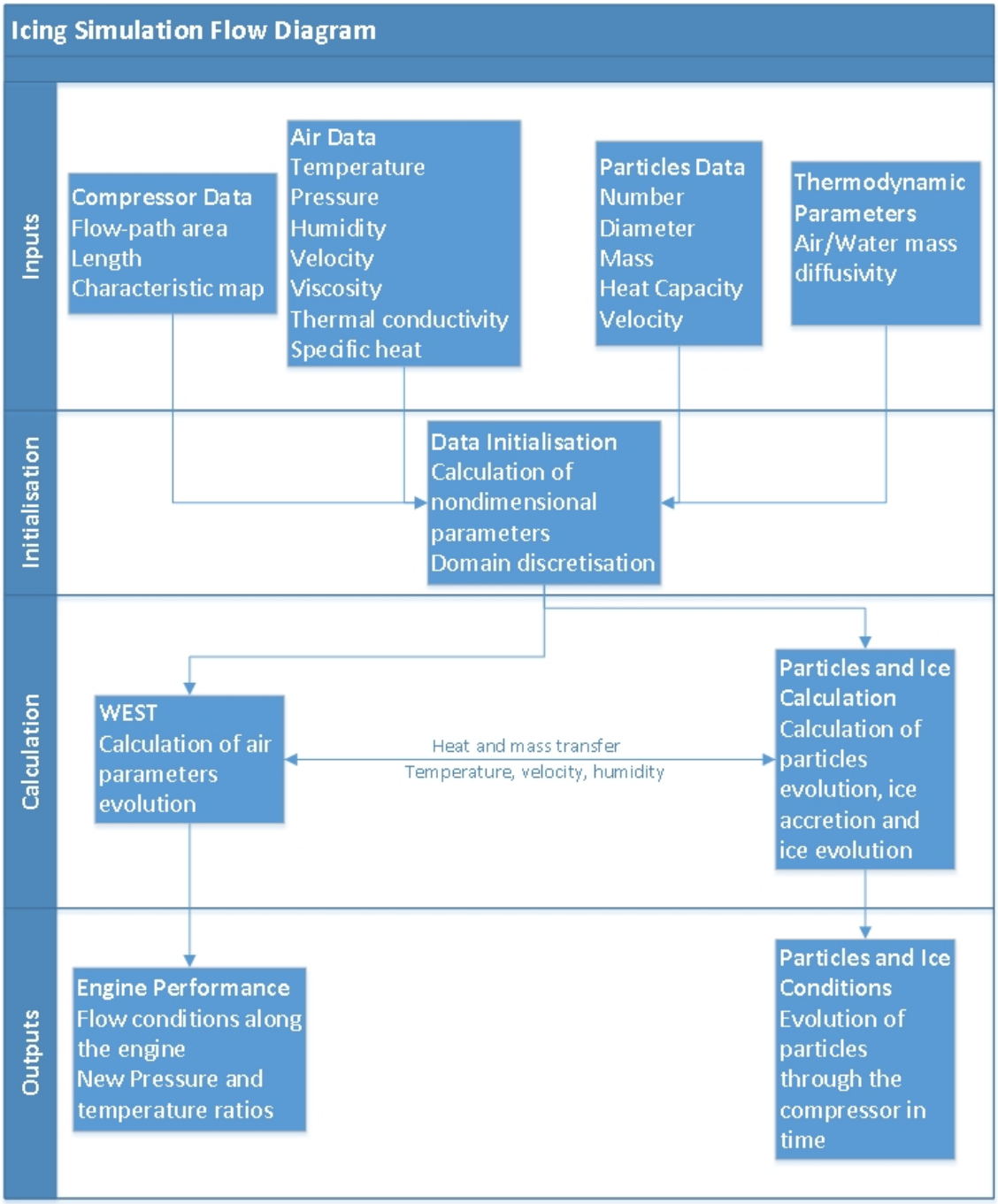


Figure 3.6: Overall simulation process

Before discussing the details of the various models used in the present method and how they are linked together, it seems to be useful to give an overall presentation of the simulation strategy that has been adopted.
Figure 3.6 is a top-level flow chart of what the typical simulation process would look

like.
WEST requires a number of design and air/ambient data, on top of that, the particles and some thermodynamic parameters are needed as inputs by the ice ingestion code.
These data are then initialised to form the nondimensional parameters required in WEST Euler equations.
After this phase, the proper calculation begins, with the aforementioned Euler equations and turbine matching on one side, and the particles and ice calculation on the other. These two calculations proceed in parallel and are mutually influenced by each other, as it was already discussed in previous sections.
Finally, the output of the code are the performance of the engine and the history of the particles evolution through the compression system at the various time steps.

# Chapter 4

# Modelling

Figure 3.1 showed how various phenomena and engine subsystems could influence each other during ice ingestion. All these components are also the building blocks of the numerical model. Hence, updating Figure 3.1 by highlighting which phenomena are modelled by WEST and which are included in the newly developed ice ingestion code, it is possible to obtain a picture that shows the basic architecture of the present model. This picture is Figure 4.1.

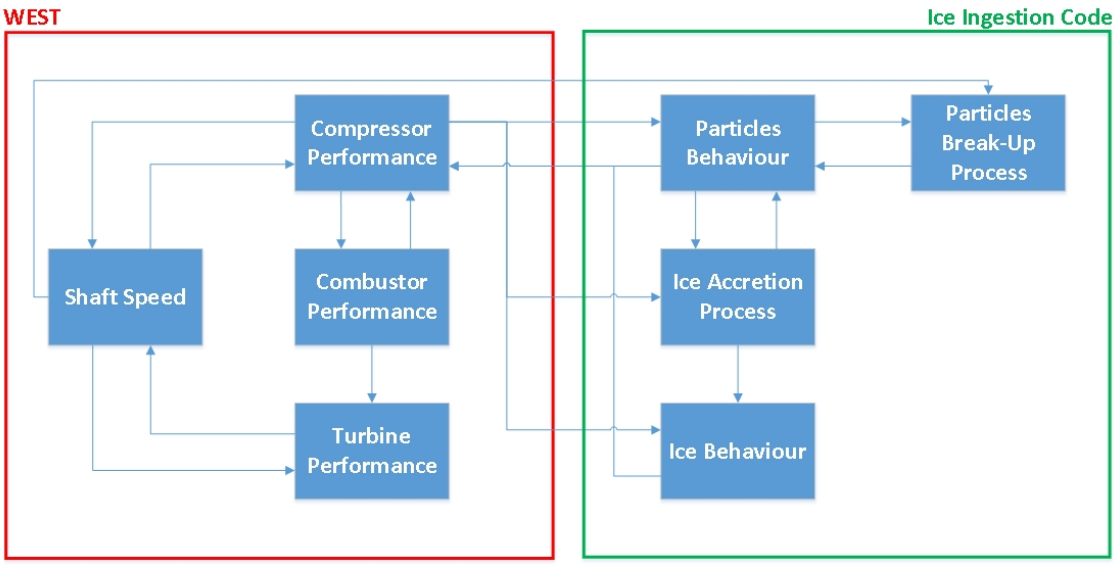


Figure 4.1: Model building blocks and connections between them

The numerical model here presented is divided in three main components, which will also be the three sections of this chapter: WEST, the ice particles code, and the links between them.

WEST will be briefly discussed in the first section, and in particular how it models the behaviour of the main components of the engine: compressors, combustion chamber and turbines, and how it calculates the shaft or shafts rotational speed.
The second section of this chapter deals with the modelling of ice particles and the eventual ice accretion. As Figure 4.1 shows, the main components of the ice ingestion code are:

- **Ice Particles** : the ice particles are modelled using a Lagrangian approach, with the evolution of various groups of particles being modelled independently, and using basic mechanical and thermodynamic principles and equations
- **Particles Break-Up Process** : when ice particles or water droplets pass across a rotor leading edge, they are broken up or splashed. The models used are taken from the literature and take into consideration both particles parameters and shaft rotational speed
- **Ice Accretion Process and Ice Behaviour** : the method also accounts for ice accretion and the behaviour of the accreted ice. The accretion model is based on NASA experimental and computational findings, while the behaviour of the accreted ice follows the same principles and equations as the ice particles.

The final section of this chapter is dedicated to all the measures that were necessary to adopt in order to assure that all the influences that the particles have on the main flow were taken into consideration. The biggest examples of these changes are the modification of WEST solving scheme to accomodate for the particles calculation and WEST solving equations to include the source terms necessary to account for the particles influence on the flow mass, momentum and energy. The model also takes into account the area reduction determined by the presence of the particles and accreted ice, and the modifications of flow thermodynamic parameters induced by the presence of water vapour.

## 4.1 WEST

As already mentioned, WEST is a Matlab code developed by Cranfield UTC to simulate the behaviour of the core engine during shaft failure overspeed events and all the phenomena related to them (compressor surge, shaft overspeed, turbine friction,...).
Figure 4.2 shows how WEST divides the core engine in different domains[66]:

- **Blue** the compression side, that goes from the engine inlet to the first nozzle guided vane's (NGV) throat, including so the combustion chamber
- **Red** the expansion side, from the first NGVs throat to the end of the exit nozzle
- **Green** the secondary air system (SAS)
- **Purple** friction, wear and tangling calculations.

It is worth noticing that, while the first three are actual computational domains, the friction, wear and tangling calculation is more of a function triggered by the shaft failure, and the purple area is where the phenomenon should take place.

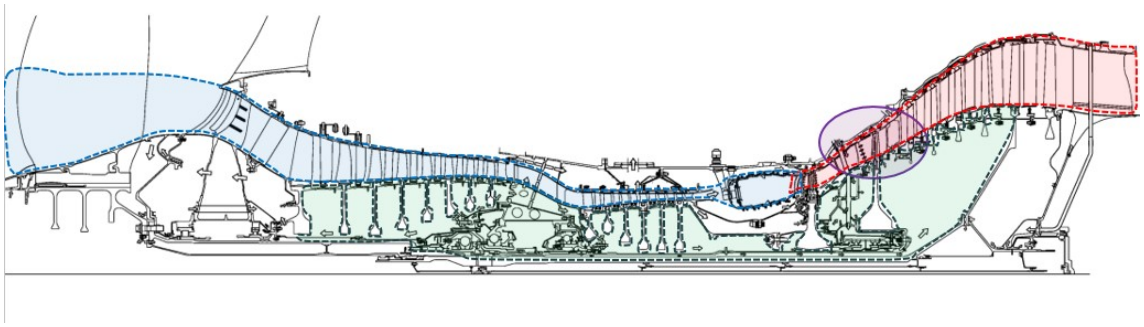

Figure 4.2: Turbofan core engine cross-section with the four main "computational domains" highlighted in different colours[66]

An important feature of WEST is its modularity. It is in fact possible to build a simulation that uses only one or more of the computational domains. For the present work, in particular, only the compression and expansion side domains will be used. The computational approach for both these domains, as well as the shaft management part of the code needed to couple the two together, will now be discussed.

### 4.1.1 Compression side

The computational domain defined as compression side includes the core engine compressors and combustion chamber until the throat section of the first row of NGVs. An important assumption that has to be made for this division to be valid is that the aforementioned throat area is choked, which is generally the case in normal operations, so that the information can not run upstream, going from the turbine to the combustion chamber.
The domain is defined as an annular duct with length and area equal to the length

and passage area of the actual engine. This duct is divided into a linear grid, and the number of its elements is defined by the user.

### Equations

The compression side is modelled using quasi 1-D Euler equations for mass, momentum and energy, plus two balancing equations for combustion results and uncombusted fuel:

$$\frac{\partial}{\partial t}\begin{bmatrix} \rho A \\ \rho u A \\ \rho A E \\ \rho A Y_{SP} \\ \rho A Y_{FNB} \end{bmatrix} + \frac{\partial}{\partial x}\begin{bmatrix} \rho u A \\ \rho u^2 A + p_s A \\ \rho u A H \\ \rho u A Y_{SP} \\ \rho u A Y_{FNB} \end{bmatrix} = \begin{bmatrix} -W_B + W_F \\ F_{comp} - F_{comb} + p_s \frac{\partial A}{\partial x} - F_B + F_F \\ Q + SW - H_B + H_F \\ \dot{\omega}_{SP} \\ \dot{\omega}_{FNB} \end{bmatrix} \tag{4.1}$$

Where $Y_{SP}$ and $Y_{FNB}$ are the mass fractions for combustion products and unburnt fuel. The operative fluid behaviour is supposed to follow the ideal gas law, Eq. 4.2, with its specific enthalpy, $h$, and internal energy, $e$, defined by Eq. 4.3 and Eq. 4.4.

$$p_s = \rho R T_s \tag{4.2}$$

$$h = h\left(T\right) \tag{4.3}$$

$$e = h - RT \tag{4.4}$$

From these formulations, the total internal energy, $E$, and enthalpy, $H$, are expressed as shown in Eq. 4.5 and Eq. 4.6:

$$E = \left(e + \frac{u^2}{2}\right) \tag{4.5}$$

$$H = h + \frac{u^2}{2} \tag{4.6}$$

As can be seen, Eq. 4.1 can be split into three different matrices, the first containing the conserved variables, $U$, the second consisting of the fluxes, $F$, and the last one including the source terms, $G$, and the pressure forces, $W = p_s \frac{\partial A}{\partial x}$.
The meaning of the different source terms are:

- $W_B$ represents the mass flow removed by the bleed valves
- $W_F$ is the amount of fuel introduced into the flow in the combustion chamber
- $F_{comp}$ represents the momentum increase induced by the compressor blades
- $F_{comb}$ takes into account the momentum losses that take place in the combustor
- $F_B$ accounts for the momentum lost due to the flow extraction at the bleeds
- $F_F$ represents the momentum gained from the fuel injection
- $Q$ is the energy introduced by the heat released from the burnt fuel
- $SW$ takes into account the work input necessary for the compressor to pressurise the flow
- $H_B$ accounts for the energy removed by removing the bled flow
- $H_F$ represents the energy added by the fuel before combustion
- $\dot{\omega}_{SP}$ is the source term for the production of combustion results
- $\dot{\omega}_{FNB}$ accounts for the presence of unburnt fuel

### Compressors, Combustor and Bleeds Modelling

The compressor source terms are derived from its design characteristics. So that at a given rotational speed, mass flow, inlet temperature and inlet pressure the values of corrected mass flow $WRTP$ and rotational speed $NRT$, defined by Eq. 4.7 and Eq. 4.8, can be calculated, and from there the values of pressure and temperature ratio are univocally defined by the compressor map.

$$WRTP = \frac{W\sqrt{T}}{P} \tag{4.7}$$

$$NRT = \frac{N}{\sqrt{T}} \tag{4.8}$$

An important assumption that is worth mentioning has to do with the fan flow splitting into core and bypass. While core fan maps do exist for this purpose, in order for this division to be possible it is necessary to assume that eventual compressor instabilites occurring in the core engine do not develop radially in the fan. Moreover, the outer part of the fan has still to be considered when it comes to engine matching. This can be performed, since the fan torque maps show that non-dimensional rotational speed is the primary factor in defining outer fan power absorption [66], which means that outer fan torque is defined solely by non-dimensional rotational speed, which is known, without considering the unknown bypass flow.
On the other side, WEST combustor model is based on the work done by Portincasa[68]. The publicly available NASA CEA software[69] was used to create a generic combustor map, and using this map, given the combustor inlet conditions, the enthalpy change and the combustor source terms are calculated.
Finally, the bled mass flow is either linearly distributed accross a component's length, or extracted at a defined point, and spread throughout a defined number of elements, so that:

$$W_B = \frac{\dot{m}_B}{\Delta x} \tag{4.9}$$

Moreover, the value of $\dot{m}_B$ can assume the form of a fixed mass flow, a percentage of the main gas path flow, or the bleed can be coupled with a boundary node of the secondary air system.
In this study, only the first two options have been used.

### Boundary Conditions

In any numerical scheme it is necessary to set appropriate conditions at the buondaries of the computational domain, called buondary conditions, and WEST is no

different.
There are two different types of boundary conditions available in WEST, and the user can choose which is better suited for the simulation at hand.
The first kind is the physical boundary conditions, where a value is set for certain physical values at the inlet and, if necessary, at the outlet of the compression domain. The second set of boundary conditions are the non-reflective ones, where the physical value can deviate to prevent wave reflections at that boundary. The latter is generally used in cases of transient simulations. However, given the fact that ice ingestion is a relatively slow phenomenon, it has been decided to adopt the physical boundary conditions.
It is then necessary to specify which physical variables have to be set for different inlet and outlet conditions.
Given the fact that WEST has been developed for performance simulations of high bypass turbofan engines, the only option available for the inlet is for it to be subsonic. In this case the total pressure $p_t$ and temperature $T_t$ have to be specified. The velocity is extrapolated from the first two grid nodes as $V_1 = 2V_2 - V_3$, $\gamma$ and the static temperature $T_s$ are iterated to match $T_t$. Finally, the static pressure is calculated as $p_s = p_t / \left[\frac{T_t}{T_s}\right]^{\frac{\gamma}{\gamma-1}}$ and density as $\rho = p_s / RT_s$.
On the other side, for the outlet, there is both the possibility of a subsonic and supersonic outlet.
In the case of a subsonic outlet, which is generally used only when it is necessary to simulate an isolated compressor followed by a plenum, it is necessary to specify a value for outlet static pressure. Then, velocity and density are linearly extrapolated for the domain as $V_N = 2V_{N-1} - V_{N-2}$ and $\rho_N = 2\rho_{N-1} - \rho_{N-2}$, where $N$ is the total number of grid nodes, and the temperature is calculated using the ideal gas law: $T_s = p_s / (\rho R)$.
In the case of a supersonic outlet, on the other side, no physical value needs to be set. Velocity, density and pressure are all extrapolated as $V_N = 2V_{N-1} - V_{N-2}$, $\rho_N = 2\rho_{N-1} - \rho_{N-2}$ and $p_{s,N} = 2p_{s,N-1} - p_{s,N-2}$, while temperature is obtained by the ideal gas law: $T_s = p_s / (\rho R)$.

### Solution Scheme

In WEST, two alternative solution strategies are available to solve the compression side governing equations: the MacCormack scheme and the Transient Roe Source Solver. In this study, only the first solution scheme is used, hence it will be the only one to be described.

Eq. 4.1 is a system of non-linear, hyperbolic equations with respect to time. In order to have a stable explicit solution in a set of non-linear hyperbolic equations, a limit has to be set on the time steps[70]. This limit is determined by the Courant number, $C$, which has to be $\leq 1$. The relation between $C$ and the local time step is given by:

$$\Delta t_i = C\frac{\Delta x_i}{a_i + |V_i|} \tag{4.10}$$

Where $a_i$ is the local speed of sound, defined as $a_i = \sqrt{\gamma R T_i}$, an $V_i$ is the local velocity.
Eq. 4.10 is known as the Courant-Friedrichs-Lewy condition for one-dimensional flow, and it has been shown to work well throughout the literature.
In order to select one single time step for the entire compression domain, Eq. 4.10 is applied to each grid node at the start of every iteration, with the smallest of the local time steps being selected to advance the solution.
This process is carried out independently from the solution method employed.
The MacCormack scheme, first applied by MacCormack for impact velocity cratering in 1969[71], is an explicit finite-difference technique. It is a predictor-corrector scheme, resulting in a second-order central difference. A more in-depth analysis of the method is given by Anderson[70], while the details of its application to WEST can be found in the work of Lucas Pawsey[66].
What is important to highlight in the context of this study is the general set-up and the two-steps nature of the MacCormack scheme.
After the time step has been selected, and the compressor and combustor performance are obtained from their respective maps, the source terms and the $F$ matrix are evaluated. At this point, the first step of the calculation, named predictor step, is performed. This takes the form of either a forward difference scheme or a backward difference scheme, alternating at every time step. In the case of a forward difference scheme the predictor step calculation will look like Eq. 4.11.

$$\bar{U}_i = U_i^n + \Delta t\left[G_i^n - \frac{F_{i+1}^n - F_i^n}{\Delta x_i}\right] + S_i^n + \Delta t W \tag{4.11}$$

Where the $S$ term represents the artificial viscosity. The introduction of this new

parameter is necessary to stabilise the solution, as the MacCormak scheme does not have per se enough numerical dispersion to sufficiently dampen oscillations due to gradients. The artificial viscosity formulation in WEST is:

$$S_i^n = C_x \frac{\left|p_{s,i+1}^n - 2p_{s,i}^n + p_{s,i-1}^n\right|}{p_{s,i+1}^n + 2p_i^{s,n} + p_{i-1}^{s,n}} \left[U_{i+1}^n - 2U_i^n + U_{i-1}^n\right] \tag{4.12}$$

Where $C_x$ defines the magnitude of the artificial viscosity, and it generally is set at 0.03 for steady state simulations and 0.3 for transient simulations.
After the predictor step, the boundary conditions are updated and flow properties are recalculated. With the new set-up of flow properties the source terms, artificial viscosity and the fluxes matrix are re-evaluated in order to perform the second step, or corrector step, of the calculation. If the predictor step has been carried out using a forward difference scheme, the corrector step will adopt a backward difference scheme, and the reverse applies if the predictor step used backward differences. So in the considered case, the corrector step will be:

$$\bar{\bar{U}}_i = U_i^n + \Delta t \left[\bar{G}_{i-1}^n - \frac{\bar{F}_i^n - \bar{F}_{i-1}^n}{\Delta x_{i-1}}\right] + \bar{S}_i^n + \Delta t \bar{W} \tag{4.13}$$

Finally, the flow set-up for the next time step is given by the average between the predictor and corrector step results:

$$U_i^{n+1} = \frac{\bar{U}_i + \bar{\bar{U}}_i}{2} \tag{4.14}$$

And the boundary conditions and flow properties are then updated for the next time step.
The overall process is schematically shown in Figure 4.3, highlighting the two-step nature of the MacCormack method.
One last feature that is important to highlight before moving on is that the force wall term included in $W$ changes its formulation depending if the forward or backward differences scheme is adopted. Eq. 4.15 shows the formulation for forward differences, and Eq. 4.16 for backward.

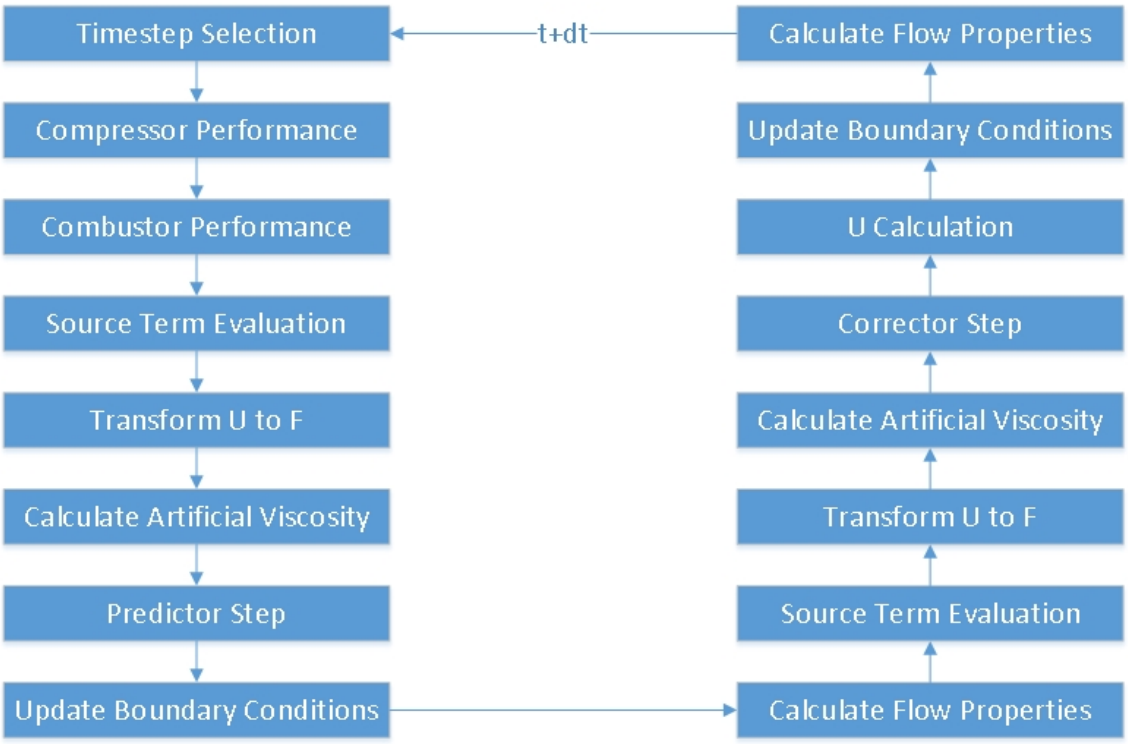


Figure 4.3: Computational routine for MacCormack scheme

$$p_s \frac{\partial A_i}{\partial x} = \left( \frac{p_{s(i+1)} + p_{s(i)}}{2} \right) \left[ \frac{A_{i+1} - A_i}{x_{i+1} - x_i} \right] \tag{4.15}$$

$$p_s \frac{\partial A_i}{\partial x} = \left( \frac{p_{s(i)} + p_{s(i-1)}}{2} \right) \left[ \frac{A_i - A_{i-1}}{x_i - x_{i-1}} \right] \tag{4.16}$$

### 4.1.2 Expansion side

The expansion side solver is a stand alone tool that calculates the performance of a system of turbines with a quasi-steady matching method.
The boundary conditions for the expansion solver at the inlet are the inlet mass flow, total pressure and total temperature, and the mass fractions of both combustion products and unburnt fuel. Additional boundary conditions are the shafts rotational speeds, the nozzle outlet static pressure, and the mass flow and temperature of all the secondary flows injected into the main gas path, together with the position of the injection ports.

Considering the boundary conditions supplied at the inlet, outlet and the secondary

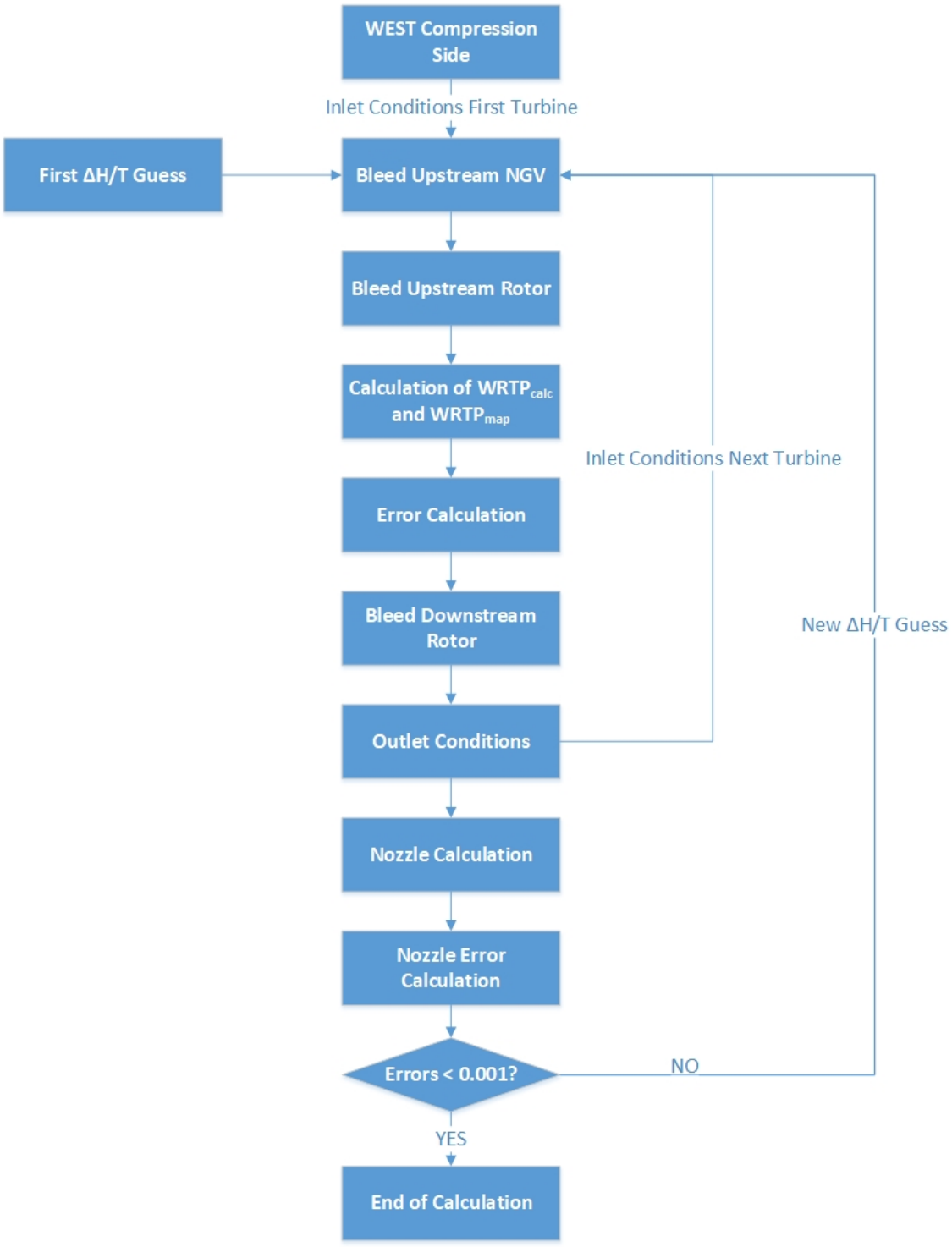


Figure 4.4: WEST expansion side computational process

flows, the tool finds a match on the turbine performance characteristics that satisfies various requirements.

The matching routine for the expansion side is shown in Figure 4.4 and can be summarized in nine steps:

1. If any injection port is present at the NGV inlet, the secondary flow is mixed to the main flow

2. If any injection port is present at the rotor inlet, the injected flow is mixed with the main flow

3. $WRTP$ is calculated to give $\frac{W\sqrt{T}}{p}|_{calc}$

4. $\frac{W\sqrt{T}}{p}|_{map}$ and $\eta_{map}$ are obtained from $NRT$ and $\Delta H/T$ at the rotor inlet, using the turbine characteristics

5. If this is not the first turbine, where the capacity is imposed by the compression domain, calculate the error value as:

$$errorValue = \left(1 - \frac{\frac{W\sqrt{T}}{p}|_{map}}{\frac{W\sqrt{T}}{p}|_{calc}}\right) \times 100 \tag{4.17}$$

6. Calculate the rotor outlet conditions using $\Delta H/T$ and $\eta_{map}$

7. If any injection port is present at the rotor outlet, the secondary flow is mixed to the main flow

8. In case this is the last turbine, the nozzle calculations are carried out as if it was an isoentropic nozzle, obtaining the last error value.

9. repeat the process for each turbine, with the outlet conditions of the previous one becoming the inlet conditions for the next. The number of error values is equal to the number of turbines. If any error value is greater than 0.001, the Broyden method, a generalisation of the secant method, is used to minimisefind a new guess for the values of $\Delta H/T$ for each turbine. Once the error values have become smaller than the target value, final $\Delta H/T$ for each turbine has been found.

A more in depth explanation of WEST expansion side solver can be found in the original study by Lucas Pawsey[66].

### 4.1.3 Shaft management

Once both the compression and expansion sides have been solved, WEST calculates the rotational speed of the shaft for the following time step.
The code does it by integrating the shaft speed, starting from an initial one for $t = 0$, based on the torque imbalance on the shaft. In WEST, there are various different torque sources that can be introduced, but for simplicity reasons, in this work only the turbine, $\tau_t$, and compressor, $\tau_c$, torques are considered, which are calculated in the expansion and compression solver respectively.
Thus, the net torque balance, $\tau$, results to be:

$$\tau = \tau_t - \tau_c \tag{4.18}$$

This net torque causes then the rotational speed, $\omega$, to change according to Eq. 4.19:

$$\frac{\partial \omega}{\partial t} = \frac{\tau}{I} \tag{4.19}$$

Where $I$ is the shaft inertia.
Equation 4.19 needs to be integrated to find the new shaft speed. WEST does it using a 2-step Adams-Bashford method, expressed in Eq. 4.20

$$\omega_{n+1} = \omega_n + \left( \left[ 1 + \frac{\Delta t_n}{\Delta t_{n-1}} \right] \frac{\tau_n}{I} - \left[ \frac{\Delta t_n}{2\Delta t_{n-1}} \right] \frac{\tau_{n-1}}{I} \right) \tag{4.20}$$

Where the subscripts $n-1$, $n$ and $n+1$ identify the previous, current and next time step respectively. The different values in $\Delta t$ reflect the variability of the time steps, so that $\Delta t_n = t_{n+1} - t_n$ and $\Delta t_{n-1} = t_n - t_{n-1}$. Finally, it is worth noticing that for the first time step, when $\Delta t_{n-1}$ and $\tau_{n-1}$ are not available, an Euler forward method is used, as expressed in Eq. 4.21:

$$\omega_n = \omega_n + \frac{\Delta t_n \tau_n}{I} \tag{4.21}$$

This process is carried out for each shaft if more than one is present, or it can be omitted for fixed rotational speed simulations, and is omitted when only the compression side is being simulated.
The overall computational sequence followed by WEST can be summarized as shown in Figure 4.5. The compression side is the first subroutine to be executed, followed by the expansion side. After these two, the subsequent rotational speed is quantified, and the calculation moves to the next time step.

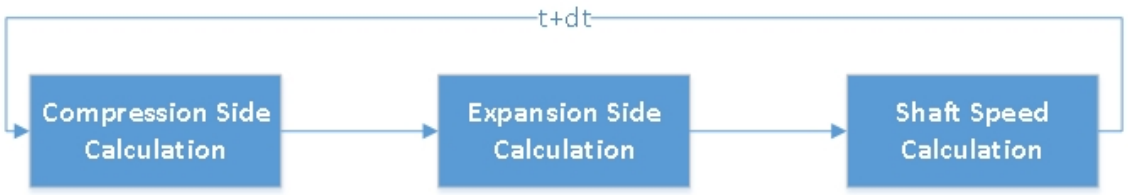


Figure 4.5: WEST Computational sequence

## 4.2 Ice ingestion code

This section describes the newly developed code for the simulation of the behaviour of ingested ice particles. As already mentioned, the modelling approach has been inspired by the publications of Kundu et al.[8].
In this method, the particles are treated as a separate entity compared to the air flow, and their development is followed with a Lagrangian approach while they travel in the compressor.
The following section will describe how the various phenomena that determine the particles evolution have been modelled and also some assumptions that it has been necessary to make for coding purposes.

### 4.2.1 Particles discretisation

The ingestion of ice particles in reality is a continuous phenomenon, which means that, in order to build a computer code able to model it, some sort of discretization is necessary. With the aim of this project being to develop a relatively simple

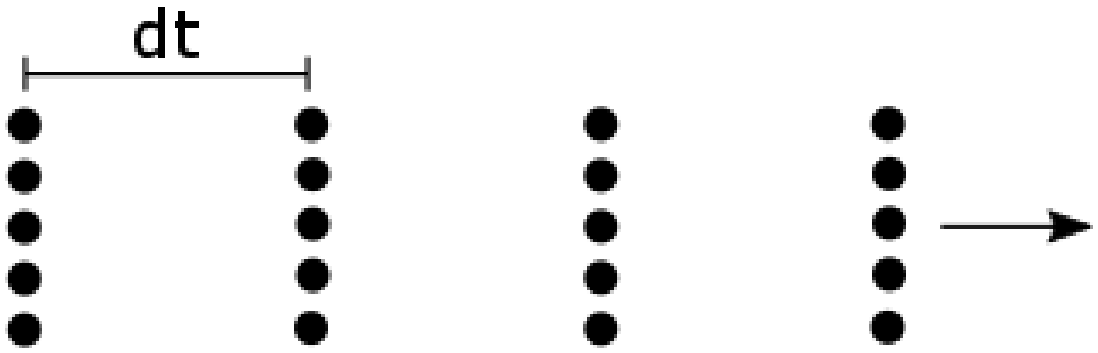


Figure 4.6: Particles discretization

simulation tool, that could represent the fundamental architecture for future development, a very simple discretization strategy has been chosen, which is depicted in Figure 4.6.

Every given time step, where this time step is independent from the Eulerian calculation one, and is imposed as an input by the user, a certain amount of particles is introduced in the engine. These particles are assumed to be spherical and to have all the same diameter, which is, as well as their temperature and velocity, an input also set by the user.

The number of particles introduced at every time step is determined by the combination between the time step itself, the mass of a single particle, which is uniquely defined by its diameter and temperature, and the total ice mass flow, which is again an input parameter, with this combination being:

$$N_p = \frac{w_p dt_p}{m_p} \tag{4.22}$$

Where $N_p$ is the number of particles introduced at that timpe step, $w_p$ is the total ingested ice mass flow, $dt_p$ is the particles ingestion time step and $m_p$ the mass of a single particle.

This discretization generates groups of homogeneous particles, where all the single particles within the group will evolve in the same way as the others in the same aforementioned group. From now on, every group of homogeneous particles $N_p$ will be called wall.

Another challenge in modelling the evolution of the ice particles is represented by the complex nature of the thermodynamic phenomena that determine this evolution (i.e. temperature change, evaporation, melting,...). Often more than one of these

phenomena acts at the same time, so it has been necessary to make some assumptions, and some of them are shown in Figure 4.7.

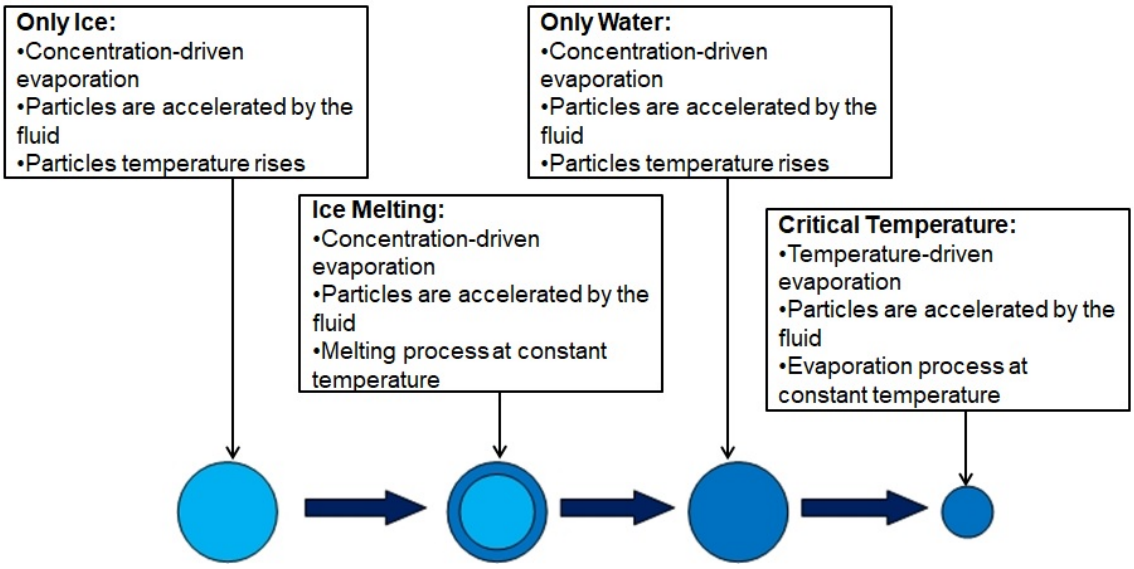


Figure 4.7: Particles evolution

It can be seen that the particles evolution is split in 4 main phases:

- **Only Ice:** when the particles are constituted only by ice, there are three main phenomena that take place. The particles lose mass due to the evaporation driven by the water concentration difference between the particles and the surrounding air, the particles are accelerated by the surrounding fluid, and their temperature rises.

- **Ice Melting:** once the ice reaches its melting temperature, it starts to become water. During this process, the evaporation and acceleration of the particles continue to take place, while the temperature is assumed to remain constant across the whole single particle, until all the ice has melt.

- **Only Water:** after the melting process, the particles temperature starts to rise again, until the critical vaporisation temperature is reached.

- **Critical Temperature:** once the critical temperature is reached, particles state change from liquid to vapour is driven by temperature instead of concentration. This process, named here as vaporisation, is essentially the same as water boiling, and it is assumed to take place at constant temperature.

As it can be noticed, more than one phenomenon take place at the same time during each phase. It is then necessary to decide how to simplify this problem. At each time step, the five main phenomena (acceleration, temperature rise, evaporation, melting and vaporisation) are taken into consideration one at a time, and for each phenomenon its governing equation is applied only to the walls that are in one of the phases that require its application. For example, acceleration applies to all the walls, ice melting only to the walls in the Ice Melting phase, while the concentration-driven evaporation influences the walls that are in the first three phases of their evolution. The order by which these phenomena are calculated is the following:

1. acceleration is calculated first. This is because it takes place throughout the whole particles evolution. Also, even though it is affected by the loss of particles mass, this change has been assumed to be negligible, given that the calculation time step ($dt$) is small enough

2. the next process whose effects are calculated is the evaporation. This is the second most common phenomenon during the four aforementioned phases, and it is unaffected by other processes, while the mass reduction that it involves affects them

3. the ice melting is then simulated

4. particles temperature rise is evaluated as fourth

5. the last calculated process is the particles vaporisation at critical temperature

The order of the last three phenomena is arbitrary, since they do not take place at the same time. However, it may happen that during one single time step one group of particles passes from the conditions that are fit for one of the three processes to those that characterize another of them (e.g. all the ice melts, requiring the temperature to start rising again). In this case, the heat absorbed by the first process is calculated, since all the three phenomena are heat driven, subtracted from the total heat that the particles can absorb from the contiuous phase during that time step, and the remaining is used for the second process.
In the next subsection the modelling of all these different processes will be explored in more detail.

### 4.2.2 Air-particles interaction phenomena

In this subsection the mathematical modelling of the various processes affecting the particles evolution will be analysed, following the computational order undergone during the simulations.
All the equations in this subsection, if not stated otherwise, are taken from "Multiphase Flows with Droplets and Particles" by Crowe et al.[67].

#### Acceleration

The first phenomenon analysed is the particles acceleration. Particles are being carried forward as a result of the drag they excert on the surrounding air, so, according to Crowe[67], the particles velocity change, $du_p$, in one time step $dt$ is equal to:

$$du_p = \frac{\rho C_D A_p \left|u - u_p\right| (u - u_p)}{2m_p} dt = \frac{F_D}{m_p} dt \tag{4.23}$$

Where $\rho$ is the air/vapour mixture density, $C_D$ the drag factor, $A_p$ the particles cross sectional area, $u$ the flow velocity, $u_p$ the particles velocity, $m_p$ the particles mass and $F_D$ the acting drag force.
With the particles being spherical, the drag coefficient has been considered to change with the Reynolds number, defined as:

$$Re = \frac{\rho \left|u - u_p\right| d_p}{\mu} \tag{4.24}$$

Where $\mu$ is the dynamic viscosity of the air/vapour mixture. Thus, there are three different expressions for $C_D$ for three different ranges of $Re$:

$$C_D = \frac{24}{Re} \quad for \quad Re < 1$$

$$C_D = \frac{24\left(1+0.15Re^{0.687}\right)}{Re} \quad for \quad 1 \leq Re \leq 1000 \tag{4.25}$$

$$C_D = 0.44 \quad for \quad Re > 1000$$

Finally, with the flow being one directional, the particles cross sectional area is:

$$A_p = \pi \frac{d_p^2}{4} \tag{4.26}$$

**Evaporation**

The amount of water evaporating or ice sublimating during every time step, $dmv_1$, is defined by the difference in vapour concentration between the area surrounding the particle, where the vapour is considered to be saturated, and the rest of the flow domain. So, according to Crowe et al.[67]:

$$dmv_1 = h_m \pi \left(\rho_{ps} - RH\rho_{vs}\right) d_p^2 dt \tag{4.27}$$

Where $h_m$ is the mass transfer coefficient, whose value will be explained in the next subsection, $\rho_{ps}$ is the saturated vapour density at the particles temperature, $RH$ is the relative humidity, $\rho_{vs}$ the saturated vapour density at the air temperature and $d_p$ the particles diameter.
The saturated vapour density is calculated as $\rho_s = \frac{p_s}{R_v T}$, following the ideal gas law, where $p_s$ is the vapour saturation pressure and $R_v$ the specific gas constant for water vapour ($R_v = 461.5 J/kgK$).
$p_s$ is calculated following the World Meteorological Organisation (WMO) formulation[72]. According to the WMO, at a given ambient pressure, a parameter $f(p)$ is defined as $f(p) = 1.0016 + 3.15 \cdot 10^{-6} p - 0.074 p^{-1}$, together with it, the saturated pressures of pure water/vapour and ice/vapour are defined with changing $t$ (temperature in °C):

$$\begin{aligned} p_{sw}^* &= 6.112 exp\left[17.62t/\left(243.12 + t\right)\right] \\ p_{si}^* &= 6.112 exp\left[22.46t/\left(272.62 + t\right)\right] \end{aligned}$$

For the saturated pressure of moist air at varying $p$ and $t$ we then have $p_s(p,t) = f(p)p_s^*(t)$, using the ice or water $p_s^*$, depending if it is required for the sublimation or evaporation calculation respectively.
Finally, as it will be shown later, the primary humidity parameter obtained from the Euler calculations is the mixing ration $q = \frac{\rho_v}{\rho_a}$, where $\rho_v$ is the vapour density, while $\rho_a$ the air density. It is also true, according to ASHRAE handbook[73], that $q = 0.622\frac{p_v}{p-p_v}$ where $p_v$ is the vapour partial pressure and $p$ the air/vapour mixture pressure, which means that $q = 0.622RH\frac{p_s}{p-RHp_s}$. So, in order to obtain the relative humidity $RH$, the following formula is applied:

$$RH = \frac{qp}{p_s(0.622+q)} \tag{4.28}$$

**Melting**

The third phenomenon taken into consideration is the particles ice melting into water at 273.15 $K$, which is calculated with the following equation:

$$dm_w = \frac{h\pi d_p^2 \left(T - T_p\right) dt - L_{vw} dmv_{1w} - L_{vi} dmv_{1i}}{L_m} \tag{4.29}$$

Where $dm_w$ is the amount of ice melted in a time step $dt$, $h$ the heat transfer coefficient between the air and the particles, $L_{vw}$ and $L_{vi}$ the latent heats respectively for water evaporation and ice sublimation, $dmv_{1w}$ and $dmv_{1i}$ the amount of water evaporated and ice sublimated, and $L_m$ the latent heat of fusion for ice. The calculation and values of all these themodynamic parameters, except the latent heat of fusion that, like the melting temperature, is considered constant at $333506.525 J/kg$, will be explained in the next subsection.
The evaporation terms have to be taken into consideration because, even though that process is driven by concentration, the energy required for the state change still is part of the total heat that the particles can extract from the main flow during one time step.
As already mentioned, in case all the ice melts within one time step, the remaining heat absorbed by the particles will result in the rising of the particles temperature, as it will be evident later.

**Temperature rise**

When the particles are not at a critical temperature, they are heated up by the surrounding air. The formula that regulates this process is:

$$dT_p = \frac{h\pi d_p^2 \left(T - T_p\right) dt - L_{vw} dmv_{1w} - L_{vi} dmv_{1i} - L_m dm_w}{C_{pp}} \tag{4.30}$$

Where $dT_p$ is the temperature rise occurred in the time step $dt$ and $C_{pp}$ the particles heat capacity.
While the evaporation terms take into account the heat absorbed by the evaporation and sublimation processes that always take place, the melting term takes into account the possibility that, within one time step, all the ice melts and the particles temperature starts to increase again.
On the other side, it might be possible that a critical temperature is reached before the end of a time step. In this case, the temperature rise is determined by the difference between the critical temperature and the particles temperature $dT_p = T_{crit} - T_p$. $T_{crit}$ will be $273.15K$ in case of melting, while for the vaporisation process it has a value $T_{vap}$ that changes with pressure, and its calculation will be shown in the next subsection. Also, in these cases the next phase will begin within the same time step, subtracting the heat quantity necessary for the temperature increase, so for the case of ice melting the result will be:

$$dm_w = \frac{h\pi d_p^2 \left(T - T_p\right) dt - L_{vw} dmv_{1w} - L_{vi} dmv_{1i} - C_{pp} \left(273.15 - T_p\right)}{L_m} \tag{4.31}$$

**Vaporisation**

Finally, the last phenomenon to be considered is the vaporisation. As already mentioned, this is the water state change from liquid to vapour when the particles reach the critical vaporisation temperature. In this case, instead of being driven by the different water concentration between saturated vapour surrounding the particles and the remaining flow, the process uses all the heat that the particles can absorb from the flow to enact the state change. The equation that models this process is:

$$dmv_2 = \frac{h\pi d_p^2 \left(T - T_p\right) dt - C_{pp} \left(T_{vap} - T_p\right)}{L_{vw}} \tag{4.32}$$

Where $dmv_2$ is the amount of water that passes from liquid to vapour in one time step $dt$ while the $C_p(T_{vap} - T_p)$ term takes into consideration the aforementioned possibility that the vaporisation begins at a time step where some absorbed heat had aready been used to increase the particles temperature.

These were the thermodynamic processes that determine the particles evolution along the compressor. In the next subsection the focus will be on the thermodynamic parameters that influence these phenomena and on how they are determined.

### 4.2.3 Particles thermodynamic parameters

The topic of this subsection is the explanation of how the different water thermodynamic parameters mentioned earlier were calculated in the ice particles ingestion code. They will be analysed in the order they have appeared in this section.
The first parameter to be considered is the mass transfer coefficient between air and ice/water, $h_m$. According to Kundu[8] the mass tranfer coefficient can be expressed as:

$$h_m = \frac{\left[2 + \left(0.4\sqrt{Re} + 0.06Re^{2/3}\right) Sc^{0.4}\right] D_\nu}{d_p} \tag{4.33}$$

Where $S_c$ is the Schmidt number, defined as $S_c = \frac{\mu}{\rho D_\nu}$, and $D_\nu$ is the diffusivity between air and ice/water. This last property is obtained following the methodology suggested by Welty [74]. Starting from the air and water collision diameters (respectively $\sigma_a = 3.617$Å and $\sigma_w = 4.055$Å), the air and water energy of molecular interactions divided by the Boltzmann constant ($\frac{\varepsilon_a}{k} = 97K$ and $\frac{\varepsilon_w}{k} = 356K$) and their respective molecular masses ($M_a = 29$ and $M_w = 18$), two parameters are defined as:

$$\begin{aligned} \sigma_{aw} &= \frac{\sigma_a + \sigma_w}{2} \\ \frac{T\varepsilon_{aw}}{k} &= T\sqrt{\frac{\varepsilon_a \varepsilon_w}{k^2}} \end{aligned}$$

A third coefficient, $\Omega$, comes from the interpolation of $\frac{T\varepsilon_{aw}}{k}$ with data taken from Welty[74] that can be found in Appendix A.
The diffusivity between water and air is then obtained by:

$$D_\nu = 0.001858 \frac{\sqrt{T^3 \left(\frac{1}{M_a} + \frac{1}{M_w}\right)}}{\frac{p}{101325}\sigma_{aw}^2 \Omega} \frac{1}{10000} \tag{4.34}$$

Where the pressure is divided by 101325 because it is required to be in $atm$, while WEST works in $Pa$, and the overall result is divided by 10000 to pass from $cm^2/s$ to $m^2/s$.
For the other transfer factor that has been mentioned, the heat transfer coefficent $h$, according to Das[75], a correlation similar to Eq. 4.33 can be applied:

$$h = \frac{\left[2 + \left(0.4\sqrt{Re} + 0.06Re^{2/3}\right) Pr^{0.4}\right] k}{d_p} \tag{4.35}$$

Where $Pr$ is the Prandtl number, defined as $Pr = \frac{C_p \mu}{k}$, and $k$ is the air/vapour mixture coefficient of thermal conduction, while $C_p$ its specific heat at constant pressure.
After the transfer coefficients, the proper thermodynamic parameters are now considered, which are the latent heats of sublimation for ice, $L_{vi}$, and vaporisation for water, $L_{vw}$, and the particles heat capacity, $C_{pp}$.
According to Murphy and Koop[76] the latent heat of sublimation for ice is:

$$L_{vi} = \left[46782.5 + 35.8925T - 0.07414T^2 + 541.5\exp\{-(T/123.75)^2\}\right] \frac{1000}{18.01528}$$

for temperatures over $30K$, the final multiplication is made to pass from $J/mol$ to

$J/kg$.
On the other side, the latent heat of evaporation for water has been calculated using XSteam, an open source MATLAB code that adopts correlations taken from IAPWS IF-97[77].
For what concerns the particles heat capacity, it has to be taken into consideration three cases: the case in which the particles are fully composed of ice, the case when they are made of just water, and the case when the two phases coexist together.
In the case of only ice, it has been adopted again a formulation taken from Murphy and Koop[76]:

$$C_{pi} = \left[-2.0572 + 0.14644T + 0.06163T \exp\{-(T/125.1)^2\}\right] \frac{1000}{18.01528}$$

for temperatures over $20K$, with the final factor introduced again to pass from $J/molK$ to $J/kgK$.
Similarly to what has been done for the latent heat of evaporation, also the water heat capacity $C_{pw}$ is calculated using XSteam.
Finally, for the case in which the particles are composed both by ice and water, the overall heat capacity is considered to be the average of $C_{pi}$ and $C_{pw}$, weighted with the mass of the respective phases:

$$C_{pp} = \frac{m_{pi}C_{pi} + m_{pw}C_{pw}}{m_p}$$

Where $m_{pi}$ and $m_{pw}$ are the masses of the particles ice and water portions respectively, and $m_p$ is the total particle mass.

### 4.2.4 Break-up models

The particles modelling code takes into consideration also the break-up process of both ice particles and water droplets.
Since the aim of this project was to develop the main architecture for ice ingestion modelling, the decision has been made to keep the break-up models as simple as possible. In order to do this, it is assumed that the break-up process takes place only at the inlet section of the compressor rotors.

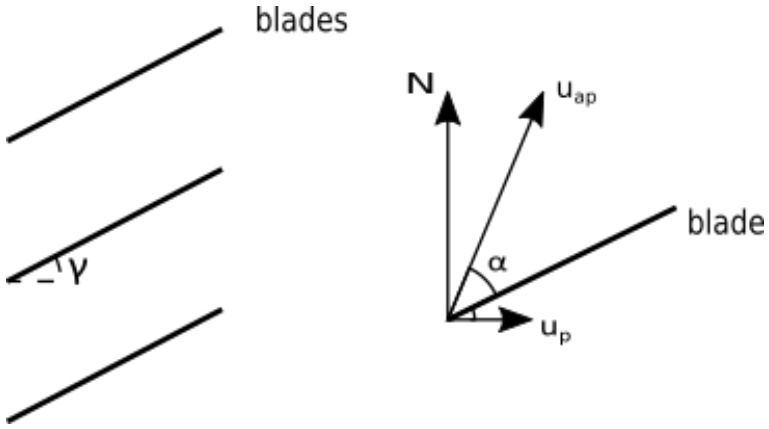


Figure 4.8: Particles impact geometry

Before analysing the different models for ice particles and water droplets, it appears to be useful to clarify the main geometric assumptions made in both these cases. These assumptions are shown in Figure 4.8.
The particles are assumed to travel in a straight line along the compressor, parallel to its axis, and the rotor blades are considered to be flat plates oriented in line with their own chord. Moreover, the particles are assumed to be all at the compressor mean radius. This assumption greatly simplifies the calculations, even though it is not perfect, as in reality more particles will be concentrated toward the case due to the centrifugal forces at play. This means that the particles apparent velocity $u_{ap}$ is $u_{ap} = \sqrt{u_p^2 + (r_m N\pi/30)^2}$, where $N$ is the rotor rotational speed expressed in $rpm$ and $r_m$ the compressor mean radius. Thus, the particles impact velocity on the blades, $u_i$, is:

$$u_i = u_{ap} \sin(\alpha) \tag{4.36}$$

With $\alpha$ being:

$$\alpha = \arctan\left(\frac{r_m N\pi/30}{u_p}\right) - \gamma$$

Where $\gamma$ is the blades stagger angle.

**Ice particles break-up model**

For simplicity purposes again, the mixed ice-water particles are assimilated to the ice particles, so they break-up as if they were fully solid.
According to Hauk et al.[52] two critical impact velocities for ice can be defined: the maximum velocity at which no particle break-up is possible, $U_{crack} = 0.046\frac{1}{\sqrt[3]{d_p^2}}$, and the maximum velocity at which only minor break-up is observed, $U_{attr} = 0.45\frac{1}{\sqrt{d_p}}$. Considering that the aim of the present model is to take into account only major particle break-ups, it has been decided to consider $U_{attr}$ as the critical impact velocity that would trigger a break-up event.
The model for the actual ice break-up has been taken from the 1995 report of the Advisory Group for Aerospace Research & Development (AGARD) titled "Recommended Practices for the Assessment of the Effects of Atmospheric Water Ingestion on the Performance and Operablity of Gas Turbine Engines"[78]. In the AGARD report, statistical correlations are used to take into consideration the fact that, in reality, not all particles have the same size and that the break-up process is not a deterministic phenomenon. So they define the maximum particles diameter after the impact as:

$$d_{max} = \left[1.2647 + 0.16001 \ln\left(\frac{1}{u_i}\right) - 0.0796\,(d_p - 1)\right] d_p \tag{4.37}$$

And after that, the average particles diameter after the impact:

$$\bar{d'_p} = \left[-0.19422 + 1.05\left(\frac{d_{max}}{d_p}\right)\right] d_p \tag{4.38}$$

Considering the simplicity requirements already mentioned, and the fact that, in the present model, all the particles impacting a defined blade have the same starting diameter, and they all impact the blade at the same radius and with the same velocity, it has been decided to consider the diameter of the new particles equal to the mean diameter in the AGARD method: $d'_p = \bar{d'_p}$.

**Water droplets break-up model**

For what concerns the break-up mechanism of the water droplets, Saxena et al.[13] carried out a sudy comparing three different droplet/blade interaction models using a computational tool similar to the one described in this thesis.
The three methods were the Mundo model[79], one where the number of child droplets after the break-up event is equal to the number of original particles multiplied by a constant factor, and a third one where there was a linear correlation between the number of child and parent particles. They also changed the frequency of the events, by allowing the break-up process to take place either only at the rotors leading edge, or both at the rotor and stator leading edges.
The Mundo model resulted to be the most aggressive of the three, however, it was also the most consistent, with similar results for the cases with break-up allowed only at the rotors, or both at the rotors and stators. Considering the fact that it was decided for this simulation set-up to limit the break-up events to the compressor rotors, the Mundo model as applied by Saxena et al. has been adopted as the water droplets break-up model.
According to Mundo et al.[79] a parameter $K$ is defined as:

$$K = \left(\frac{\rho_p^3 d_p^3 u_i^5}{\gamma^2 \mu_p}\right)^{1/4} \tag{4.39}$$

Where $\gamma$ is the particles surface tension and $\mu_p$ their dynamic viscosity. $\gamma$ is obtained interpolating particles temperature with a table reporting data from Welty et al.[74], and this table can be found in Appendix A. On the other side, the dynamic viscosity is calculated by interpolation of particles temperature and flow pressure with values calculated using the IAPWS-IF97[77] formulations.
Once the $K$ parameter is defined, according to Mundo[79] only droplets with $K \geq 57.7$ break up, and the number of child droplets resulting from a given particles wall is:

$$N_p' = 1.676 \cdot 10^{-5} K^{2.539} N_p \tag{4.40}$$

Like in the work of Saxena[13], here also a limiting factor has been applied, so that

$N'_p/N_p$ can never be greater than 50.

The overall computational method for particles break-up and droplets splashing can be summarized as shown in Figure 4.9. It is worth noting that the two models apply opposite strategies to define the outcome of the disruptive process. While the AGARD model defines the average diameter of the particles after the impact, and from there it is possible to obtain their number, the Mundo model first calculates the number of child droplets, from which one can quantify their average diameter.

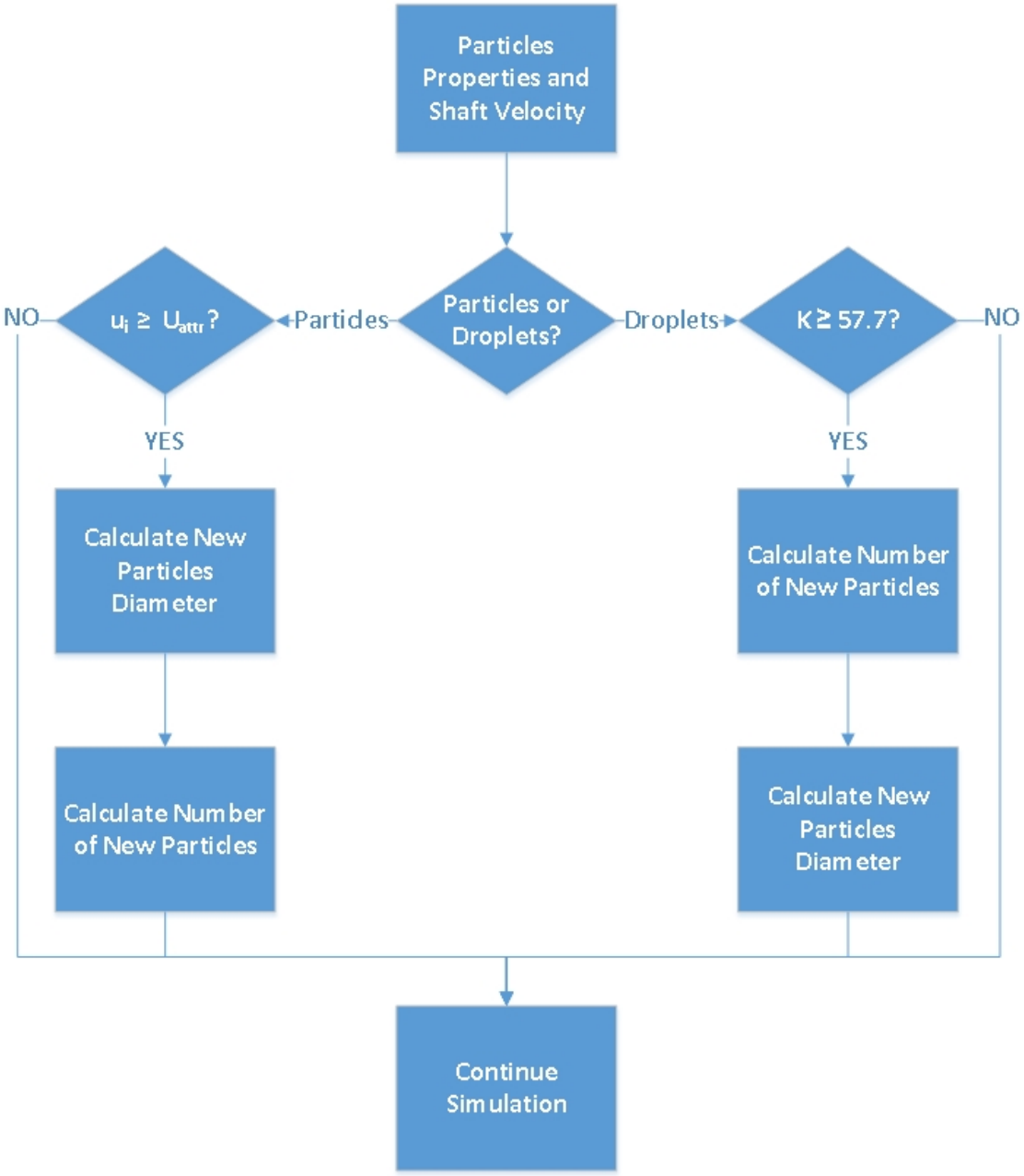


Figure 4.9: Break-up model computational process

### 4.2.5 Ice Accretion

Part of this project has been also to implement a simple way to identify the occurrence of ice accretion on compressor stator vanes, and model the accretion process and its effects. The process applied to identify and quantify the eventual ice accretion can be summarized as seen in Figure 4.10.

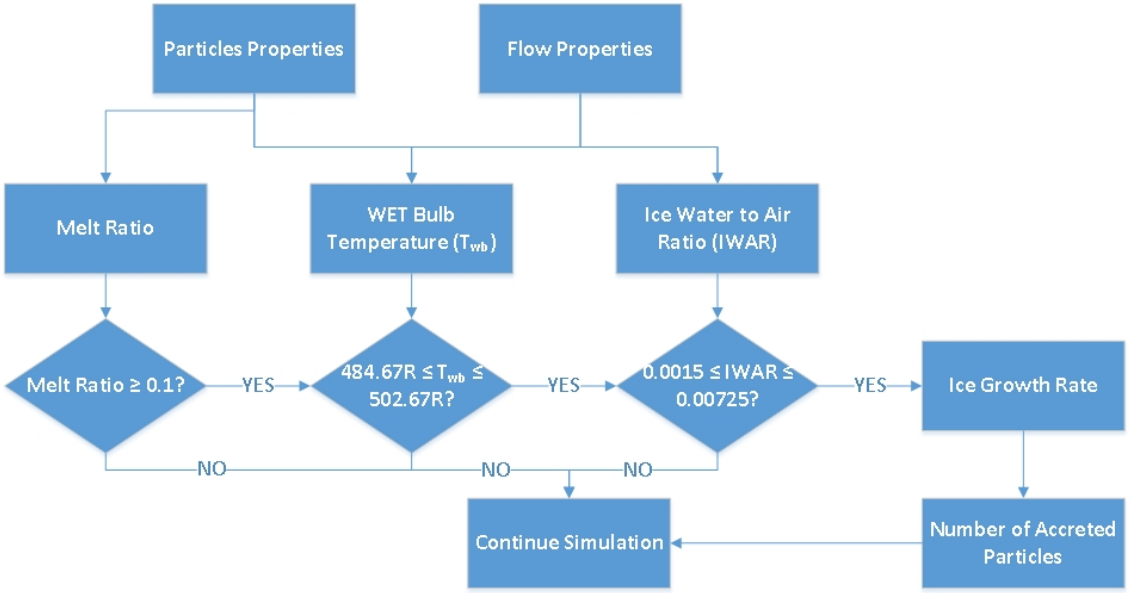


Figure 4.10: Ice accretion model computational process

Several studies from NASA showed that the two most critical factors for ice accretion are wet bulb temperature and particles melt ratio[49], which is the percentage of particles mass that has melt over the total mass. It was seen that generally, in cases where ice accretion had occurred, the average static wet bulb temperature was $2R$ above freezing, and within a range of $9R$ to $14R$, while the average melt ratio was always greater that 10%. For this reason, in the simulations the ice accretion conditions are identified if simultaneously the flow presents a static wet bulb temperature between $484.67R$ and $502.67R$, equal to $269.26K$ and $279.26K$ respectively, and the particles melt ratio is greater or equal than 10%.
NASA investigated also the growth rate[49], they found that, once the criteria for ice accretion are met, the two main parameters that define ice growth rate are $T_{wb}$ and ice-water flow to air ratio, $IWAR$, which is the ratio between the total mass of water, wether it is solid or liquid, entering the engine, and the mass flow rate of air. Figure 4.11 is an example of their findings[5]. It can be observed that the results take the shape of a wedge, named "Icing Wedge".
In the present code, these data have been used, by interpolation, to determine the

ice growth rate at varying wet bulb temperature and $IWAR$. Even though the results were obtained only for a small window of particle sizes, the lack of better data made it necessary to rely on them, and apply them to any particle size. The limitations of the experimental campaign, however, had to be considered for what concerns the range of IWAR that was tested. As it can be seen in Figure 4.10 a third requirement is present in this model for ice accretion which has not been mentioned yet: the limitations on IWAR, whose values have to be between 0.0015 and 0.00725. This was because of the lack of data for ice growth rate outside of this range, making the interpolation impossible. The aforementioned range, however, included all the simulations performed in this study.

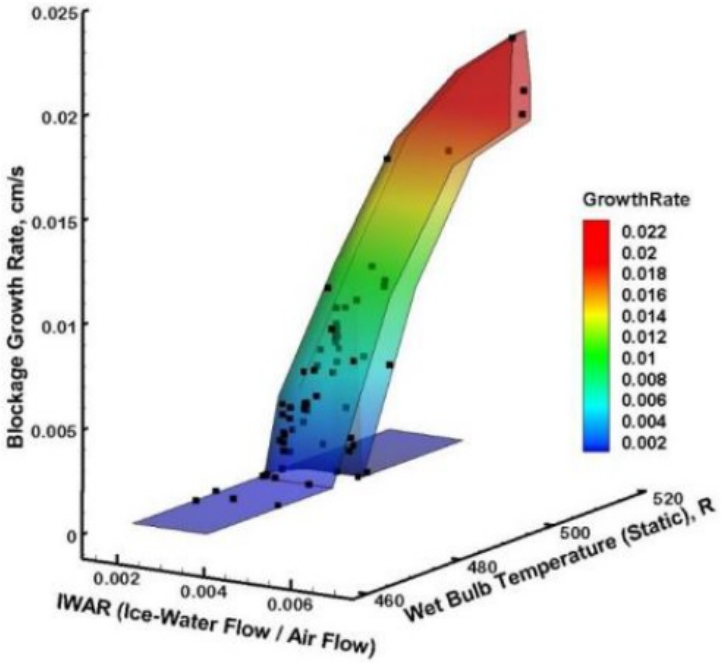


Figure 4.11: Refined "Icing Wedge" based on $1 - 9.5\mu m$ Particle size[5]

Once the stator stations with ice accretion are identified, and the growth rate is set, particles are taken from the flow to stick to the outer wall of the compressor annulus, in a number that matches the mass required by the determined growth, creating an iced outer ring, with length equal to the distance between the $x$ station with ice accretion and the successive station, outer radius equal to the compressor annulus outer radius, and thickness given by the ice accretion code.
The particles are pulled from the walls that are in the area where the ice is forming, which is between the $x$ point where the icing conditions where matched and the next one. If there is only one wall between these two poins, the number of particles after

a time step $dt$ will be:

$$N_p'' = \frac{N_p m_p - 2\pi d\delta \left(r_{ext} - \delta - \frac{d\delta}{2}\right) dx \rho_p}{m_p} \tag{4.41}$$

Where $N_p''$ is the number of particles after $dt$, $r_{ext}$ the compressor annulus external radius, $\delta$ is the ice thickness and $d\delta$ the ice growth in the time $dt$. On the other side, if there is more than one wall of particles in the area where the ice is forming, the number of particles taken from each wall will be inversely proportional to the distance between the wall and the mean point of the icing zone.
Moreover, the accreted ice behaviour is regulated by correlations that resemble exactly those used for the particles development, with the obvious exception of the momentum equation, which is not present, given the static nature of accreted ice. For brevity reasons, the aforementioned equations will not be repeated here, but the extensive explanation of their adaptation to the accreted ice can be found in Appendix B.
This is the end of this section, the next one will discuss the changes that was necessary to make on WEST to take into account the effects that ice particles and accreted ice have on the continuous phase of the flow.

## 4.3 WEST modifications

In order to make it possible for the particles and accreted ice to have an effect on the performance of the compressor, a series of changes had to be made to the core WEST code.
Both the solving scheme and the equations had to be modified. Moreover, to have a better understanding of the internal dynamics that take place within the compressor during an ice ingestion event, some simulations had to be performed splitting the compressor in single stages, which involved some changes in WEST input files, all these topics will be discussed in the present section.

### 4.3.1 Solving scheme

As it can be seen in Figure 4.12, the introduction of the ice simulating code has made it necessary to introduce some drastic changes in the WEST solution scheme. In the figure, both the expansion side and the shaft speed calculations are condensed in one single block because their solving process has not been changed by the introduction of the particles.
At the beginning of every time step, a subroutine is present to introduce a new group of particles if necessary. The calculations regarding the evolution of ice particles

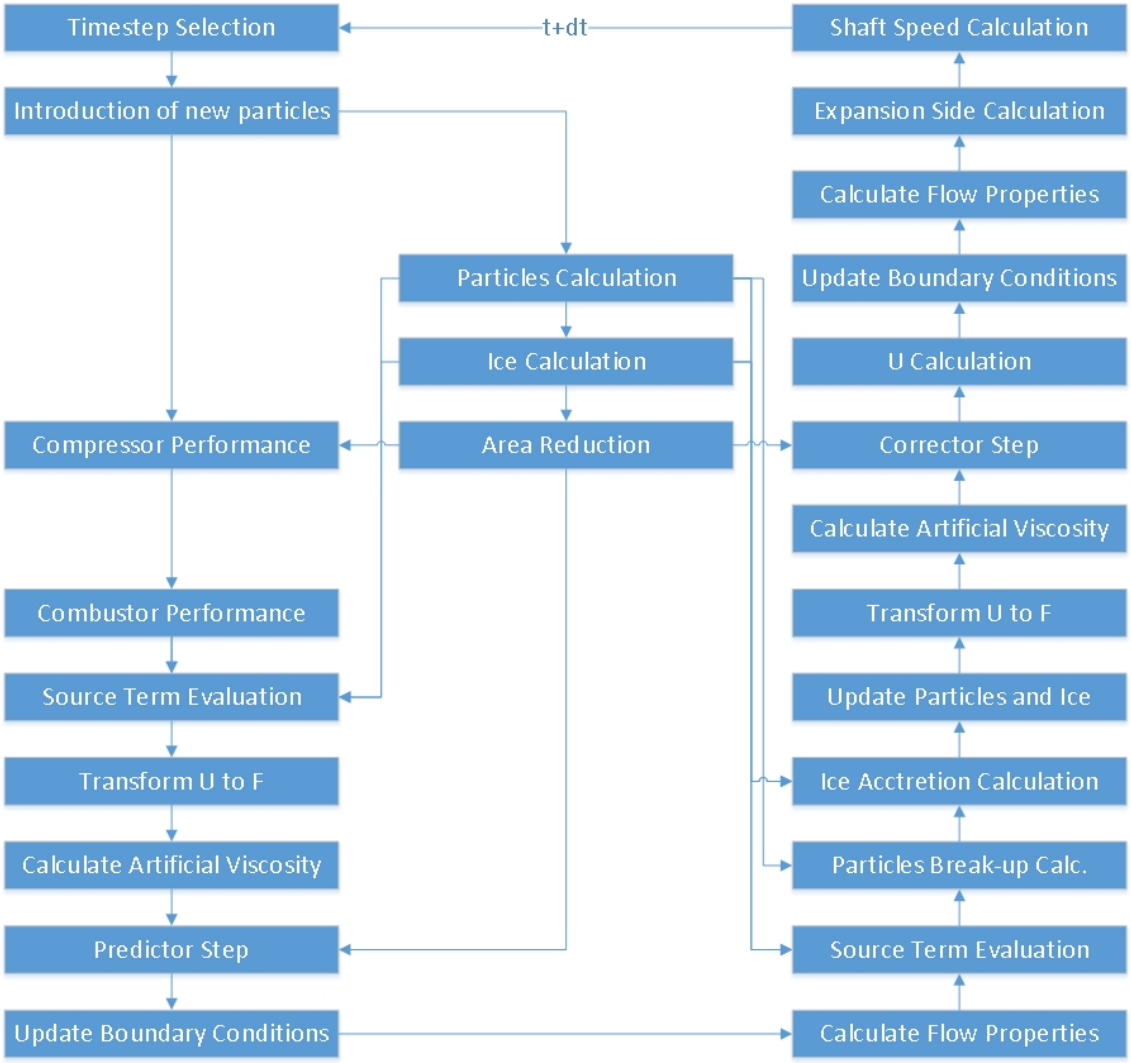


Figure 4.12: Computational routine modified for the inclusion of ice

and accreted ice had to be placed before the compressor performance evaluation, because the area blockage effect that they both generate influences the compressor behaviour, on top of the effect that it has on the solution of the Euler equations. The

particles break-up and the ice accretion calculations, as well as the update of both particles and ice properties for the following time step, are both performed after the calculation of the source terms for the corrector step, since neither the particles nor the ice will be involved in the solving process anymore at that point. It is also worth noting that the ice and particles calculation is performed only once, and does not follow the two-step rule of the MacCormack scheme. This is because the equations that regulate the behaviour of ice have, given a set of starting conditions, all very well defined solutions.
Moreover, the physical effects on the main flow caused by the phenomena described in the previous section are taken into account in additional source terms and changes to the solving equations, which will be described in the next subsection.

### 4.3.2 Equations

The inclusion of the particles and ice calculation required some major changes to be made to the core WEST equations. First of all, the evaporation of ice and water implies the inclusion in the system of water vapour. In order to accomodate for this, the mass equation has been split in two parts, like the bleeds mass source term, where the portion of air, $W_{Ba}$, and vapour, $W_{Bv}$, that they absorb is defined by the local humidity. On the other side, the momentum and energy equations did not need to be split, as it is assumed that the water, once evaporated, will have the same temperature and velocity of the surrounding air.
On top of this change, it was necessary to include three new source terms to account for the effects of the particles and ice on the mass, momentum and energy of the main flow. With the additional mass flow coming from the ice being solely consituted by vapour, the relative source term is added to the vapour mass equation only.
As a result of all these changes, the matrices $U$, $F$ and $G + W$ will look like what is shown in Eq. 4.42, Eq. 4.43 and Eq. 4.44.

$$U = \frac{\partial}{\partial t} \begin{bmatrix} \rho_a A \\ \rho_v A \\ \rho u A \\ \rho A E \\ \rho A Y_{SP} \\ \rho A Y_{FNB} \end{bmatrix} \tag{4.42}$$

$$F = \frac{\partial}{\partial x} \begin{bmatrix} \rho_a u A \\ \rho_v u A \\ \rho u^2 A + p_s A \\ \rho u A H \\ \rho u A Y_{SP} \\ \rho u A Y_{FNB} \end{bmatrix} \tag{4.43}$$

$$G + W = \begin{bmatrix} -W_{Ba} + W_F \\ -W_{Bv} + S_{mp} + S_{mi} \\ F_{comp} - F_{comb} + p_s \frac{\partial A}{\partial x} - F_B + F_F + S_{mop} + \\ Q + SW - H_B + H_F + S_{ep} + S_{ei} \\ \dot{\omega}_{SP} \\ \dot{\omega}_{FNB} \end{bmatrix} \tag{4.44}$$

Where $\rho_a$ is the air density, $\rho_v$ the vapour density, and $\rho$ the total flow density, equal to $\rho = \rho_a + \rho_v$. Finally, $S_{mp}$, $S_{mi}$, $S_{mop}$, $S_{ep}$ and $S_{ei}$ are respectively the mass, momentum and energy source terms respectively resulting from the particles and ice calculations, and their formulation will be the next topic of this subsection.

### Source terms formulation

The aforementioned source terms take the form of a differential over $x$. The main challenge in the formulation of the particles source terms is the fact that the positions of the particle walls does not coincide with the WEST grid nodes.
In order to overcome this problem, the source terms have been formulated as:

$$S = \frac{s}{dx} \tag{4.45}$$

Where $S$ is the general source term, and $s$ the value that needs to be differentiated, from now on named source value, for each interval $dx$.
Every wall of particles brings a certain amount of mass, momentum and energy source values $s_p$, and these values are associated to one or more intervals, proportially to the distance between the wall and their center. Figure 4.13 shows a general case that will help understand the logic for this association.

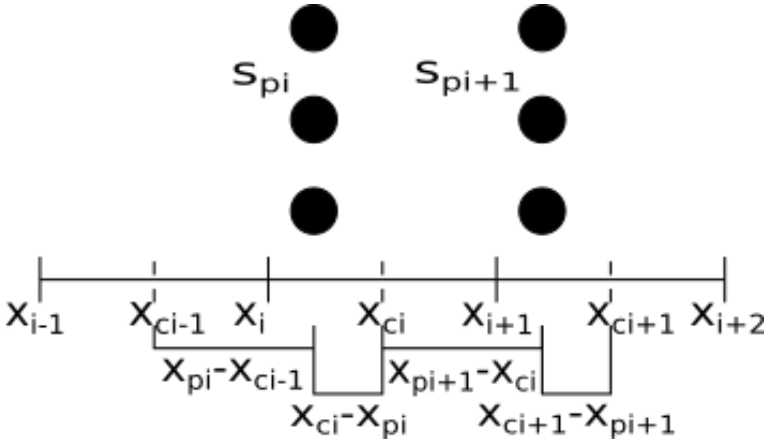


Figure 4.13: Source terms association logic

In this case, $x$ are the WEST grid nodes, $x_c$ the intervals center points, $x_p$ the position of the particle walls and $s_p$ the walls source values, that may be $s_{pm}$ for mass, $s_{pmo}$ for momentum and $s_{pe}$ for energy.
The values of $s$ for the three different intervals here displayed will be:

$$s_{i-1} = \frac{s_{pi}(x_{ci}-x_{pi})}{x_{ci}-x_{ci-1}}, s_i = \frac{s_{pi}(x_{pi}-x_{ci-1})}{x_{ci}-x_{ci-1}} + \frac{s_{pi+1}(x_{ci+1}-x_{pi+1})}{x_{ci+1}-x_{ci}}, s_{i+1} = \frac{s_{pi+1}(x_{pi+1}-x_{ci})}{x_{ci+1}-x_{ci}}$$

It is now necessary to define the source values for mass, momentum, and energy.
The evaporation and sublimation processes lead to a positive flux of vapour into the main flow:

$$s_{pm} = N_p \frac{dmv_1 + dmv_2}{dt} \tag{4.46}$$

For what concerns momentum, on one side there is the positive contribution brought by the added vapour, while on the other you have the negative effect of the particles being carried forward by the main flow:

$$s_{pmo} = u_p s_{pm} - N_p F_D \tag{4.47}$$

Finally, for the energy source value there is the positive term coming from the new

vapour in the flow and the negative terms generated by the heat absorption caused by the processes already described (evaporation, melting, temperature rise,...) and by the work done by the air/vapour mixture to accelerate the particles:

$$s_{pe} = s_{pm} H_p - N_p \left( \frac{dQ}{dt} - F_D u_p \right) \tag{4.48}$$

Where $H_p$ is the specific energy of the vapour being released by the particles and $dQ$ the amount of heat that the particles absorbed in the time step $dt$.
$H_p$ has two terms, one expressing the specific enthalpy of the vapour, and the second its specific kinetic energy: $H_p = h_p + \frac{1}{2} C_{pv} u_p^2$, where $C_{pv}$ is the vapour specific heat at the temperature $T_p$.
Finally, the heat absorbed by the particles includes the amount necessary to cause the evaporation/sublimation, the temperature rise and the melting of ice:

$$dQ = L_{vi} dmv_i + L_{vw} dmv_w + C_{pp} \left( m_p - dmv \right) dT_p + L_m dm_w$$

The same source terms are applied to the ice accreted on the stator vanes, with the exception of the momentum energy, which is absent given the fact that the ice is static, and the obvious simplification brought by the fact that in this case the origin of the source terms matches the WEST grid. Again, the calculations for the ice source terms can be found in Appendix B.
It is important to remind here that the particles and ice calculation is not repeated after the corrector step. The difference for the particles and ice source terms between the predictor and the corrector step is that, while the exchange values remain the same (e.g. $dmv_1$, $dQ$), for the other terms, such as $u_p$, the initial value is taken for the predictor step source terms, and the final for the corrector.

### 4.3.3 Area blockage

The next effect to be taken into consideration is the reduction of the actual passage area caused by the simple presence of the particles and accreted ice.
According to Crowe et al.[67], the area reduction induced by the particles at any given point in the compressor is:

$$dA_p = \frac{4}{3} n_p \pi r_p^2 A \tag{4.49}$$

Where $n_p$ is the particles volumetric density, $r_p$ the particles radius at that point, here obtained by interpolation, and $A$ the original cross-sectional area.
It is then necessary to calculate $n_p$. In order to do this, a new parameter, $N_{pIi}$, has been introduced, whose value is defined in a similar way as the aforementioned $s_i$ parameters for the source terms. Thus, the number of particles included in every particles wall will be distributed between the intervals whose center points include the position of the wall, with a criteria that is inversely proportional to the distance between the wall and those center points.
Finally, the particles density at a given mesh grid point $i$ will be:

$$n_{pi} = \frac{N_{pIi-1} + N_{pIi}}{\frac{1}{8}\left(A_{i-1} + 2A_i + A_{i+1}\right)\left(x_{i+1} - x_{i-1}\right)} \tag{4.50}$$

On the other side, the area reduction due to the accreted ice is simply the one due to the ice ring forming on the outer case of the compressor, since the accretion points match the WEST grid points:

$$dA_i = 2\pi \left(r_{ext} - \frac{\delta}{2}\right) \delta \tag{4.51}$$

### 4.3.4 Stage by stage division

As it will be seen in the next chapter, the ingestion of ice particles produces an interesting dynamic between the stages of a single compressor. In order to better capture this behaviour, it was necessary to split the map of the compressor in single stage maps.
The assumption that was made is that the overall pressure and temperature ratios of the compressor were equally spread among the stages, so that the pressure and temperature ratios of the $i$ stage are:

$$PR_i = PR^{1/N_s}, \quad TR_i = TR^{1/N_s} \tag{4.52}$$

Where $PR$ and $TR$ are the overall pressure and temperature ratios and $N_s$ is the number of total stages.
It is then necessary to change the values of $NRT$ and $WRTP$. Considering that $NRT$ is based on the inlet temperature, its value for the stage $i$ will be:

$$NRT_i = \frac{NRT}{\sqrt{TR_i^{i-1}}} \tag{4.53}$$

On the other side, $WRTP$ is based on the outlet values of pressure and temperature, so the formulation of the conversion from whole compressor to single stage will be:

$$WRTP_i = \frac{WRTP \cdot PR_i^{N_s-1}}{\sqrt{TR_i^{N_s-i}}} \tag{4.54}$$

### 4.3.5 Flow parameters and map reading changes

As it has already been highlighted, the particles evaporation introduces a new substance in the flow with the water vapour. This means that the compressor operative fluid is not pure air anymore, and some key parameters need to be changed in order to take into account the new conditions.
The main parameters affected by the introduction of vapour are the dynamic viscosity, $\mu$, the specific heat, $C_p$, and the operative gas specific constant, $R$.
All these parameters for the air/vapour mixture are defined as the weighted average between the values of those for air and vapour. So for a general property $X$ we will have that:

$$X = \frac{X_a \dot{m}_a + X_v \dot{m}_v}{\dot{m}}$$

The dynamic viscosity value $\mu_v$ for vapour comes from the interpolation of the flow temperature and pressure with a table whose values were obtained following IAPWS-IF97[77] calculations.
The vapour specific heat $C_{pv}$ is also obtained by interpolation of the flow temperature, and its data were taken from the website www.engineeringtoolbox.com[80]. Again, the table with the data is available in Appendix A.
Finally, the value of the vapour gas specific constant is the universally recognised $R_v = 461.5\frac{J}{kgK}$.
The change of this last property, however, made it necessary to change also how the input maps were read by the code. In fact, the two parameters that define the compressors characteristic in WEST, $NRT = \frac{N}{\sqrt{T}}$ and $WRTP = \frac{\dot{m}\sqrt{T}}{p}$, are actually the simplifications of $\frac{ND}{\sqrt{\gamma RT}}$ and $\frac{\dot{m}\sqrt{\frac{R}{\gamma}T}}{p}$, with $D$ representing the compressor diameter, given that the dimension and the operative fluid of the machine remain the same.
As already mentioned, the introduction of vapour obviously changes the operative fluid, which means that it is not possible anymore to simplify those parameters.
In order to be able to use the same compressor characteristics with the new operative fluid, two correction factors have been introduced:

$$corr_N = \frac{\sqrt{\gamma RT}}{\sqrt{\gamma_a R_a T}} \quad and \quad corr_W = \frac{\sqrt{\frac{R}{\gamma}T}}{\sqrt{\frac{R_a}{\gamma_a}T}} \tag{4.55}$$

Where the subscript $a$ indicates the $\gamma$ and $R$ values for pure air.
These factors are applied to the calculated $NRT$ and $WRTP$ to obtain $NRT' = \frac{NRT}{corr_n}$ $WRTP' = WRTP \cdot corr_W$, which are the actual values used to read the compressor maps. In this way the operative point is shifted as much as needed to counterbalance the changed operative fluid.

# Chapter 5

# Results and Discussion

In this section, the results of the simulations carried out during this study are presented and discussed.
The section structure reflects the progression of the simulations performed. The first simulations that were carried out modelled a single, isolated compressor followed by a plenum. After those a single shaft engine has been simulated to test if the ice ingestion model would cause any problem to the running of the turbine and shaft speed calculators. The main body of simulations has then been performed modelling the whole core of a commercial high bypass turbofan engine and testing its behaviour in response to ice particles ingestion at cruise under different ambient conditions. Finally, a few more simulations were carried out to try to show the capability of the model to simulate ice accretion and to test the sensitivity of the method to the way the compressors were modelled: if considered as a whole or split into stages.

## 5.1 Isolated compressor

A series of simulations on an isolated 8 stage intermediate pressure compressor (IPC) of a three spool commercial high bypass turbofan engine at take-off conditions connected to a tank have been carried out. Here the results of a simulation with an ice mass flow equal to 0.75 percent of air mass flow and particles diameter of 140 microns are presented.

### 5.1.1 Compressor Behaviour

Figure 5.1 shows the static temperature ratio between the inlet station of each subcomponent of the system and the overall compressor inlet. This displays how the particles progressing into the compressor make the air temperature drop, and how this behaviour becomes more and more evident in the last stages, where the particles are melting and heating up as liquid droplets, which are phenomena that absorb more heat than heating ice.
In Figure 5.2, instead, the mass flow at the beginning and at the end of the simulation are depicted. In this figure, and in all the figures present in this chapter that have **X [m]** on the abscissa, the X co-ordinate corresponds to the physical distance between the inlet and outlet section of the WEST compression domain. It can be noticed that the lower air temperature causes an increase in total mass flow, which further increases along the compressor due to the evaporation of ice particles.
The combination of these results explains what can be seen in Figure 5.3, where it is represented the evolution of the operative point on the maps of the eight stages, with the final operative condition marked by a dot. The increase in total mass flow drives the first stages away from the surge line, but the further increase due to particles evaporation is not enough to compensate for the air temperature drop,

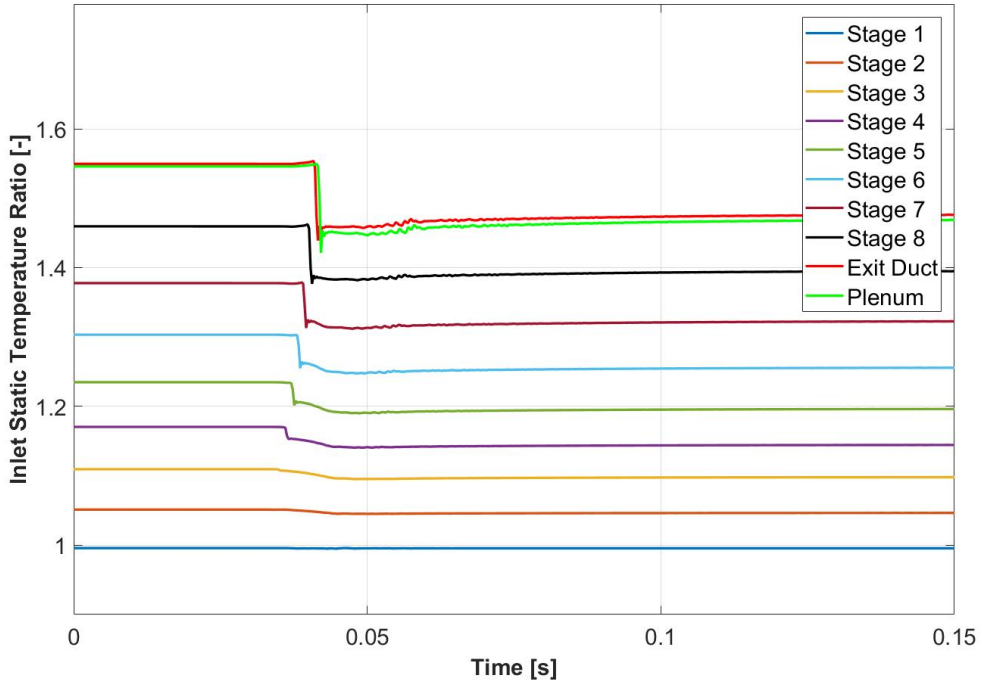


Figure 5.1: Inlet static temperature ratio

causing the operative point of the last stages to move towards surge. Moreover, the drop in temperature causes also the nondimensional rotational speed $NRT$ to increase along the compressor.

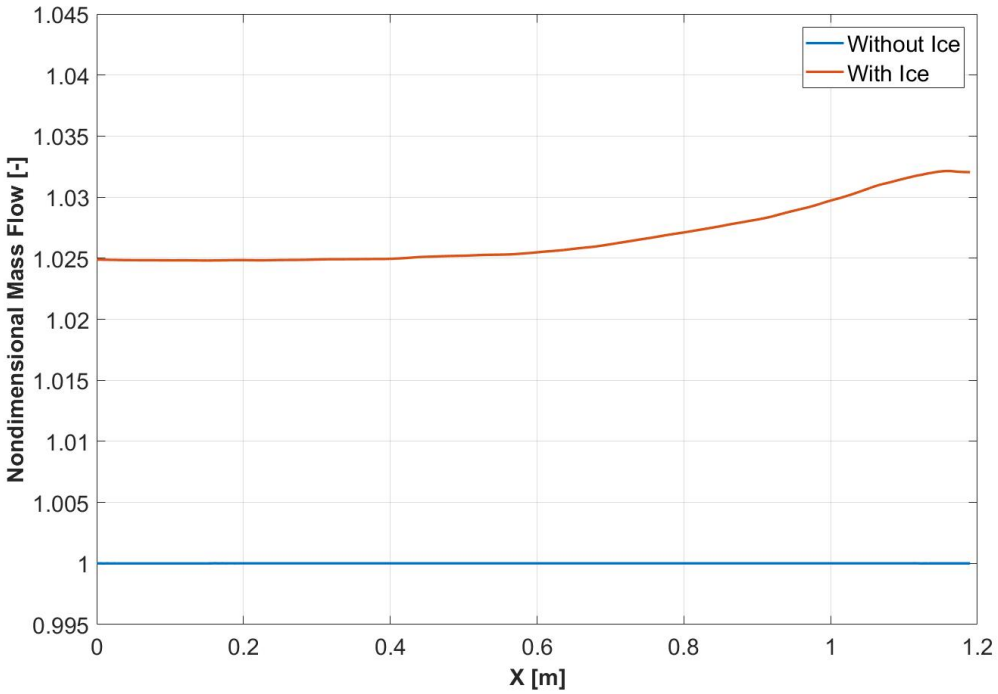


Figure 5.2: Normalised mass flow

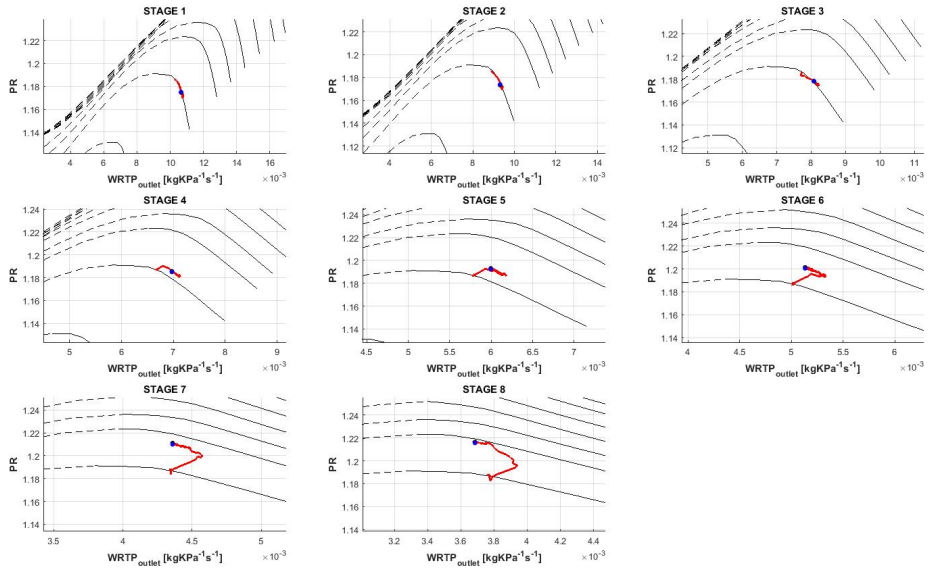


Figure 5.3: Stages operative point movement during ice ingestion

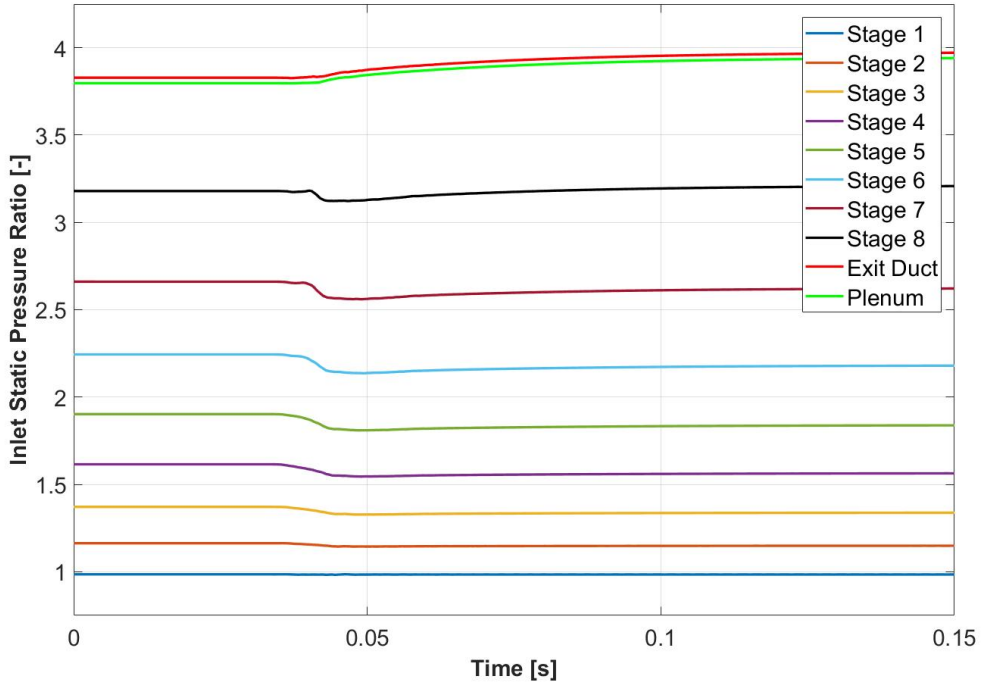


Figure 5.4: Stages operative point movement during ice ingestion

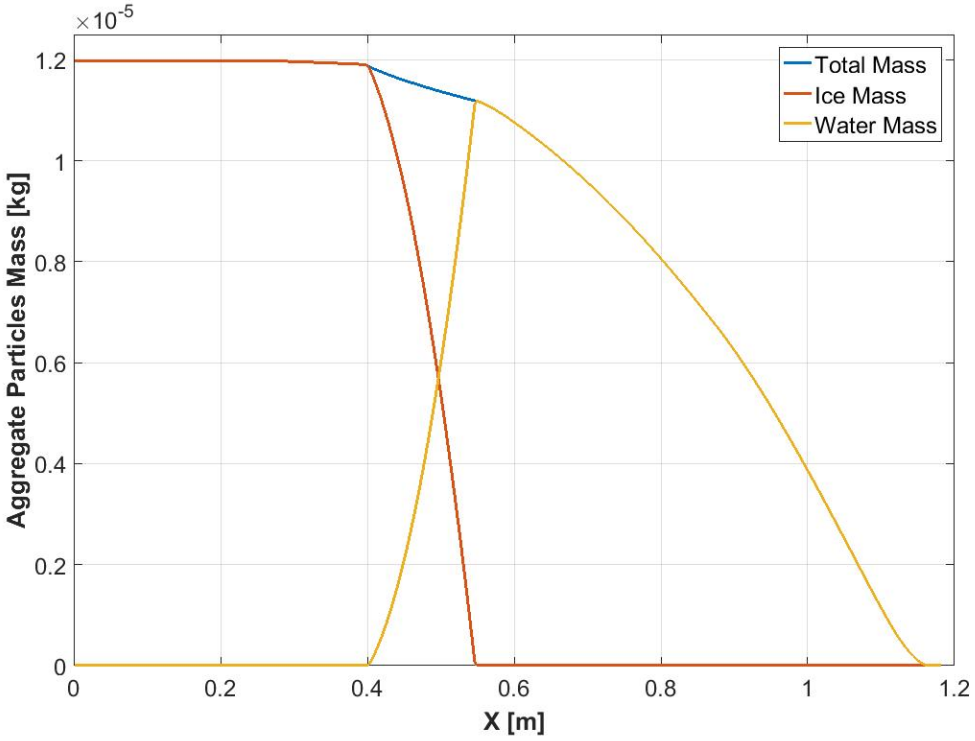


Figure 5.5: Ice particles aggregate mass along the compressor

Furthermore, looking at Figure 5.3 it is possible to understand what happens in Figure 5.4, where the ratio between the inlet static pressure of each component and the overall inlet pressure is shown. With the operative points of the first stages moving away from the surge line, the pressure ratio of those stages decreases. On the other hand, the operative points of the stages in the second half of the compressor move to higher nondimensional rotational speeds and, for the last stage, toward the surge line. This causes the the pressure ratio of these stages to drop progressively less than the previous ones until, in the last couple of them, after an initial drop the pressure ratio becomes actually higher than what it was before the ice ingestion.
These results closely mimic those obtained, on a different compressor, by Kundu et al.[8]. This has been interpreted as a sign of the validity of the ice ingestion model, which led to the continuation of its development and its progressive integration into a whole engine simulation.

### 5.1.2 Ice Particles Behaviour

It is interesting now, before moving to the results of more complex simulations, to show and explain the general behaviour of the ice particles as they penetrate the engine.
One of the most important characteristics of the particles behaviour is their progressive evaporation and change in composition. This can be seen in Figure 5.5, where the aggregate mass of the particles, defined as $am = N_p \cdot m_p$, is depicted, together with their aggregate ice and water mass portions. It is possible to notice that, as soon as a film of water is formed due to the ice melting, the evaporation accelerates, due to the water having a higher diffusivity with air compared to ice. This result is in agreement with what was found in Figure 5.2, where the increase in mass flow along the compressor due to the particles evaporation starts to be relevant only in the second half of the compressor.
It has been decided to show the aggregate particles mass instead of the single particles mass and their ice and water portions because the particles break-up process makes it difficult to use these parameters to analyse particles composition when considering the particles development along the whole compressor. In fact, the mass of a single particle is greatly reduced after just a couple of stages, to the point that it is not even comparable anymore to its initial value, as can be seen in Figure 5.6. On the other hand, the impact of the particles against the blades determines an abrupt increase in the number of particles with each break-up event, phenomenon that is

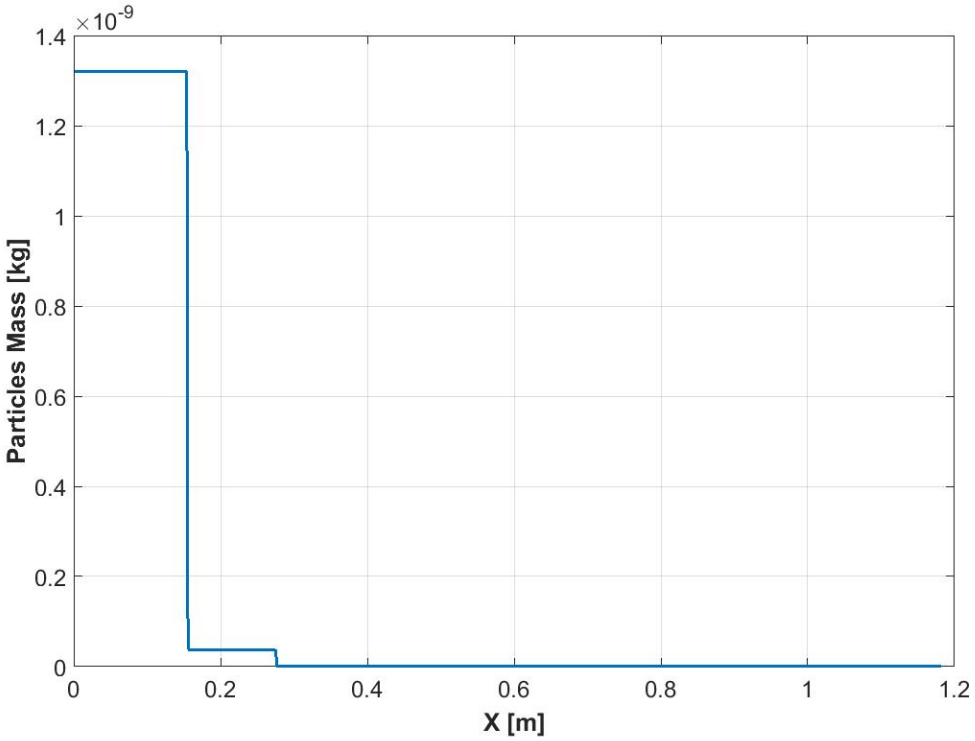


Figure 5.6: Ice particles mass along the compressor

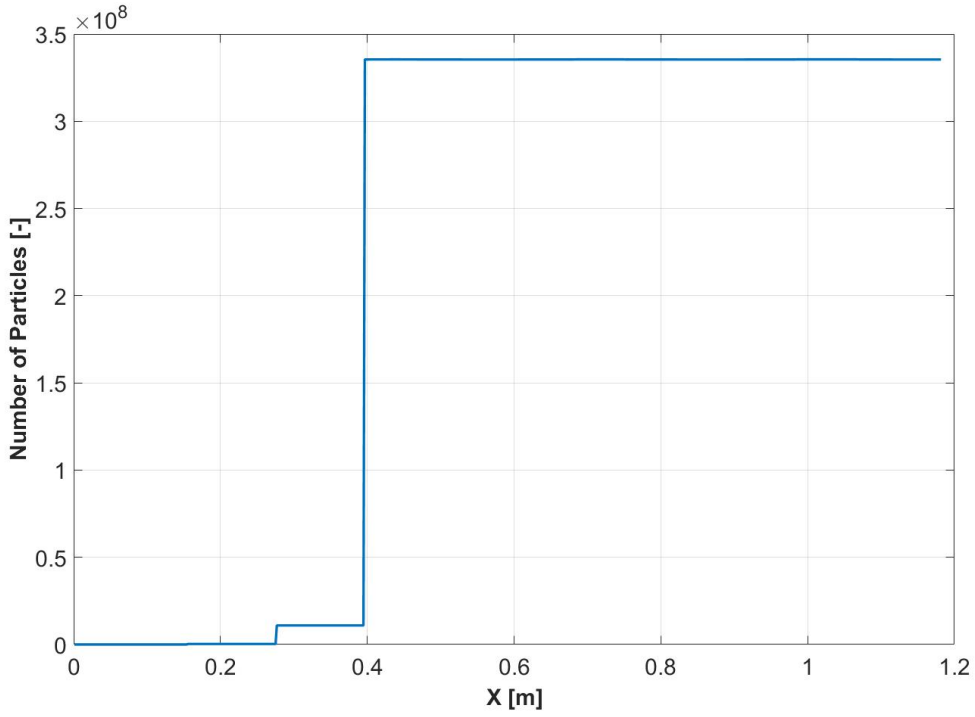


Figure 5.7: Number of ice particles along the compressor

shown in Figure 5.7. It is interesting to note that after the third stage there are no additional break-up events. This is due to the very small dimensions already reached by the particles, that do not meet the requirements for the break-up models to intervene anymore. Furthermore, by comparing these last three figures with Figure 5.1, it is possible to verify that the real drop in temperature ratio takes place after the beginning of the melting process.

Figure 5.8 shows how the particles temperature changes as they move through the compressor. As expected, during the ice melting process the temperature remains constant. It is also interesting to notice how to every break-up event corresponds an acceleration in the temperature rising process, induced by the sudden reduction in particles mass.

An unexpected feature of the temperature behaviour is the final stabilisation and subsequent peak that can be noticed in Figure 5.8. The reason for this phenomenon can be found in the complex interaction between the main flow conditions and the different processes that characterise the particles development. As it can be seen in Figure 5.9 the initial stabilisation of the particles temperature corresponds to the end of the flow static temperature increase at the exit of the compressor, which happens while the particles are still evaporating. The reason for this correspondence can be found in the way that the particles behaviour is modelled. As it was explained

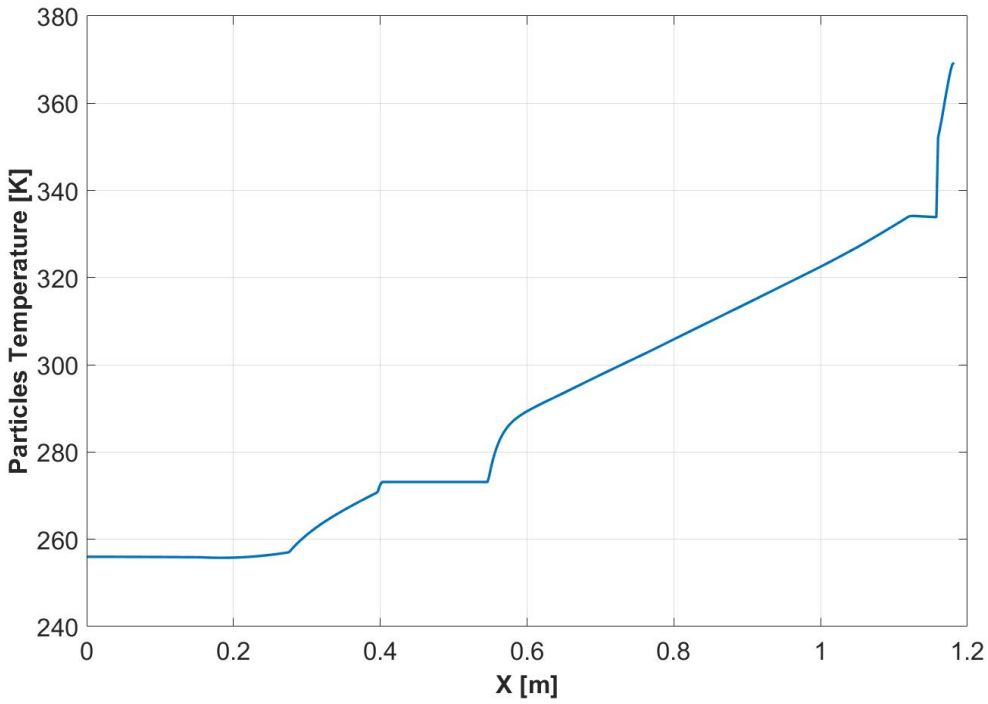


Figure 5.8: Particles temperature along the compressor

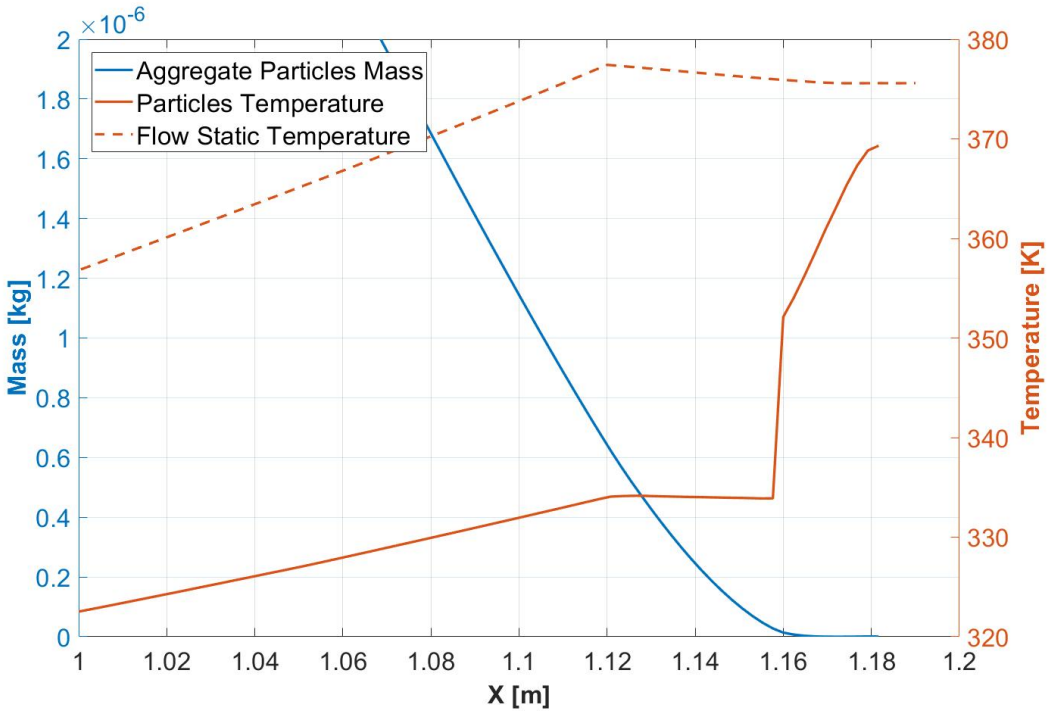


Figure 5.9: Aggregate particles mass, particles temperature and main flow static temperature in the last part of the domain

in the previous section, the evaporation process is calculated before the temperature rise, and the energy necessary for it to happen is subtracted from the total heat absorbed by the particles, hence reducing the energy available to increase the particles temperature. Thus, if the flow temperature stabilises and the evaporation rate remains constant, it is possible that there is not enough energy left for raising the ice temperature, and this is the case in the area that goes from 1.12 $m$ to 1.16 $m$ in Figure 5.9.

After 1.16 $m$ it is possible to see that the particles mass assumes an asymptotic behaviour, hence reducing the evaporation rate. This enables the particles temperature to rise again, in a quite abrupt fashion due to the extremely low particles mass.

Finally, Figure 5.10 shows the particles velocity compared to the one of the air/vapour mixture. It can be seen that, as it could be expected, each time the particles were broken up this caused a rapid increase in particles acceleration. Moreover, a lag can be observed between the air and particles deceleration once the continuous phase velocity reaches its maximum value, which is in perfect agreement with the fact that the particles are carried by the main flow, so that their inertia causes them to decelerate as a consequence of the air velocity reduction.

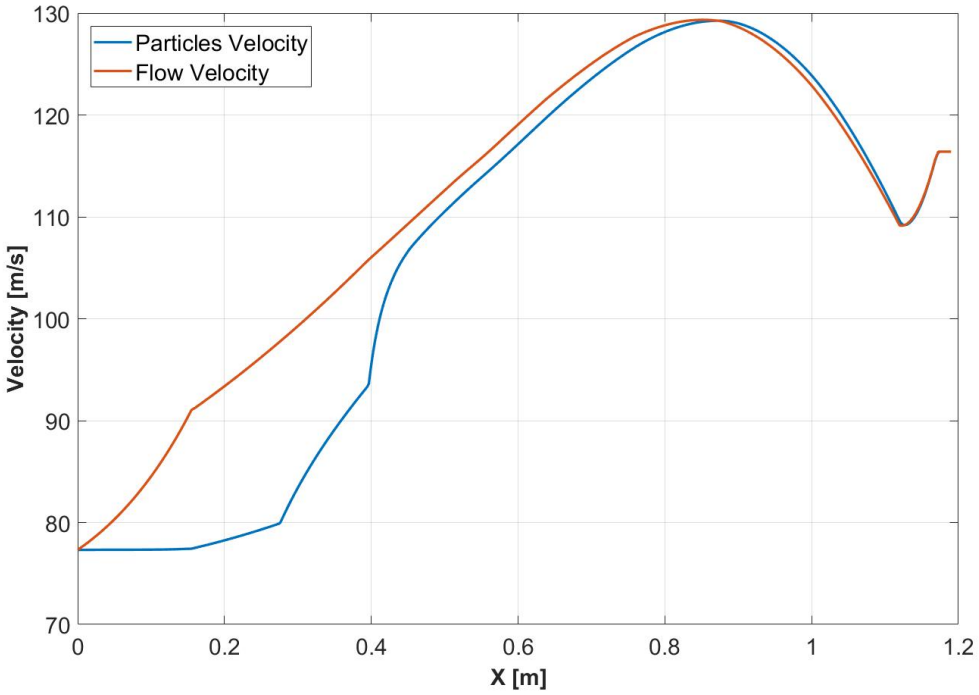


Figure 5.10: Particles and flow velocity along the compressor

## 5.2 Single shaft

The single shaft simulations have been only a stepping stone to test if the code introduced any problems to the operations of WEST when the compression system is complete of the combustion chamber and coupled with the expansion system and the mechanical management routine.
For these simulations the HP compressor of a three spool high bypass commercial turbofan engine at take-off was considered. The introduced ice particles had a diameter of 140 $\mu m$ and a temperature of 250 $K$. A series of simulations was carried out with varying ice particles ingestion rates. The amount of ice ingested per second was equal to 1 %, 1.25 % and 1.5 % of the air inlet mass flow.
Figure 5.11 shows the effects of ice ingestion on the compression side mass flow of air and water vapour. As already seen for the isolated compressor, the introduction of ice particles has two main effects on the mass flow. On one hand, there is an overall increase in continuous phase mass flow, on the other, there is also a mass flow increment along the compressor, due to the evaporation and sublimation of the particles and their passage from the discrete to the continuous phase. Both these effects accentuate with higher particles ingestion rates.

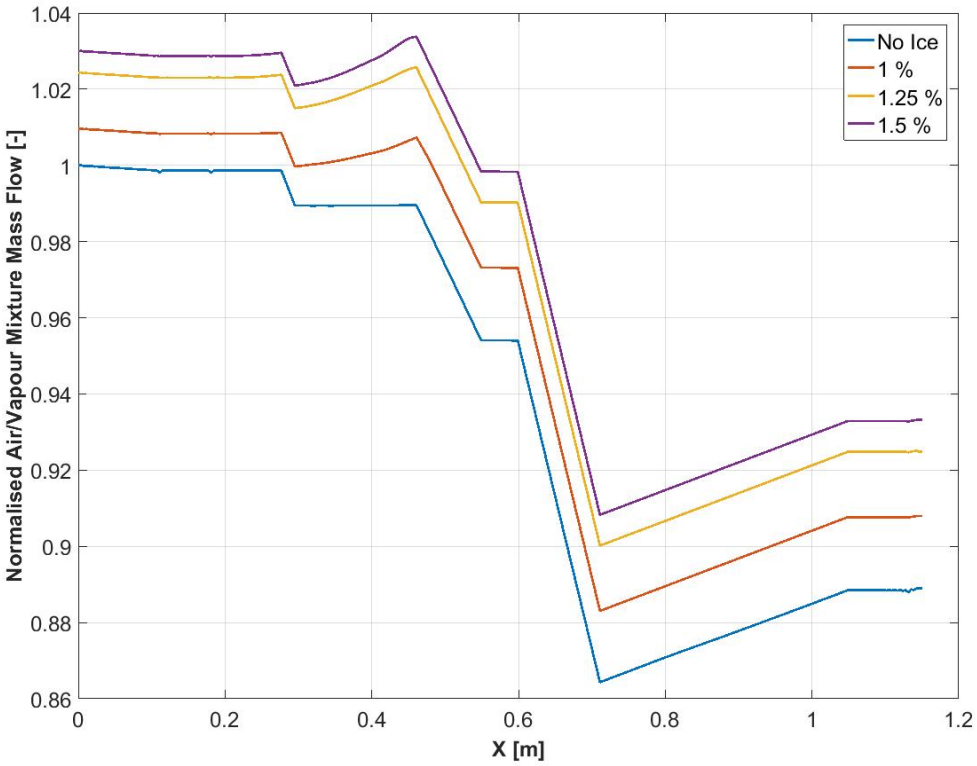


Figure 5.11: Normalised air/vapour mass flow along the compressor with different ice particles ingestion rates

The main reasons for the overall increase in air/vapour mass flow is the phenomenon shown in Figure 5.12. The ice particles, with the heat they absorb evaporating, melting and being heated up, cause a reduction in temperature along the compressor, which corresponds to an increased air density and leads to a higher mass flow.
Figure 5.13 highlights the novelty of these simulations. The particles ingestion induces an increase in shaft rotational speed, which is accentuated with higher particles ingestion rates. Figure 5.14 helps understand the reason for this phenomenon. The introduction of ice particles leads, with the increase in mass flow that they cause, to a slightly increased power demand by the compressor. The turbine, which has not been reached by the increased mass flow yet, cannot keep up with the compressor demand, leading to an initial reduction in rotational speed. Around the 0.02 seconds mark, a spike in turbine torque is visible. This is due to the fact that the colder extra mass flow has now reached the turbine. In these conditions, the presence of ice particles actually causes the compressor to require less power than the one that the turbine is capable to deliver, due to the cooling effect that they have on the working fluid. This leads to an overall acceleration in shaft rotational speed.

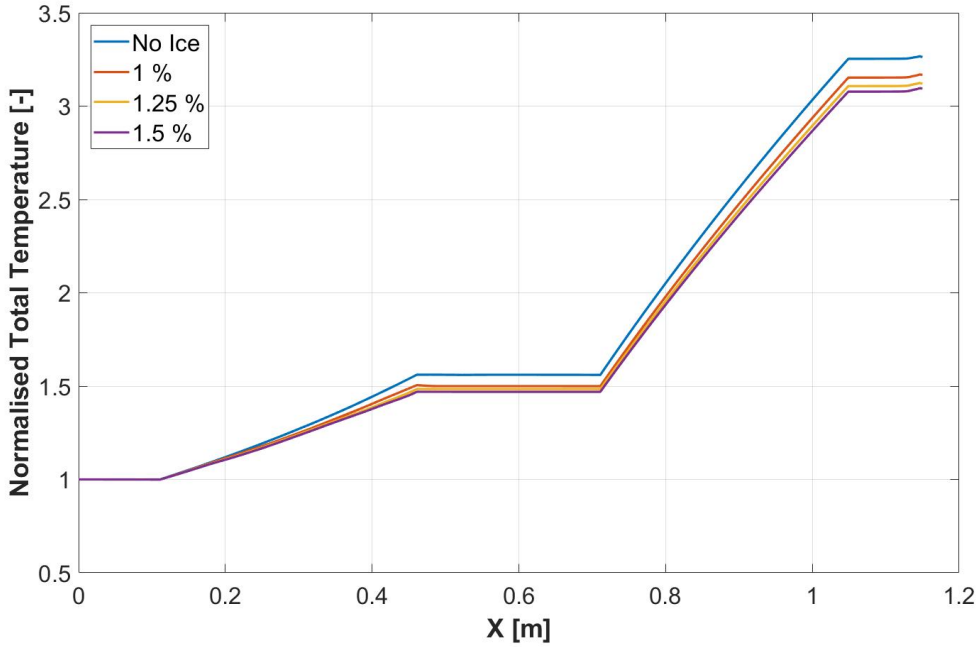


Figure 5.12: Normalised flow total temperature with different ice particles ingestion rates

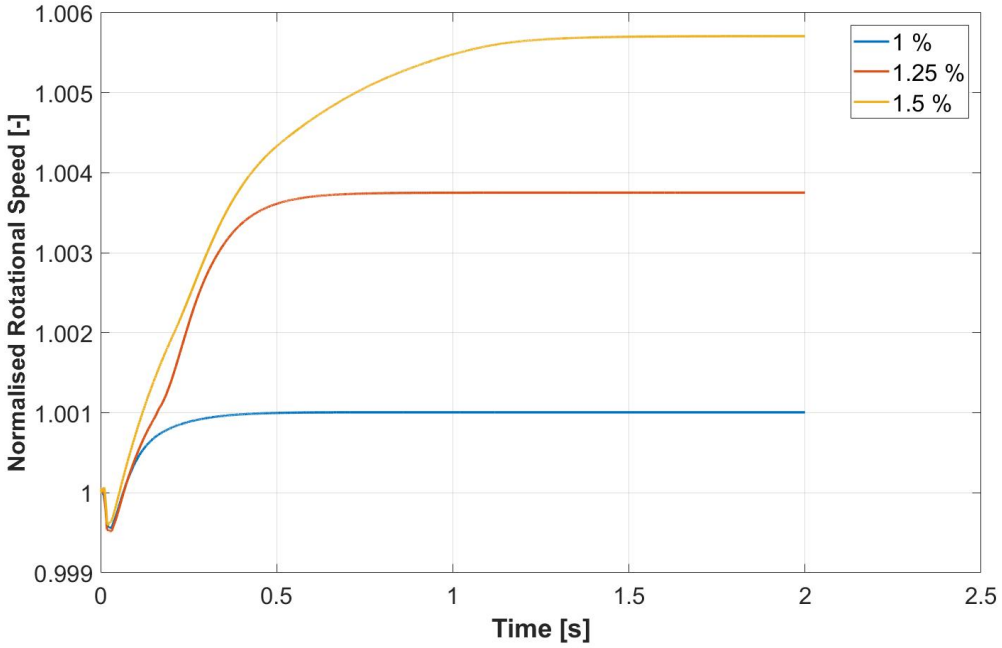


Figure 5.13: Normalised shaft rotational speed with different ice particles ingestion rates

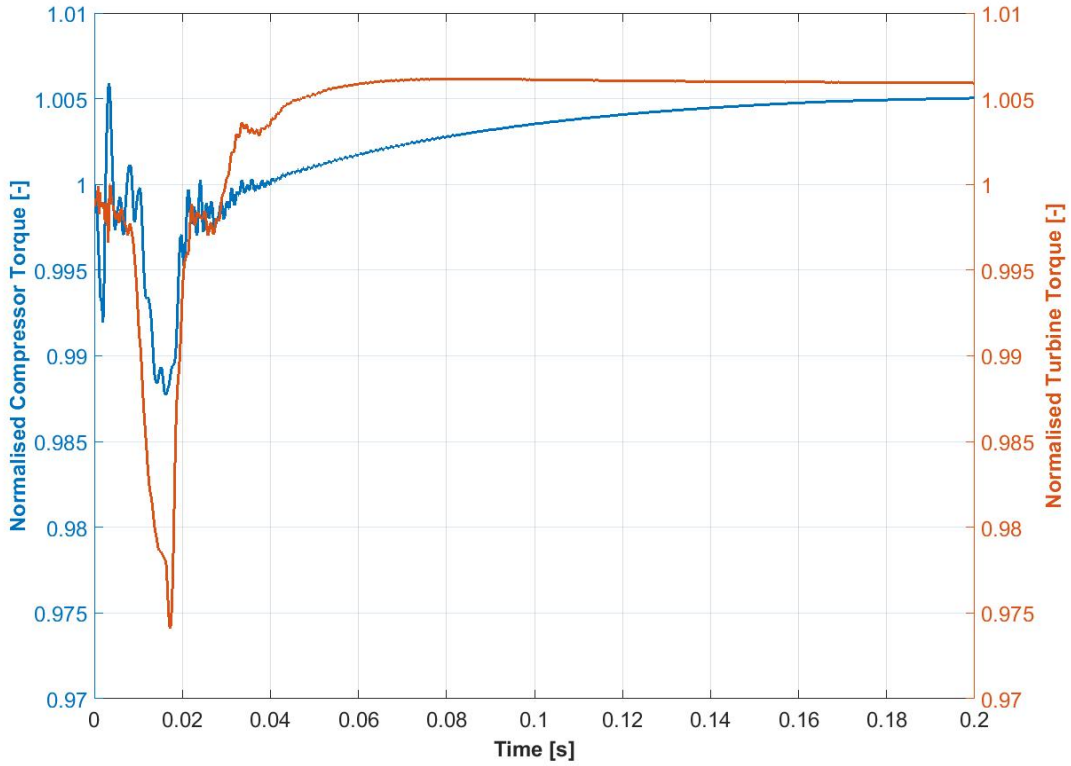


Figure 5.14: Normalised compressor and turbine torques with ice inlet mass flow equal to 1 % of air inlet mass flow

## 5.3 Whole engine

### 5.3.1 Inlet parameters analysis

The engine taken into consideration was a high bypass commercial turbofan engine at cruise conditions, the parameters whose influence was investigated are the ice ingestion rate, particles dimension and ambient temperature.

#### Ice ingestion rate

For these simulations the inlet temperature was 10 $K$ higher than the international standard atmosphere temperature at 37000 feet.
With the whole engine simulations, the particles ingestion rates are expressed in grams per cubic meter of ingested air instead of percentages of air mass flow. The

particles ingested are 140 $\mu m$ in diameter, with a temperature of 226.6 $K$, equal to the inlet static temperature, have a speed of 250 $m/s$, and the analysed ingestion rates are 2, 3 and 4 $g/m^3$.
In whole engine simulations, the effects of varying particles ingestion rates on mass flow and temperature are the same that have been shown for the single shaft case: increase in overall mass flow and increase in mass flow along the compression side, and temperature reduction. The only feature that is worth to highlight is that all the particles seem to melt and evaporate within the IPC, causing the real shift in temperature to happen there, as it is shown in Figure 5.15.

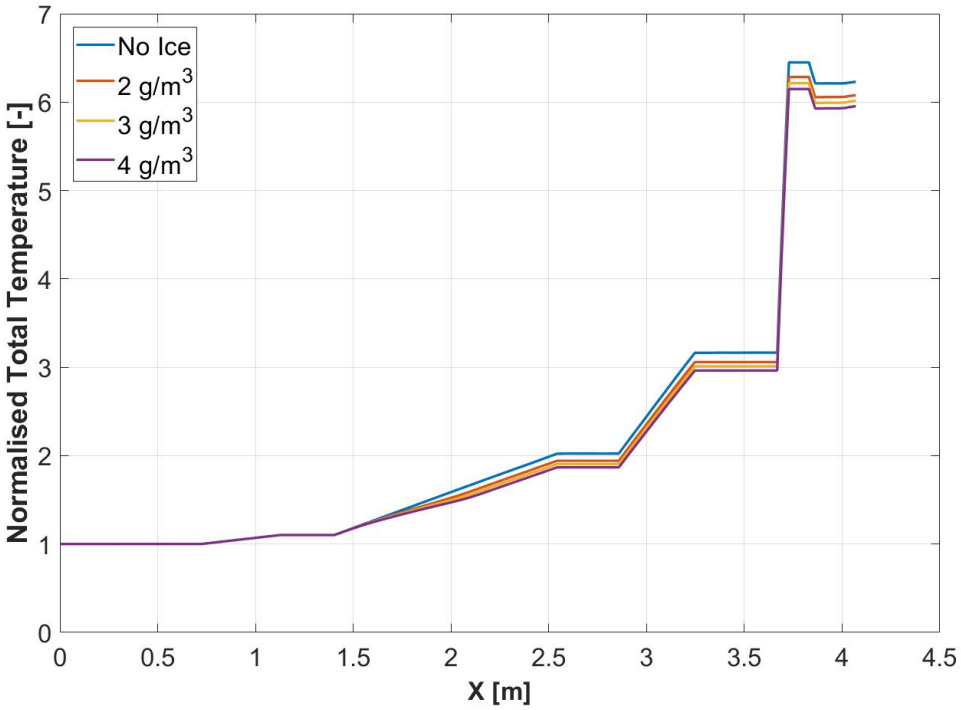


Figure 5.15: Normalised total temperature throughout the compression domain with different ice ingestion rates

For what concerns rotational speed and HPC outlet pressure and temperature, Figure 5.16 and Figure 5.17 show that the general trends observed in the in-flight data are qualitatively maintained in the simulations. As it can be seen, the rotational speeds, which are normalised with their respective take-off speed, tend to converge, while P30 and T30, normalised with their initial values, diverge, with P30 increasing and T30 decreasing. Both these trends are accentuated by increasing the particles' ingestion rate. While the divergence of P30 and T30 is easy to explain, with the temperature drop caused by the particles heat absorption and the pressure rising

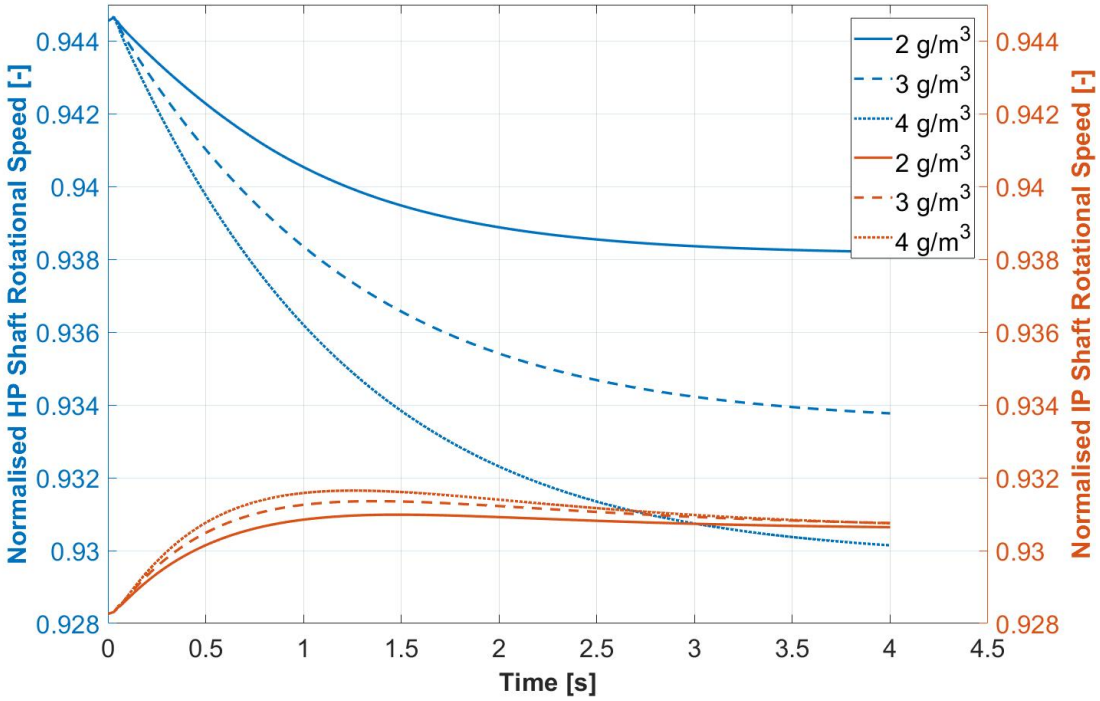


Figure 5.16: Normalised rotational speed for IP and HP shafts with different ice ingestion rates

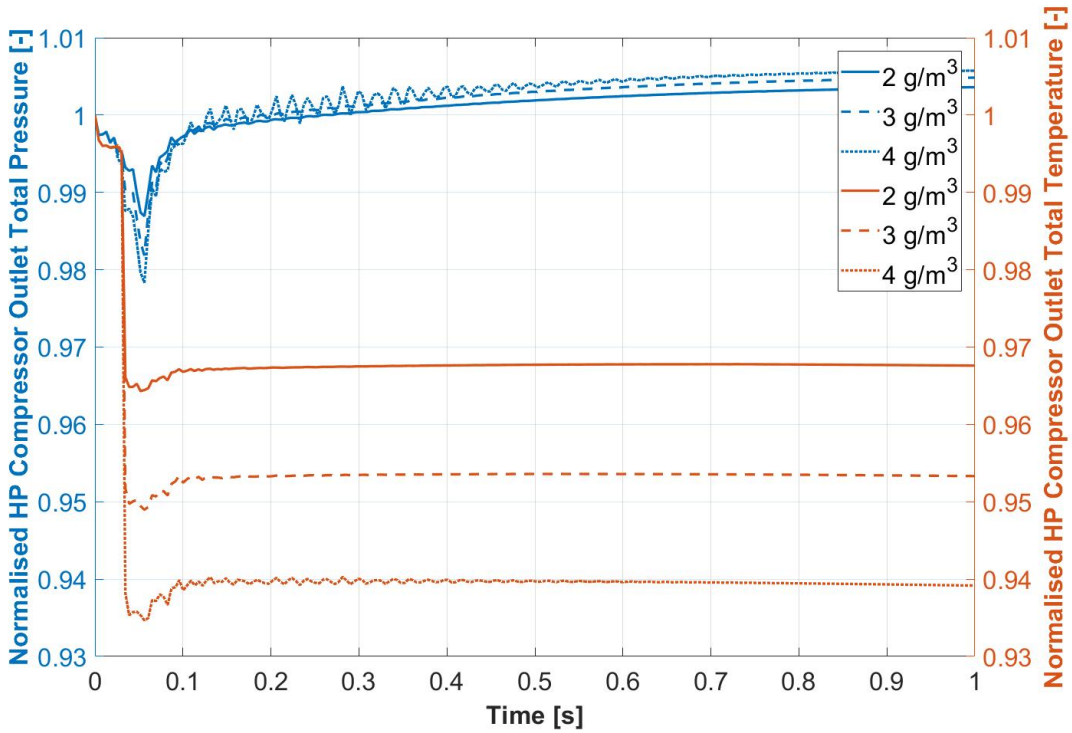


Figure 5.17: Normalised HPC outlet total pressure and temperature with different ice ingestion rates

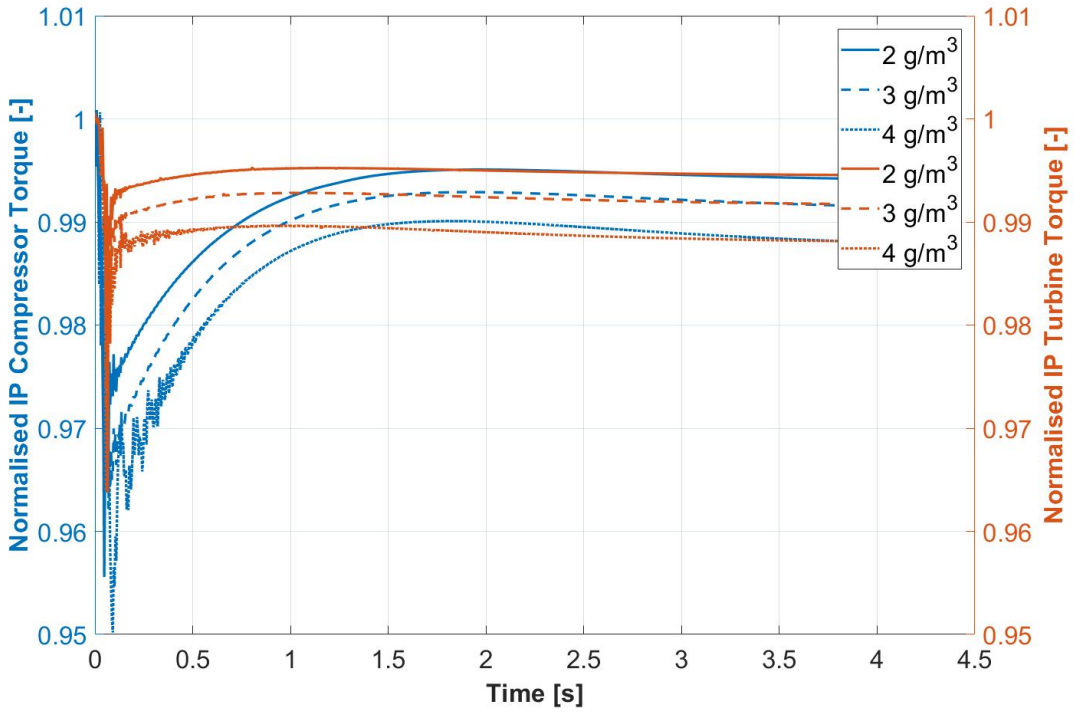


Figure 5.18: Normalised IP compressor and turbine torques with different ice ingestion rates

because of the better compression of a colder fluid, the reason for the behaviour of the shaft speeds can be more difficult to understand.
Figure 5.18 and Figure 5.19 can help understand this phenomenon. As already mentioned, the transformation of ice particles into vapour happens mainly in the IPC, and it does not reach at all the HPC. Moreover, the mass flow increase due to the ice ingestion has a bigger impact, proportionally, on the smaller mass flow of the HPC. This means that, while in the IPC the main effect that the particles have is making the compression process more efficient, thus requiring less power from the turbine, in the case of the HPC the main phenomenon to be considered is the increased mass flow that requires more power to be compressed.

### Ice particles size

The following investigation was meant to analyse the influence of different particles sizes, keeping the inlet temperature and ice ingestion ratio constant.
Figure 5.20 shows how the mass flow of the considered engine changes ingesting the same amount of ice ($4\ g/m^3$) but with particles dimensions respectively of 140, 70 and 35

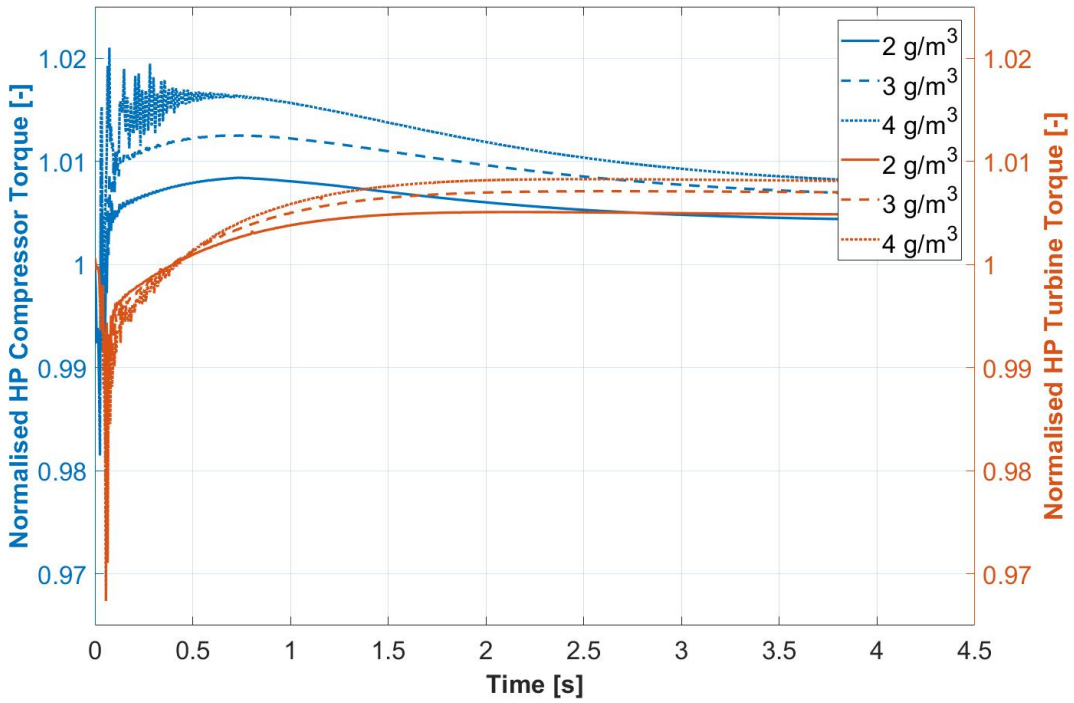


Figure 5.19: Normalised HP compressor and turbine torques with different ice ingestion rates

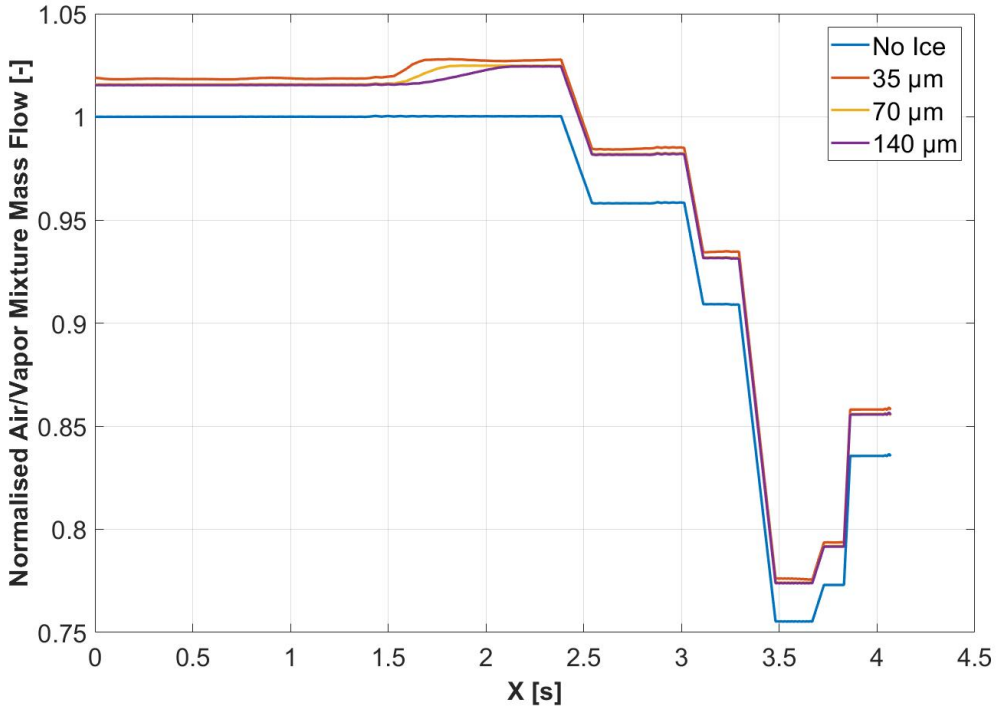


Figure 5.20: Normalised air/vapour mixture mass flow thoughout the compressor with different ice particles diameters

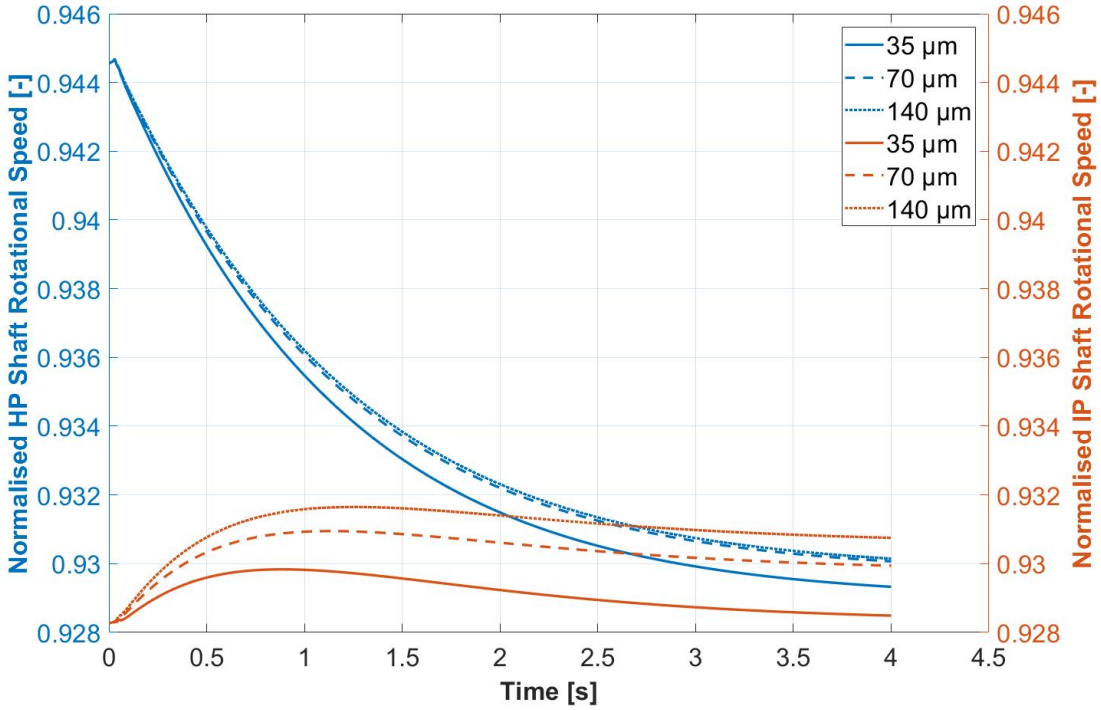


Figure 5.21: Normalised IP and HP shaft rotational speeds with different ice particles diameters

$\mu m$. It is worth noting that smaller particles induce bigger mass flow increases and that the further increase in mass flow taking place throughout the IPC is anticipated. This is because, intuitively, smaller particles end up evaporating earlier.

Figure 5.21 and Figure 5.22, on the other hand, show the effects of particles size on rotational speed, P30 and T30. It can be seen that, in this case, while the overall effect on the shaft rotational speeds is less accentuated by the ingestion of smaller particles, with the two adimensional speeds coming closer and closer together with bigger particles, a difference in the behaviour of the two shafts can be observed. In fact, the effect on the IP shaft rotational speed is smaller with smaller particles, while the effect on the HP shaft rotational speed increases with the reduction of particles size.

This phenomenon can be understood looking at Figure 5.23. It can be seen that reducing the particles size causes a bigger portion of particles induced temperature drop to occur before the inlet of the IPC, leading to a smaller drop in temperature ratio, hence a smaller decrease in compressor required power. On the other side, the main driver for the HP shaft behaviour is the transient effect caused by the mass flow variation. As it was seen in Figure 5.20, smaller particles induce a bigger increase in mass flow, causing a higher HP shaft rotational speed reduction, even

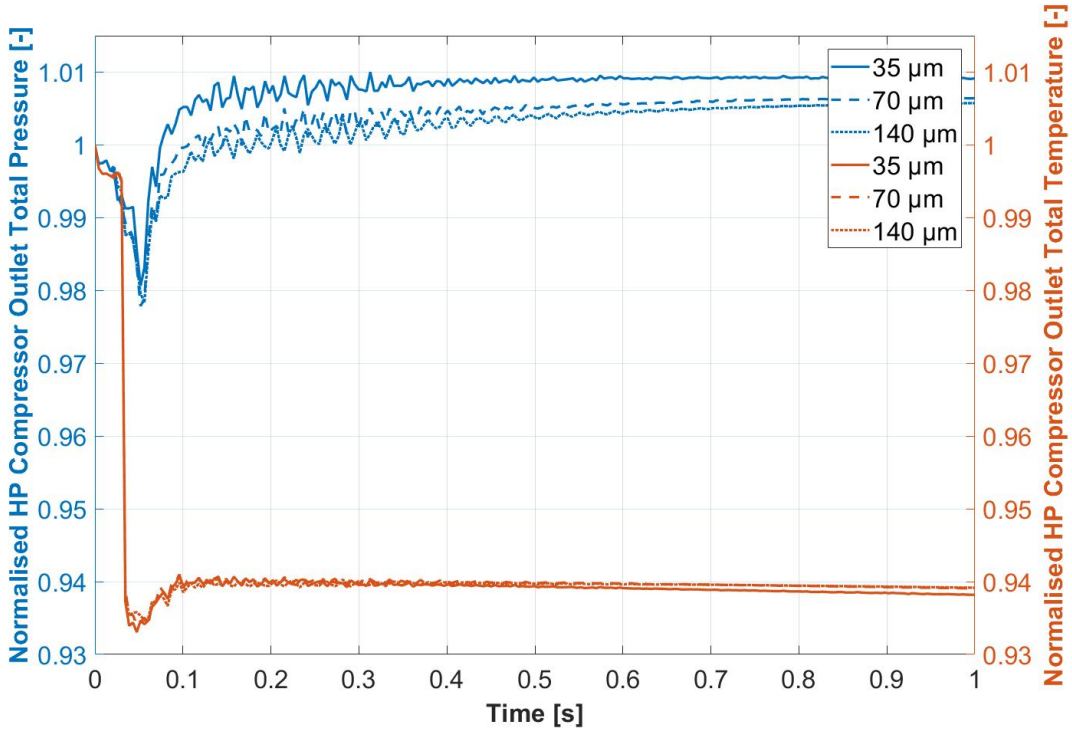


Figure 5.22: Normalised HPC outlet total pressure and temperature with different ice particles diameters

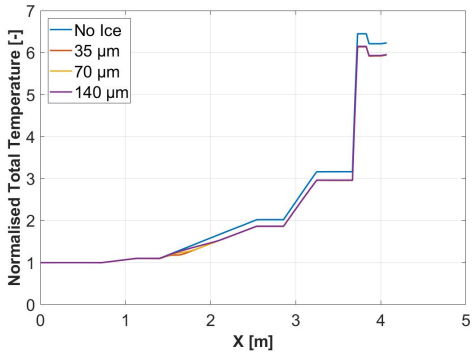


(a) Normalised total temperature

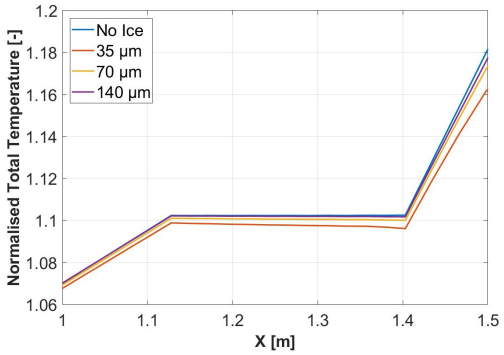


(b) Normalised total temperature at the IPC inlet

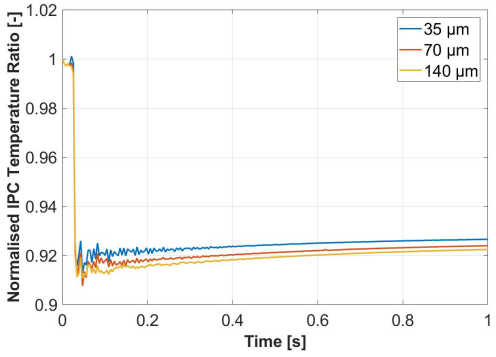


(c) Normalised IPC temperature ratio

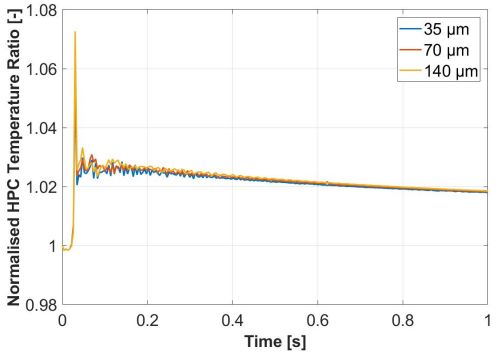


(d) Normalised HPC temperature ratio

Figure 5.23: Effects on total temperature and temperature ratios of different ice particles diameters

though the HPC temperature ratio rise is slightly reduced by the reduction of particles size.

### Ambient temperature

The last parametric analysis of this study was performed changing the ambient temperature from 216.6 $K$ to 226.6 and 236.6 $K$, keeping the particles diameter at 140 $\mu m$ and the ice ingestion rate at 4 $g/m^3$.
Figure 5.24 shows how the effects on the rotational speeds are increased by higher ambient temperatures.

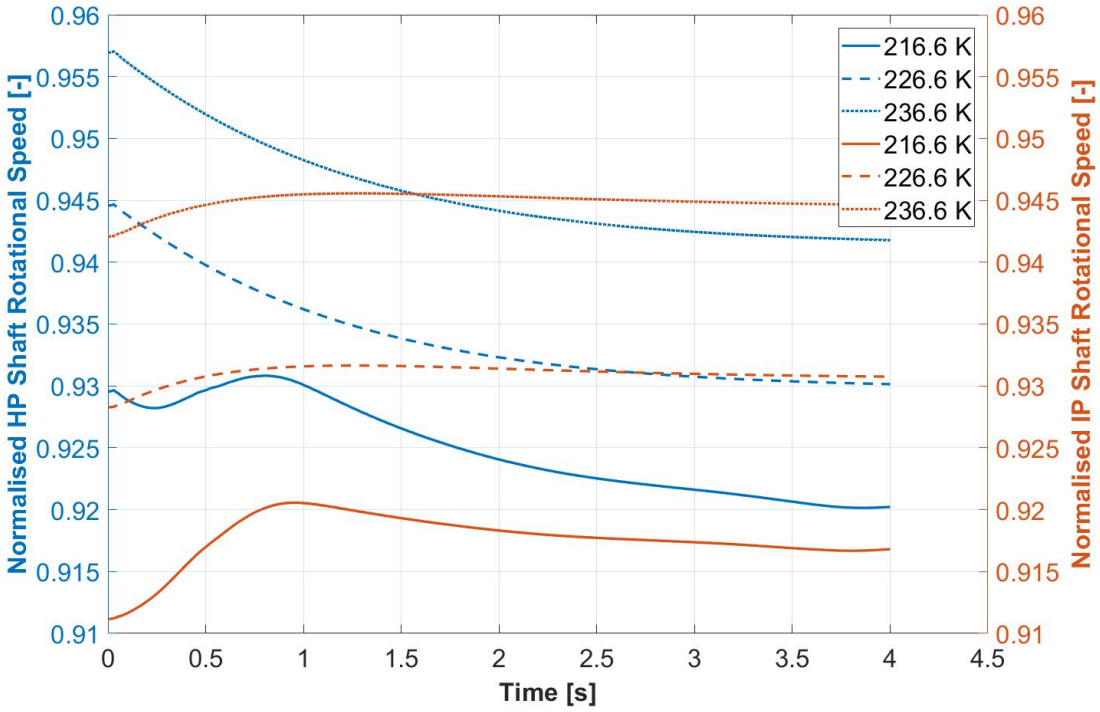


Figure 5.24: Normalised HP and IP shafts rotational speeds at different ambient temperatures

This behaviour can be explained by looking at how the ice ingestion rate is formulated. In fact, while rising the ambient temperature causes the air density to drop, hence a lower air mass flow, the ice ingestion rate, being expressed in $g/m^3$, is unaffected by this change. This leads to a higher ice over air mass flow ratio, as it can be seen in Table 5.1, causing the particles to have a greater effect at higher temperatures.

| $T_{amb}$ $[K]$ | $V_a$ $[m/s]$ | $\rho_a$ $[kg/s]$ | $\dot{m}_a$ $[kg/s]$ | $\dot{m}_i$ $[kg/s]$ | $\dot{m}_i/\dot{m}_a$ [%] |
|---|---|---|---|---|---|
| 216.6 | 57.78 | 0.4359 | 37.35 | 0.3427 | 0.9176 |
| 226.6 | 58.09 | 0.4160 | 35.84 | 0.3446 | 0.9614 |
| 236.6 | 58.26 | 0.4008 | 34.63 | 0.3456 | 0.9979 |

Table 5.1: Initial inlet flow conditions at different ambient temperatures

Even though the increases in ice to air mass ratio might not seem so impressive, if the percentage increase is calculated it can be noticed that there is a 4.773 % increase in ice to air ratio between 216.6 $K$ and 226.6 $K$ and a 3.797 % increase between 226.6 $K$ and 236.6 $K$. These differences, however small, are still significant, and can explain the slightly different behaviours that can be observed in Figure 5.24.

### 5.3.2 Ice accretion

A series of simulations were performed after implementing the ice accretion model. The aim of these simulatios, rather than to rigorously test the reliability of the ice accretion model, was to try to showcase this code capability to perform an ice accretion simulation. The different ambient conditions and particles parameters for these various simulations can be found in Table 5.2. Even though a wide range of conditions has been tested, and in some of these the relative humidity had extreme or even impossible values, none of the tested scenarios produced the conditions required for ice accretion at the compressor stator vanes.

| $T_{amb}$ $[K]$ | $P_{amb}$ $[Pa]$ | Rel. Humidity $[-]$ | $d_p$ $[\mu m]$ | Ice Ingestion Rate $[g/m^3]$ |
|---|---|---|---|---|
| 226.6 | 31557.3 | 0 | 35 | 4 |
| 226.6 | 31557.3 | 0 | 70 | 4 |
| 216.6 | 31557.3 | 0 | 140 | 4 |
| 226.6 | 31557.3 | 0 | 140 | 4 |
| 236.6 | 31557.3 | 0 | 140 | 4 |
| 226.6 | 31557.3 | 0.1 | 140 | 4 |
| 226.6 | 31557.3 | 0.3 | 140 | 4 |
| 226.6 | 31557.3 | 1 | 140 | 4 |
| 226.6 | 31557.3 | 1.3 | 140 | 4 |

Table 5.2: Ambient conditions and particles properties for ice accretion simulations

While, considering its aim, this series of simulations could be considered a failure, it has to be highlighted that the simulated engine has never experienced any ice accretion event during its hours of service. Hence, while it could be argued that the

absence of ice accretion would be the outcome that a correct model would give, more work on the subject is necessary, possibly adopting an engine known for experiencing ice accretion.

### 5.3.3 Stage by stage division

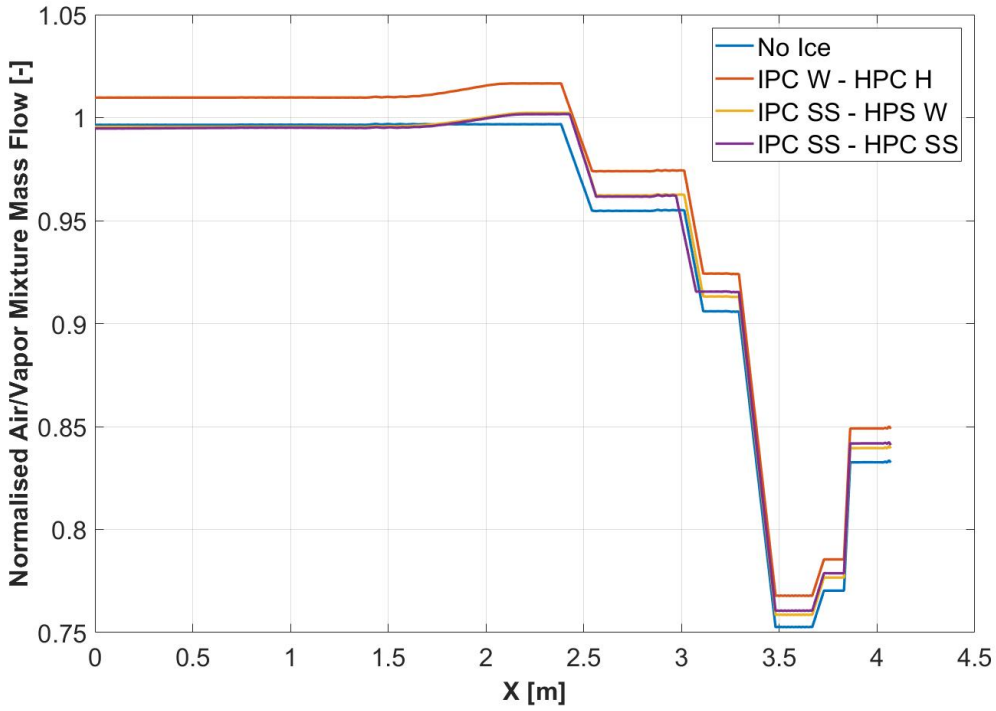


Figure 5.25: Normalised air/vapour mixture mass flow with different splitting set-ups

While the isolated compressor and the single shaft studies were performed splitting the compressor stage by stage, following the procedure described in section 4.3.4, the whole engine simulations were carried out considering each compressor as a single component, in order to save computational time.
The final analysis of this project has been to investigate the sensitivity of the solution to the compressor splitting procedure. Taking the simulation of the considered engine at an ambient temperature of 226.6 $K$ and with an ice ingestion rate of 4 $g/m^3$ as a baseline (case A), its results have been compared with two simulations that present different splitting set ups. In the first of the new simulations the IPC was divided into its 8 stages while the HPC was still considered as a single component (case B), and in the second one both the IPC and the HPC were splitted into their

respective 8 and 6 stages (case C).

The stage splitting induces a couple of main differences in the engine behaviour, in particular the division of the IPC in its composing stages. These main changes regarding the behaviour of the air/vapour mixture mass flow and of the IP and HP shafts rotational speeds are shown in Figure 5.25 and Figure 5.26.

Figure 5.25 shows the air/vapour mass flow through the compression system without ice ingestion and under three different splitting set ups: one where both the IPC and HPC are considered as whole components (W), one where the IPC its splitted stage by stage (SS) and the HPC is one component, and the third one where both compressors are splitted stage by stage. The most visible diffference is the lack of the overall mass flow increase during the ice ingestion for the last two cases.

On the other side, the main feature in the rotational speed behaviour, that can be observed in Figure 5.26, is the fact that modelling the IPC as a succession of its stages causes the intermediate pressure shaft rotational speed to actually drop. This, together with the progressive reduction of the HP shaft rotational speed drop, which is the second salient characteristic of the speeds behaviour, may induce to think that the two speeds do not converge anymore.

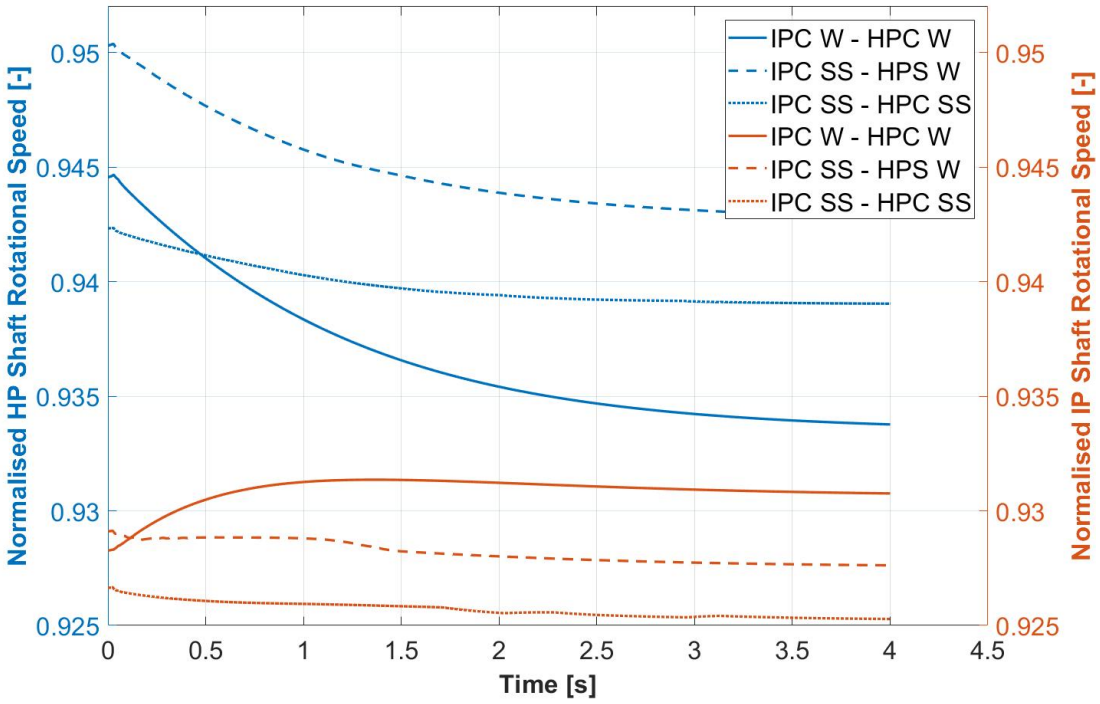


Figure 5.26: Normalised IP and HP shaft rotational speeds with different splitting set-ups

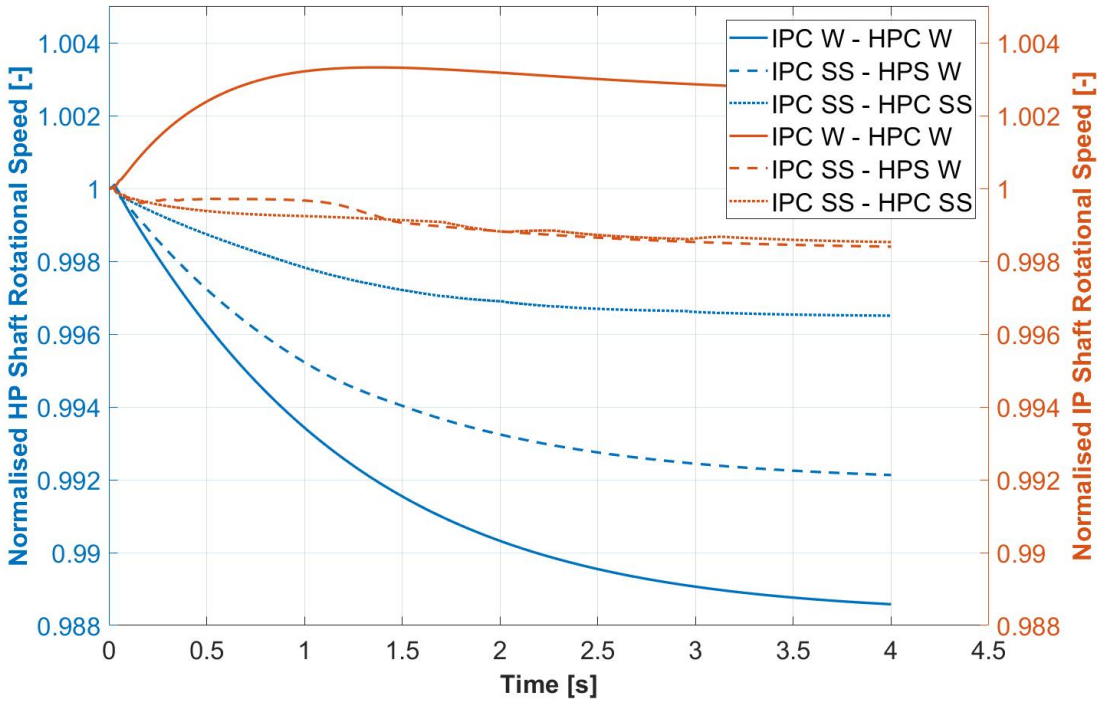


Figure 5.27: IP and HP shaft rotational speeds with different splitting set-ups, normalised with their initial value

However, this is only an optical illusion due to the different starting points that the rotational speeds have and the decreasing magnitude of their convergence. In fact, looking at Figure 5.27, where all the speeds are normalised with their respective inilital values, it is clear that, with the HP shaft speed decreasing always more than the IP shaft one, the two keep converging under all the different splitting strategies. The main reason for the aforementioned different outcomes that we have changing the splitting set-up is that, by splitting the compressor in its composing stages, we allow the stages to rematch and shift loading, as it was seen in section 5.1. This is particularly evident when looking at the IPC total temperature. Figure 5.28 shows the total temperature throughout the IPC in cases A and B, both with and without ice ingestion, each of them normalised with their own initial values. In this figure, it is clearly visible the different slope of the total temperature profile between cases A and B. With no ice ingestion the total temperature grows linearly throughout the compressor for case A, while its slope gradually increases when the compressor is split into its stages. When the particles are introduced, case A total temperature profile is parallel to the one without particles once these are completely vaporised, on the other side, in case B the latter stages are more loaded than they were without particles, as it was seen in section 5.1, leading to a slightly reduced temperature drop

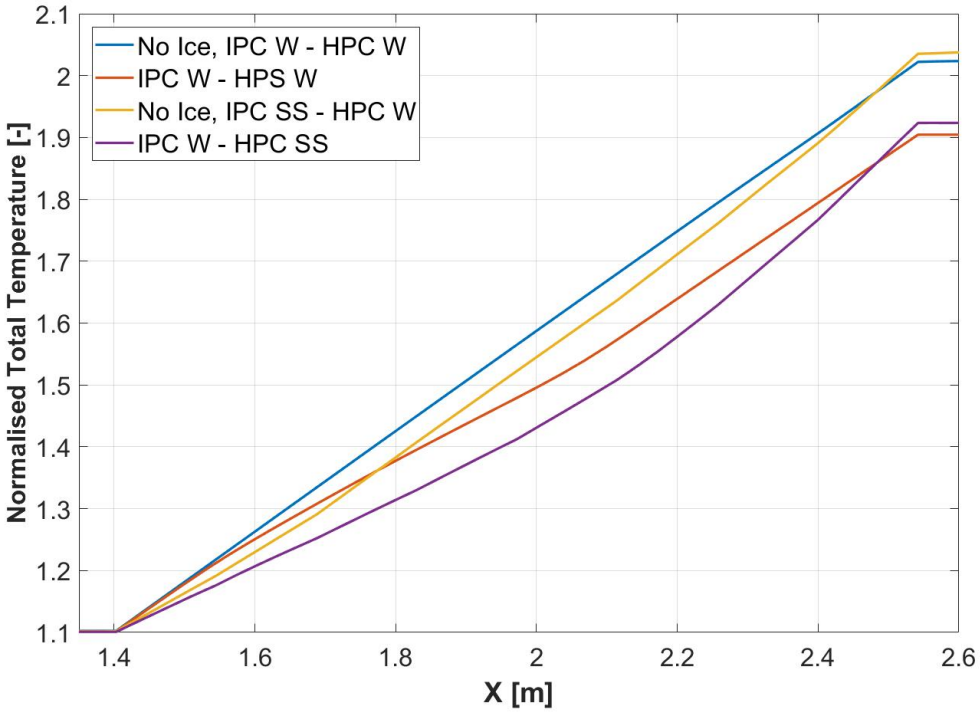


Figure 5.28: Normalised IPC total temperature with different splitting set-ups

compared to case A.
This reduced drop can be noticed also in the static temperature, and is transferred until the end of the compression domain, as it is reported in Table 5.3.

| Splitting set-up | No ingestion $[K]$ | Ice ingestion $[K]$ | $T_s$ drop [%] |
|---|---|---|---|
| IPC W - HPC W | 1307.2 | 1263.0 | 3.38 |
| IPC SS - HPC W | 1323.2 | 1291.0 | 2.43 |
| IPC SS - HPS SS | 1330.5 | 1297.2 | 2.50 |

Table 5.3: NGV throat static temperature behaviour

With the NGVs being choked, the static temperature at that point defines the mass flow of the whole compression system, and this reduced drop in static temperature at the throat of the NGVs explaines the lack of overall increase in mass flow when splitting the compressors into single stages. In fact, if the additional mass flow available thanks to the NGVs throat area temperature drop is equal or lower to the total vapour mass being introduced by the particles evaporation, it is not possible for the overall mass flow to increase, and it might actually potentially decrease.
The second main difference in behaviour when comparing the three simulated cases is the fact that, when splitting the IPC stage by stage, the IP shaft slows down instead of accelerating. The reason for this can be found again in the stage rematching that

takes place when introducing the particles. As Table 5.4 shows, in fact, while there is a drop in the temperature ratio performed by the early stages, once the particles are completely dissolved the latter stages present actually an increase in temperature ratio.

| | Stage 1 | Stage 2 | Stage 3 | Stage 4 | Stage 5 | Stage 6 | Stage 7 | Stage 8 |
|---|---|---|---|---|---|---|---|---|
| No Ice | 1.0818 | 1.0827 | 1.0905 | 1.0819 | 1.0754 | 1.0746 | 1.0747 | 1.0770 |
| Ice | 1.0687 | 1.0643 | 1.0624 | 1.0618 | 1.0679 | 1.0799 | 1.0845 | 1.0888 |

Table 5.4: IPC stages temperature ratios

Moreover, the later stages also have to process an increased mass flow due to the particles vaporization. These two effects coupled together lead to a reduction of the power requirement for the first stages, but an increase for the latter ones. This is confirmed by Figure 5.29, where the value of $\dot{m}\Delta T$ is shown over time for the different stages. Considering that the value of air heat capacity increases with temperature, it is easy to understand how the last few stages are the main contributors to the total compressor power requirement, causing it to actually increase with the ingestion of ice particles, instead of decrease as it was found when considering the compressor as a single component.

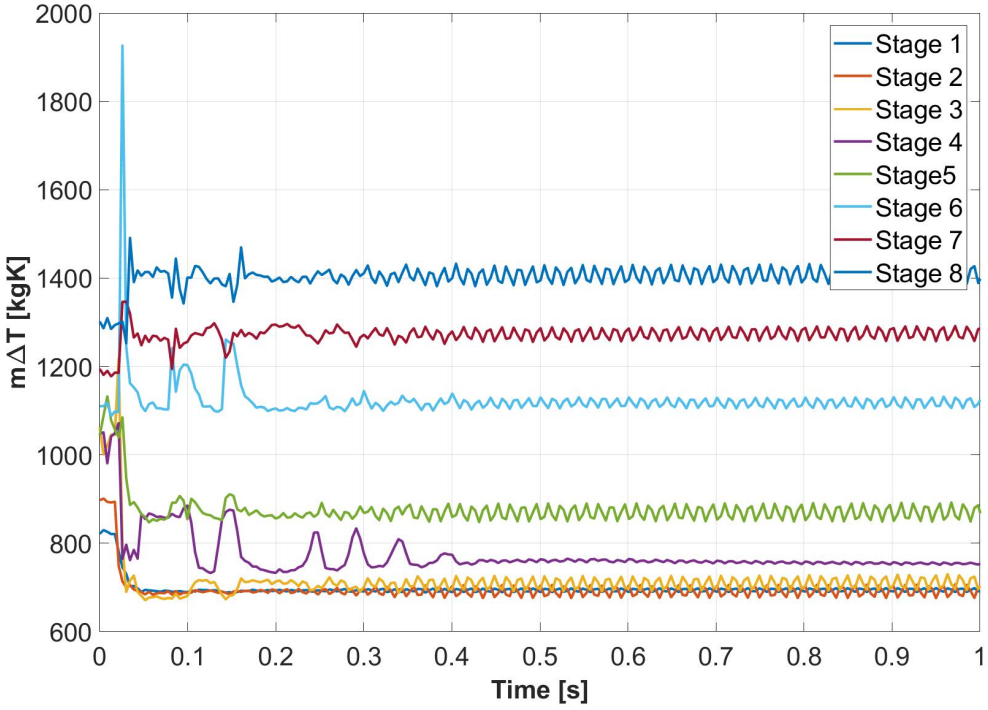


Figure 5.29: $\dot{m}\Delta T$ for the different IPC stages

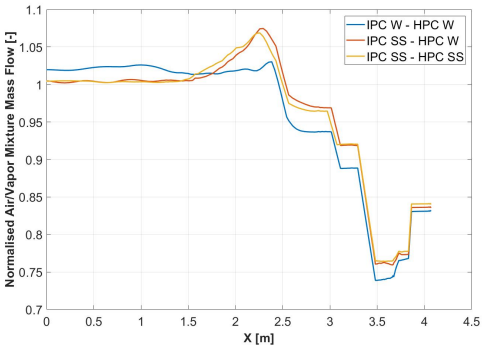


(a) Normalised mass flow at $t = 0.0275\ s$

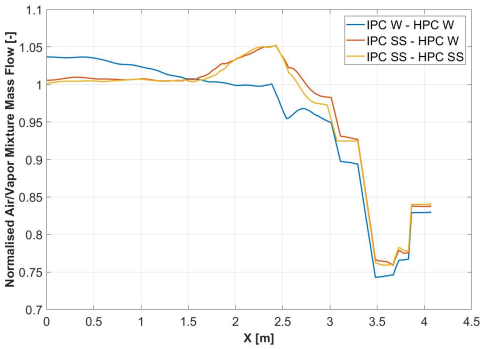


(b) Normalised mass flow at $t = 0.0300\ s$

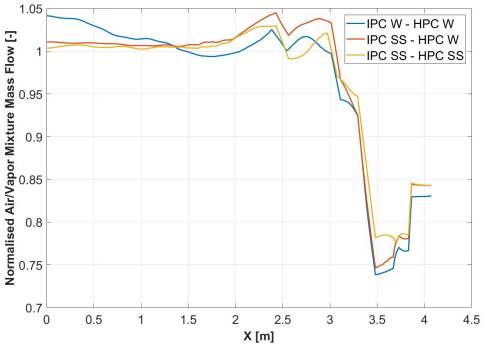


(c) Normalised mass flow at $t = 0.0325\ s$

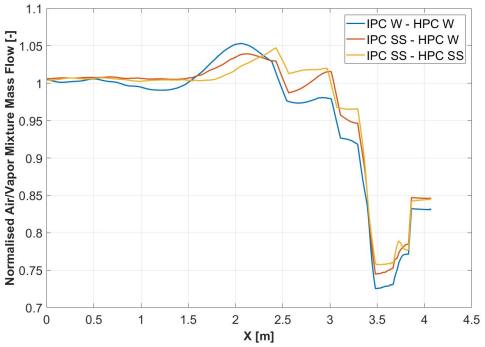


(d) Normalised mass flow at $t = 0.0350\ s$

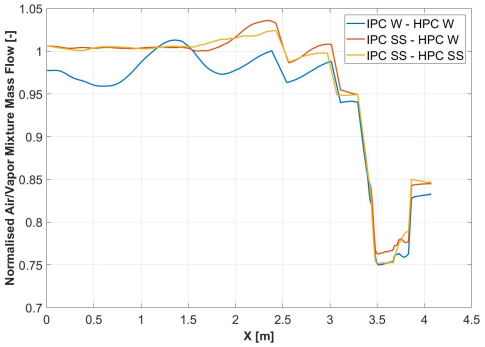


(e) Normalised mass flow at $t = 0.0375\ s$

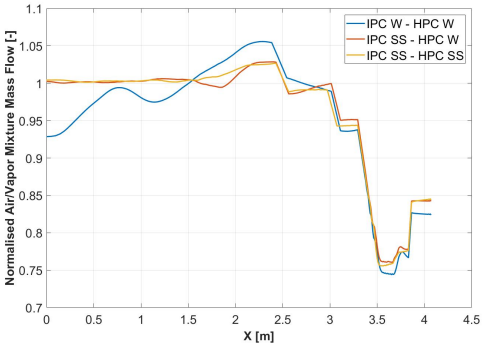


(f) Normalised mass flow at $t = 0.0400\ s$

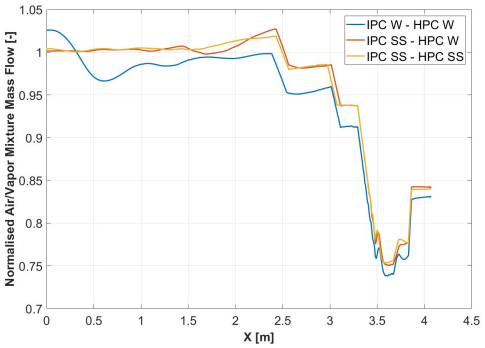


(g) Normalised mass flow at $t = 0.0425\ s$

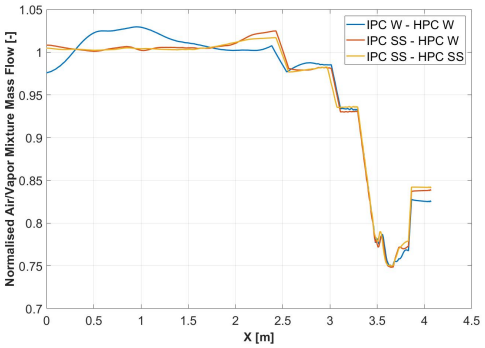


(h) Normalised mass flow at $t = 0.0450\ s$

Figure 5.30: Air/vapour mixture mass flow throughout the compressor at different time steps with variour splitting set-ups

However, these findings are in contrast with what was found analysing the single shaft case, where the compressor was also split stage by stage. Hence, more research is necessary to understand which parameters influence the behaviour of the shaft connected to the compressor that hosts the bigger portion of the particles evolution (e.g. compressor and turbine design, operative conditions, ice particles characteristics).

Finally, the last effect induced by the compressor splitting is the progressive reduction of HP rotational speed drop from case A to case B and C. As it can be seen in Figure 5.30, the splitting of the compressor leads to a progressive reduction of the mass flow variation, hence a smaller change in the HPC mass flow, which was the main driver of the HP shaft behaviour.

# Chapter 6

# Conclusions and Future Work

This last chapter of the thesis will be divided into three main sections.
In the first one, the whole project will be summarised, starting from its aim and motivations, followed by a description of the methodology and the simulations results and findings. The limitations of the presented model and of its results will also be discussed.
The second part of this chapter will be focused on the future work that the author considers to be helpful for either overcoming the limitations of the present study, expand the capabilities of the presented model, or could result in new findings and a better understanding of the ice ingestion phenomenon using this same method.
The last part will discuss the impact that this project will and could have on both the aerospace industry and future research. On one side, in fact, there are the possible applications of the present model for the industry, and on the other the potential new findings of the future projects that could start from this research effort and the industrial applications of those same findings.

## 6.1 Summary

Engine ice ingestion is a complex phenomenon, that has started to gain attention only recently. This research has looked at it from a different perspective from the rest of the literature because of the background and the motivations for this project. In fact, while many of the previous publications looked at specific events related to ice ingestion or specific aspects of it, the rationale for this research was to analyse the general behaviour of the engine during ice ingestion in order to be able to characterise

it and identify its main features. In order to do so, a simulation method had to be formulated. The results of these simulations could then generate enough data to train a data base model capable of identifying the ice ingestion behaviour and communicate its occurence to the pilots, possibly improving their decision making capabilities.

### 6.1.1 Method

The cornerstone of the method that was followed to simulate the phenomenon of ice crystals ingestion was the division between the fluid flow entering the engine and the ice particles and water droplets being ingested.
On one side the flow behaviour was modelled using a MATLAB code already in development by the Cranfield UTC called WEST. WEST simulates the transient behaviour of the core engine main gas path by dividing it between the compression side and the expansion side. The compression side is modelled using 1-D Euler equations with source terms to take into account the effects of bleed valves, compressors and combustion chamber. The expansion side is solved via quasi steady state matching. Once both the compression and the expansion sides are solved, a mechanical manager calculates the torque on the two sides of each shaft of the engine and determines the shafts rotational speeds for the subsequent time step.
On the other side, the particles were modelled adopting a Lagrangian approach. Every given time step, a defined number of particles is introduced in the main gas path. The model then follows their evolution as they heat up, accelerate, melt and evaporate/sublimate. A series of assumptions are made: all the particles have the same diameter, the particles temperature remains constant within the particle itself, melting process and vaporisation at critical temperature take place at constant temperature. Moreover, particles break-up and droplets splashing were taken into consideration as well, with the assumptions that the particles can break up and the droplets splash only when crossing the rotor blades leading edge sections. Additionally, there is also the possibility to simulate ice particles accretion, using a model based on findings obtained by NASA.
The influence of the particles on the fluid flow is accounted for using three additional source terms to the Euler equations and one new mass equation. The new mass equation is required by the introduction of a new species, the water vapour, and the three new source terms model the effects of the particles on mass, in the new mass equation, momentum and energy. Finally, also the particles blockage effect and the changes in the fluid thermodynamic properties due to the change in the

fluid composition were taken into consideration. One by changing the passage area and the other by modifying the fluid properties according to the humidity ratio.

### 6.1.2 Findings

The described model was used to simulate increasingly complex systems.

#### Isolated compressor

At first, a three spool commercial engine IPC compressor was run at take-off conditions and constant rotational speed. This set of simulations was compared with those performed by Kundu at al.[8], showing the same stage rematching highlighted in their study.
The main part of the study, was then to use the present model toperform single shaft and whole engine simulations.

#### Overview of ice ingestion physical effects

The particles are ingested together with air into the engine. As the air is heated up, compressed and accelerated by the engine compression system, it drags forward the particles making them accelerate, and a temperature difference is established between air and particles. This temperature gradient, coupled with the difference in water concentration between the ice and water particles and the surrounding air, causes the particles to evaporate, heat up and melt. All these phenomena determine an absorbtion of energy and release of mass by the particles towards the main flow. These two phenomena have two opposing effects on the engine behaviour: On one side, the energy absorbtion has an intercooling effect on the operative fluid, allowing the compressor to operate more efficiently. On the other side, the reduced temperature and the release of water vapor from the ice particles and water droplets causes an increase in massflow, which determines an increase in power demand from the compressor. The combination of these two phenomena, one that would determine an acceleration of the engine shaft, and the other that would cause the shaft to slow down, and the magnitude of their effects determines the behaviour of the engine at a system level, according to the different operative conditions.
A series of operative conditions have also been analysed in the study, and the results are summarised in the remaining of this section.

**Single shaft analysis**

For the second part of this computational effort, the full HP portion of a commercial high bypass turbofan engine (compressor, combustion chamber and turbine) at take-off conditions was modelled. Even though this set of simulations was only meant to be a stepping stone before simulating a full engine, it gave some interesting insight about the effects of ice ingestion and the interactions between different components. The HP shaft rotational speed was found in fact to accelerate as a response to the ingestion of ice, despite the increase in mass flow that was registered. This was due to the fact that, once the increased mass flow reached the turbine, the heat absorbed by the ice particles caused the compressor power demand to be lower than the one generated by the turbine.

**Whole engine analysis**

Finally, the bulk of this work was the modelling of the full core engine of a commercial three spool high bypass turbofan engine at cruise conditions. A series of analyses were performed, and the results can be summarised as follows:

- The simulations were successful in reproducing the convergence of shafts rotational speeds, increase in P30 and decrease in T30 observed in in-flight data
- Overall engine mass flow was increased by ice ingestion, with further increase throughout the compression domain due to particles evaporation
- Total temperature along the compression domain was reduced by the introduction of ice particles, especially after the beginning of the particles melting process, causing T30 to decrease
- With the reduction of temperature, the operating fluid became more easily compressible, causing P30 to increase
- The aforementioned intercooling effect that the particles have on the compressor working fluid caused the IP shaft to accelerate
- With the particles being completely evaporated by the end of the IPC, no heat absorbtion took place in the HPC, causing the HP shaft to decelerate due to the transient effect of the mass increase within the high pressure compressor
- Higher ice ingestion rates increased the effects of the ice crystals

- Smaller particles had a smaller impact on the engine behaviour, since they would heat up and evaporate much more quickly and absorb a bigger portion of the total heat necessary for them to vaporise before even entering the IPC, hence modifying its performance to a smaller degree

- Increasing the ambient temperature produced an increase of the particles effects due to the lower air mass flow ingested by the engine. This was due to the fact that, with the ice mass flow being linked to the air volumetric flow, which is not influenced by the ambient temperature, the ratio between ice and air ingested mass flows was increased

A series of whole engine simulations were carried out to try to showcase the capability of the code to perform ice accretion simulations. Unfortunately none of the attempts produced the right conditions for ice accretion. However disappointing, this result was most likely induced by the fact that the considered engine is not known for experiencing ice particles accretion in flight. Additional research is then necessary to verify the validity of the implemented ice accretion model.
In the last part of the research, a comparison was done between different simulation set-ups for the full engine simulations. The usual set-up, with both the IPC and the HPC considered as single components, was compared with one where only the IPC was modelled as an ensemble of its eight stages, and with a third one were both compressors were divided stage by stage. There were a few differences between the three simulations. The first one of these differences was that, once the IPC was divided in its stages, the overall increase in mass flow disappeared, which is explained by the fact that, due to the stage rematching phenomenon already highlighted by Kundu et al.[8] and observed in the isolated compressor simulations, the temperature drop at the NGVs is reduced compared to when the IPC is considered to be a whole component. The second main difference was in the behaviour of the IP shaft. While in the first simulation the IP shaft would accelerate and the HP one would decelerate, in the second and third cases they would both decelerate. However, with the rate at which the HP shaft decelerated being higher than the IP shaft one, the two rotational speeds were still converging. This second difference can still be explained by the stage rematching, since the later stages of the IPC, unaffected by the particles, ended up delivering a higher temperature ratio than before, requiring an increased power. Finally, the splitting of the HPC resulted in a much more stable simulation, which induced a slight reduction of the HP shaft deceleration. While it could be argued, and the author would agree, that the most reliable simulations performed are those where the compressors were divided stage by stage, since they better capture

an important feature of the engine behaviour such as the stage rematching, more research is needed to thoroughly compare the three set-ups. Moreover, the stage by stage simulations are more computationally demanding than those where the compressors are taken as a whole component. Hence, depending on the application, all three simulation strategies could be applied, since they all qualitatively captured the main characteristics of the engine behaviour.
In conclusion, the modelling method presented in this dissertation showed some very promising results for what concerns the simulation of engine behaviour under ice ingestion conditions, reproducing some of the features observed in in-flight data. However, like any other computational tool, it is not free of limitations, which will be the topic of the next subsection.

### 6.1.3 Limitations

Before discussing the limitations of the modelling method itself, it is necessary to highlight what could be considered the main limitation of the present study as a whole, which is the lack of validation. The presented results, in fact, were not quantitatively compared with any experimental or already validated data. There has been only a qualitative comparison of compressor behaviour against previous studies in literature for the isolated compressor, while for the full engine simulations the qualitative detection of the same shaft speed, P30 and T30 trends found in in-flight data were considered. Considering in particular the case of the full engine simulations, it would have been impossible to validate the results against the available in-flight data due to the lack of information which would have been needed to appropriately simulate even just one case. In the data received, in fact, there was no information about the ice ingestion rate, the ambient humidity, or even the thrust handle, fuel flow or bleed management. Thus, in order to validate the results of this method, an experimental campaign might be needed, which will be discussed in the next section.
On the other hand, the method does present some limitations, some of which, such as the lack of complexity of a monodimensional model, are unavoidable considering that the aim of the project was to capture the overall behaviour of a full engine. In fact, an increased level of complexity, while theoretically bringing the model closer to mimic the actual mechanisms of ice ingestion, would have likely caused the method to be excessively computationally demanding.
Instead, the focus of this analysis will be mainly on the assumptions and the models used for the particles and their evaluation, as well as the modelling of their influence on the main flow.

First of all, the ingested particles were all considered to be spheres having all the same diameter. Both these assumptions are inaccurate, as the ice crystals in the atmosphere would have a statistical distribution around a mean diameter value, if not even a random diameter distribution, and shapes that vary greatly from one to another.
A second issue (even though its effects were not present in the research due to the fact that no simulations showed ice accretion) has to do with the ice accretion rate. In fact, the values of ice growth rate were taken from the literature, and in particular from NASA publications on the topic[5]. These values, however, were obtained from an experimental and computational campaign conducted on an engine very different from the one considered for this study, and is very likely that a parameter like the accreted ice growth rate is extremely dependant on the engine architecture.
Changing now the focus from the particles and ice modelling to the way these influence the fluid flow, it is necessary to highlight how the proposed method does not take into consideration the fact that the water vapour, once it has been generated by particles evaporation and/or sublimation, has to be heated by the surrounding fluid from the original particles temperature until it reaches the fluid flow temperature. Instead, the vapour in the model is considered to be already at the flow temperature, neglecting the aforementioned last passage, resulting in a reduced estimation of the enthalpy absorbtion.
Finally, it has to be noted that there was no thermodynamic modelling of the bypass duct and of the performance of the bypass portion of the fan. While this was a characteristic that was carried over from WEST, and allowed to simplify the method by not having to model the portion of the particles that would be ingested by the bypass duct against those entering the core (scooping effect), it could be argued that the engine performance modelling is not really complete without taking into consideration the full fan performance.
All these limitations that were just discussed could be considered also hints for where to direct the future work on this subject, and how to further develop the modelling tool presented in this thesis, which will be the subject of the next section.

## 6.2 Future work

While this research project did accomplish the objective of developing a new method to simulate ice particles ingestion, it also opened a lot of room for further research, going from improving the method itself to applying it for new purposes. The aim of

this section is to explore these possibilities, and possibly give some suggestions on how to pursue them.

### 6.2.1 Validation

As already mentioned, one of the main limitations of this study results is their lack of validation. It will then be necessary for the future to provide some experimental data that could be compared against the model results.
In order to pursue this goal, three alternatives are proposed here, each having their own advantages and disadvantages, and are presented here in order of decreasing complexity.
The first strategy would be to fly a highly instrumented aircraft throught ice ingestion conditions. While this option is the one that would most closely mimic the results of a real in-flight event, it also presents numerous problems. First of all, again the data that would need to be provided for the validation could not be limited to the engine performance, but would have to include the engine control logic, including fuel flow and bleed valves management, and eventual changes to the thrust handle operated by the pilot. Moreover, ambient parameters would need to be controlled, such as pressure, temperature and relative or specific humidity. Finally, probably the most complex measurement to accomplish would be the estimation of the ice ingestion rate, and possibly of the mean diameter of the ice crystals.
The second option would be to set up an experimental rig where most of the aforementioned variables could be controlled. Thanks to the work done by NASA on the subject of ice particles accretion induced rollbacks there would also be a good amount of literature on the subject and on how to emulate the ice ingestion conditions in a controlled environment[2, 3, 35]. Moreover, in order to validate the method, it might not be necessary to build an experimental facility which would have to accomodate for a large high bypass turbofan, as it would be probably prohibitively expensive. It could be possible to arrange a smaller facility, given that the design parameters necessary to run a simulation are known for the tested engine. A small multiple shaft engine would be the best option for a validation campaign. It is the opinion of the author, however, that also a single shaft engine might be enough to test the method, as long as there is the posibility for the shaft rotational speed to vary, as the power demand required by the compressor and the power output generated by the turbine change with the ingestion of the ice particles.
Finally, the last option would be to start a cooperation between Cranfield UTC, Rolls-Royce, NASA and eventually Honeywell, provider of the engine tested by the

American agency, to obtain their experimental results and the tested engine characteristics. In this way, a series of simulations could be set up modelling the exact same conditions tested by NASA, and their experimental results could be used for validation purposes. Even though this might seem the easiest of the options, it might present some problems due to the eventual resistance of either Honeywell to provide design parameters to a research entity tied to a competing engine manufacturer, or NASA to provide experimental data to another research institution.

### 6.2.2 Ice accretion modelling

Closely related to the necessity for validation, is the one to carry out ice accretion simulations that actually show presence of ice accretion. As already mentioned, the ice accretion test cases resulted to be highly inconclusive. While none of the cases showed ice accretion, it is most likely that this lack of results is due to the engine being simulated, which has never shown to suffer of ice particles accretion.
It is then necessary, for future research, to address this gap by carrying out a simulation campaign using an engine known for experiencing ice particles accretion. For this second need, adopting for validation purposes the last strategy proposed in the previous subsection would be the preferred option. In fact, the engine that was being tested by NASA has shown to experience ice accretion, and the specific event that NASA was replicating was an ice accretion induced engine rollback. These characteristics would allow at the same time to validate the overall method and show its capability to perform simulations involving ice accretion.

### 6.2.3 Model improvements

A second potential stream of research originating from this work could be focused on improving the current model.
When performing an ice ingestion simulation with new ambient conditions, an ice free simulations had to be run and reach stability and steady state starting from an educated guess for what concerns the initial conditions. This first simulation gave the initial conditions for the following ice ingestion ones. One of the main challenges of the project has been to actually find the right starting conditions for a stable ice free simulation. This was due to the fact that, as it was mentioned earlier, WEST is a UTC developed tool, which was still being developed and refined as this project was being carried out. One of the main issues encountered was that the version of

WEST used for this study was not able to simlulate compressor operations in unstable regions of the compressor maps, so that the initial conditions had to closely mimic the actual conditions for a certain operating point. Most of these stability issues have however been corrected along the past few years. Thus, the first model improvement suggested here is to transfer the ice ingestion code and its modifications to WEST into the latest version of the Whole Engine Simulation Tool. This would most certainy guarantee a more efficient workflow for the future. Moreover, WEST latest version has also some surge modelling capabilities, having passed the TRL4 gate for surge modelling.

Most of the method improvements, however, would be ways to address the limitations mentioned in the previous section.

The first of the limitations that would need to be addressed, for its potential impact on the results, is the introduction of a method to take into account the enthalpy necessary to raise the water vapour temperature from the particles temperature to the flow one.

A rigorous formulation might require to introduce a series of new equations to track the motion and evolution of different portions of vapour that have evaporated at different times, thus having a different temperature. This, however, would introduce such a level of complexity that it would likely completely nullify the purpose of using a 1D method.

On the other hand, the most simple way to take into account for the vapour temperature increase would be to calculate the enthalpy needed, and subtract it from the flow during the very same time step as the vapour is produced, or during the following one. While it might seem too simplistic, if the time needed for the vapour to reach the flow temperature is of the same order of magnitude of a calculation time step, this second option would most likely be the best trade off for taking into consideration this phenomenon while still reducing the computational demands of the method as much as possible.

Other two factors that influence the simulations results are particles size and shape. As already stated, the current method considers the ingested particles to all be spheres with a determined diameter. A good improvement of the model would be to consider the variability in shape and mass of the particles. While the solution proposed by Kundu et al.[8, 9, 10, 11, 12] of separately modelling each single particle would be the most rigorous one, a good option to not cause an excessive increase in the simulations computational requirements would be to introduce the possibility to have different subgroups of particles introduced at each time step, each with its own shape and size.

As already mentioned, the method is not capable at the moment of estimating the engine thrust, due to the lack of bypass duct modelling. While this would probably need some rethinking of part of the WEST structure, it would also present a series of ice particles modelling challenges, such as the definition of the portion of particles that are ingested by the bypass duct instead of entering the core (scoop effect[27]).
The final improvement that could be made on the present method is the modification of the ice accretion growth rate values to update them with new data, that would be relative to the actual engine being simulated. This improvement has been listed as the last, as it would require an experimental campaign for every major engine architecture that needs to be modelled, which would result in a substantial economic burden for the financing institution.

### 6.2.4 Additional functionalities

The third direction towards which research could head starting from this dissertation is the addition of new functions to the method presented in this thesis.
While WEST already has the possibility to simulate the full Secondary Air System (SAS), this subsystem was not modelled in the present work, in order to focus the effort on building the fundamental ice ingestion capability. This, however, together with the addition of a fuel flow and bleeds management logic, would result in the possibility to carry out a true full engine simulation.
The most obvious functionality that could be added to a method already accounting for ice particles ingestion and ice accretion is the possibility to include ice shedding. This could be done, for example, by simply setting a limit for ice accretion that, once met, triggers the release of a determined amount of ice in the form of one or more pieces, that would then be treated as an additional group of particles. This mehod could then be refined by including specific models for ice shedding, which would include parameters such as the maximum size of ice accretion or the sizes of the detatching ice pieces.
Finally, the same modelling methodology could be used to model the ingestion of other particulate objects such as ash or sand, and analyse their thermodynamic effects on the engine performance. In particular, the main changes would only need to take into account the differences between the thermodynamic properties of the new substances compared to ice and water. In fact, such modelling efforts could result to be even less complex than simulating the ingestion of ice particles, since materials such as volcanic ash and sand would not evaporate, hence not requiring the introduction of the second mass equation.

Moreover, the methodology could be used to model other ingestion problems such as inflammable materials, where the main difference would be that in this case the ingested substance would release heat instead of absorb it.

### 6.2.5 New analyses

Finally, the method as it is could actually already be used for some very interesting new analyses.
It has already been stated that some engine architectures are more prone than others to ice particles accretion. The same could be said about engine instabilities caused by ice ingestion, such as compressor surge. The present model and its modularity offer the chance to change many different design parameters, such as for example the stage loading scheme, and simulate different engine architectures, for example two or three spool engines. Comparing these results could help understand which parameters have the most influence on the capability of an engine to be resilient to ice ingestion conditions, and which architectures perform better in those hostile conditions.

## 6.3 Impact

The last section of this thesis is dedicated to the impact that this project will potentially have on the aerospace industry, on top of its possible applications.
The first, most obvious application for the modelling capability developed during this study would be to produce, through simulations, the amount of engine performance data required to train a data-based model capable of recognizing the engine behaviour during ice particles ingestion. The developed detection capability will then be used to inform the pilots about the flying conditions and improve their decision making capability. As it was described in the introduction, this was the main reason for this project to start in the first place.
The method described in this dissertation could also find an application during the preliminary design phase of a new engine. In fact, once the overall design characteristics of an engine are defined, the present tool could be used to assess how vulnerable the new engine would be to ice ingestion conditions, allowing the manufacturer to make the appropriate modifications, if necessary.
While those already mentioned are the most direct applications of the work pre-

sented in this thesis, it is worth mentioning that all the new possibilities for future work and future projects listed in the previous section will have their own impact and applications. In particular, the author would like to list two examples for the impact of some of the possible future projects: one of them being the modelling of other particles ingestion, and the other the identification of the most influential design parameters for engine ice ingestion resilience.

The modelling of other particles ingestion, such as volcanic ashes or sand, could be applied, similarly to the modelling of ice ingestion, to the training of a data-based model capable of recognising the engine behaviour in those conditions, which would increase the number of scenarios where the engine would be able to communicate to the pilots useful information about the flying environment.

On the other hand, the identification of the best engine architecture or the design parameters that have the most influence on the capability of the engine to resist to ice ingestion conditions could be used as indications for the design of future engines, to the point where ice ingestion does not really represent a problem anymore.

In conclusion, is the author opinion that one of the most important contributions of this research effort has been the opening of a vast number of possibilities for new projects, with each of these projects producing meaningful results and new possibilities for their application in the aerospace industry.

# References

[1] Philip C. E. Jorgenson, Joseph P. Veres, William B. Wright, and Ryan D. May. Engine icing modeling and simulation (part I): Ice crystal accretion on compression system components and modeling its effects on engine performance. *SAE 2011 International Conference on Aircraft and Engine Icing and Ground Deicing*, 2011.

[2] Joseph P. Veres and Philip C. E. Jorgenson. Modeling commercial turbofan engine icing risk with ice crystal ingestion. *5th AIAA Atmospheric and Space Environments Conference*, 24-27 June 2013.

[3] Joseph P. Veres, Philip C. E. Jorgenson, and Ryan Coennen. Modeling of commercial turbofan engine with ice crystal ingestion; follow-on. *6th AIAA Atmospheric and Space Environments Conference*, 16-20 June 2014.

[4] Jospeh P. Veres, Philip C. E. Jorgenson, and Scott M. Jones. Modeling of highly instrumented Honeywell turbofan engine tested with ice crystal ingestion in the nasa propulsion system laboratory. *8th AIAA Atmospheric and Space Environments Conference*, 13-17 June 2016.

[5] Joseph P. Veres, Philip C. E. Jorgenson, Scott M. Jones, and Samaun Nili. Modeling of a turbofan engine with ice crystal ingestion in the NASA propulsion system laboratory. *Proceedings of ASME Turbo Expo 2017: Turbomachinery Technical Conference Exposition*, 16-30 June 2017.

[6] Philip C. E. Jorgenson, Jospeh P. Veres, and Scott M. Moses. Modeling the deterioration of engine and low pressure compressor performance during a roll back event due to ice accretion. *50th AIAA/ASME/SAE/ASEE Joint Propulsion Conference*, 28-30 July 2014.

[7] Donald L. Simon, Aidan W. Rinehart, and Scott M. Jones. A dynamic model for the evaluation of aircraft engine icing detection and control-based mitigation

strategies. *ASME Turbo Expo 2017: Turbomachinery Technical Conference Exposition*, 26-30 June 2017.

[8] Reema Kundu, J. V. R. Prasad, Prashant Tiwari, Andy Breeze-Stringfellow, Peter Szucs, Tsuguji Nakano, and Byron Pritchard. Impact of engine icing on jet engine compressor flow dynamics. *48th AIAA/ASME/SAE/ASEE Joint Propulsion Conference and Exibit*, 30 July - 01 August 2012.

[9] Reema Kundu, J. V. R. Prasad, Swati Saxena, Rajkeshar Singh, Andy Breeze-Stringfellow, and Tsuguji Nakano. Analysis of stall onset in a multistage axial flow compressor in response to engine icing. *AIAA Propulsion Energy Forum*, 28-30 June 2014.

[10] Reema Kundu, J. V. R. Prasad, Swati Saxena, Rajkeshar Singh, Andy Breeze-Stringfellow, and Tsuguji Nakano. Modeling and analysis of ice shed in multistage compressor of jet engine. *6th AIAA Atmospheric and Space Environments Conference*, 16-20 June 2014.

[11] Reema Kundu. *Impact of Engine Icing on Jet Engine Compressor Flow Dynamics*. PhD thesis, Georgia Institute of Technology, 2015.

[12] Swati Saxena, Rajkeshar Singh, Andy Breeze-Stringfellow, and Tsuguji Nakano. Transient behavior in axial compressors in event of ice shed. *Proceedings of ASME Turbo Expo 2015: Turbine Technical Conference and Exposition*, 15-19 June 2015.

[13] Swati Saxena, George T. K. Woo, Rajkeshar Singh, Andre Breeze-Stringfellow, Tsuguji Nakano, and Peter Szucs. Effects of ice and blade interaction models on compressor stability. *Journal of Turbomachinery*, April 2017.

[14] Ryan D. May, The-Huei Guo, Joseph P. Veres, and Philip C. E. Jorgenson. Engine icing modeling and simulation (part 2): Performance simulation of engine rollback phenomena. *SAE 2011 International Conference on Aircraft and Engine Icing and Ground Deicing*, 13-17 June 2011.

[15] Joseph P. Veres, Scott M. Jones, and Philip C. E. Jorgenson. Performance modeling of honeywell turbofan engine tested with ice crystal ingestion in the nasa propulsion system laboratory. *SAE 2015 International Conference on Icing of Aircraft, Engines, and Structure*, June 2015.

[16] G. P. Sallee and D. M. Gibbons. Propulsion system malfunction plus inappropiate crew response (PSM + ICR). Technical report, Aerospace Industries Association/The European Association of Aerospace Industries, November 1998.

[17] R. Paul Lawson, Leigh J. Angus, and Andrew J. Heymsfield. Cloud particles measurements in thunderstorm anvils and possible weather threat to aviation. *AIAA 34th Aerospace Sciences Meeting and Exhibition*, January 1996.

[18] Jeanne G. Mason, J. Walter Strapp, and Philip Chow. The ice particle threat to engines in flight. *44th AIAA Aerospace Sciences Meeting and Exhibition*, January 2006.

[19] E. J. Jensen, P. Lawson, B. Baker, B. Pilson, Q. Mo, A. J. Heymsfield, A. Bansemer, T. P. Bui, M. McGill, D. Hlavka, G. Heymsfield, S. Platnick, G. T. Arnold, and S. Tanelli. On the importance of small ice crystals in tropical anvil cirrus. *Atmospheric Chemistry and Physics*, August 2009.

[20] Andrew J. Heymsfield. Ice particle evolution in the anvil of a severe thunderstorm during CCOPE. *Journal of the Atmospheric Sciences*, November 1986.

[21] Matthew L. Grzych and Jeanne G. Mason. Weather conditions associated with jet engine power loss and dmage due to ingestion of ice particles: What we've learned throug 2009. *14th Conference on Aviation, Range, and Aerospace Meteorology*, January 2010.

[22] Jeanne G. Mason and Matthew Grzych. The challenges identifying weather associated with jet engine crystal icing. *SAE 2011 International Conference on Aircraft and Engine Icing and Ground Deicing*, 2011.

[23] A. Heinrich, R. Ross, G. Zumwalt, J. Provorse, V. Padmanabhan, J. Thompson, and J. Riley. Aircraft icing handbook - volume 1 of 3. Technical report, Department of Transportation Federal Aviation Administration Techincal Center, 1991.

[24] Hussein Kefel. A classic anvil cloud. [photograph]. *Available at: https://commons.wikipedia.org/wiki/File:A_Classic_Anvil_Cloud_Over_Europe.jpg (Accessed 12 December 2017).*

[25] Kamel Al-Khalil. Assessment of effects of mixed-phase icing conditions on thermal ice protection systems. Technical report, U.S. Department of Transportation Federal Aviation Administration, 2003.

[26] Manuel A. Rios and Young I. Cho. Analysis of ice crystal ingestion as a source of ice accretion inside turbofans. *38th Fluid Dynamics Conference and Exhibition*, 23-26 June 2008.

[27] Matthew Feulner, Shengfang Liao, Becky Rose, and Xuejun Liu. Ice crystal ingestion in a turbofan engine. *SAE 2015 International Conference of Aircraft, Engines and Structures*, June 2015.

[28] Peter Struk, Tom Currie, William Benjamin Wright, Daniel C. Knezevici, Dan Fuleki, Andy Broeren, Mario Vargas, and Jen-Ching Tsao. Fundamental ice crystal accretion physics studies. *SAE 2011 International Conference on Aircraft and Engine Icing and Ground Deicing*, 13-17 June 2011.

[29] Tom C. Currie, Peter M. Struk, Jen-Ching Tsao, Dan Fuleki, and Daniel C. Knezevici. Fundamental study of mixed-phase icing with application to ice crystal accretion in aircraft jet engines. *4th AIAA Atmospheric and Space Environments Conference*, 25-28 June 2012.

[30] Peter M. Struk and Christopher J. Lynch. Ice growth measurements from image data to support ice-crystal and mixed-phase accretion testing. *4th AIAA Atmospheric and Space Environments Conference*, 25-28 June 2012.

[31] Peter Struk, Tadas Bartkus, Jen-Ching Tsao, Tom Currie, and Dan Fuleki. Ice accretion measurements on an airfoil and wedge in mixed-phase conditions. *SAE 2015 International Conference on Icing of Aircraft, Engines, and Structures*, June 2015.

[32] Peter M. Struk, Jen-Ching Tsao, and Tadas Bartkus. Plans and preliminary results of fundamental studies of ice crystal icing physics in the NASA propulsion system laboratory. *8th AIAA Atmospheric and Space Environments Conference*, 13-17 June 2016.

[33] Peter M. Struk, Thomas P. Ratvasky andn Timothy J. Bencic, Judith F. Van Zante, Michael C. King, Jen-Ching Tsao, and Tadas P. Bartkus. An initial study of the fundamentals of ice crystal icing physiscs in the NASA propulsion system laboratory. *9th AIAA Atmospheric and Space Environments Conference*, 5-9 June 2017.

[34] Ronald V. Goodwin and David G. Dischinger. Turbofan ice crystal rollback investigation and preparations leading to inaugural ice crystal engine test at NASA PSL-3 test facility. *6th AIAA Atmospheric and Space Environments Conference*, 16-20 June 2014.

[35] Michael Oliver. Validation crystal icing engine test in the propulsion systems laboratory at NASA Glenn Research Center. *6th AIAA Atmospheric and Space Environments Conference*, 16-20 June 2014.

[36] Ashlie B. Flegel and Michael J. Oliver. Preliminary results from a heavily instrumented engine ice crystal test in a ground based altitude test facility. *8th AIAA Atmospheric and Space Environments Conference*, 13-17 June 2016.

[37] H. Beaugendre, F. Morency, and W. G. Habashi. Ice3d, fensap-ice's 3d in-flight ice accretion module. *40th AIAA Aerospace Sciences Meeting & Exhibition*, 14-17 January 2002.

[38] G. Croce, H. Beaugendre, and W. Habashi. Cht3d: Fensap-ice conjugate heat transfer computations with droplet impingement and runback effects, 14-17 January 2002.

[39] Colin S. Bidwell and Mark G. Potapczuk. Users manual for the NASA Lewis three-dimensional ice accretion code (LEWICE3D). Technical report, NASA, 1993.

[40] Xavier Veillard, Cristhian Aliaga, and Wagdi G. Habashi. Fensap-ice modeling of the ice particle threat to engines in flight. *2007 SAE Aircraft and Engine Icing International Conference*, September 2007.

[41] Shezad Nilamdeen and Wagdi G. Habashi. Multiphase approach toward simulating ice crystal ingestion in jet engines. *Journal of Propulsion and Power*, September 2011.

[42] Shezad Nilamdeen, Wagdi Habashi, Martin Aubé, and Guido Baruzzi. Fensap-ice: Modeling of water droplets and ice crystals, 22-25 June 2009.

[43] Colin S. Bidwell. Ice particle transport analysis with phase change for the $e^3$ turbofan engine using lewice3d version 3.2. *4th AIAA Atmospheric and Space Environments Conference*, 25-28 June 2012.

[44] Willima B. Wright, Philip C. E. Jorgenson, and Joseph P. Veres. Mixed phase modeling in glennice with application to engine icing. *AIAA Atmospheric and Space Environments Conference*, 2-5 August 2010.

[45] E. Steinthorsson, M. S. Liou, and L. A. Povinelli. Development of an explicit multiblock/multigrid flow solver for viscous flows in complex geometries. *29th Joint Propulsion Conference and Exhibition*, 28-30 June 1993.

[46] Ali A. Ameri. NASA Rotor 37 CFD code validation Glenn-HT code. *47th AIAA Aerospace Sciences Meeting Including The New Horizons Forum and Aerospace Exposition*, 5-8 January 2009.

[47] Colin Bidwell and David Rigby. Ice particle analysis of the honeywell alf502 engine booster. *SAE 2015 International Conference on Icing of Aircraft, Engines, and Structures*, June 2015.

[48] David L. Rigby, Joseph Veres, and Colin Bidwell. Three dimensional simulation of flow in an axial low pressure compressor at engine icing operating points. *SAE 2015 International Conference on Icing of Aircraft, Engines, and Structures*, June 2015.

[49] Aslie B. Flegel. Ice crystal icing research at NASA. *AIAA AVIATION Forum, 9th AIAA Atmospheric and Space Environments Conference*, 5-9 June 2017.

[50] William Wright, Mark Potapczuk, and Laurie Levinson. Comparison of LEWICE and GlennICE in the SLD regime. *46th AIAA Aerospace Sciences Meeting and Exhibition*, 7-10 January 2008.

[51] William B. Wright, Peter Struk, Tadas Bartkus, and Gene Addy. Recent advances in the LEWICE icing model. *SAE 2015 International Conference on Icing of Aircraft, Engines, and Structures*, June 2015.

[52] Tobias Hauk, Ilia Roisman, and Cameron Tropea. Invesigation of the impact behaviour of ice particles. *AIAA AVIATION Forum, 6th AIAA Atmospheric and Space Environments Conference*, 16-20 June 2014.

[53] Jose Palacios, Sihong Yan, Jason Tan, and Richard E. Kreeger. Experimental measurements of frozen and partially melted water droplet impact dynamics. *6th AIAA Atmospheric and Space Environments Conference*, 16-20 June 2014.

[54] Tom C. Currie, Dan Fuleki, and Ali Mahallati. Experimental studies of mixed-phase sticking efficiency for ice crystal accretion in jet engines. *6th AIAA Atmospheric and Space Environments Conference*, 16-20 June 2014.

[55] Philippe Villedieu, Pierre Trontin, and Rémi Chauvin. Glaciated and mixed-phase ice accretion modeling using ONERA 2D icing suite. *6th AIAA Atmospheric and Space Environments Conference*, 16-20 June 2014.

[56] E. Ayan and S. Ozgen. In-flight ice accretion simulation in mixed-phase conditions. *The Aeronautical Journal*, March 2018.

[57] Alexander Bucknell, Matthew McGilvray, David Gillespie, Xin Yang, Geoffrey Jones, and Benjamin Collier. Icicle: A model for glaciated & mixed phase icing for application to aircraft engines. *SAE 2019 International Conference on Icing of Aircraft, Engines, and Structures*, June 2019.

[58] John K. Lytle. The numerical propulsion system simulation: An overview. Technical report, NASA, 2000.

[59] Scott M. Jones. An introduction to thermodynamic performance analysis of aircraft gas turbine engine cycles using the numerical propulsion system simulation code. Technical report, NASA, 2007.

[60] Mark G. Turner, John A. Reed, Robert Ryder, and Joseph P. Veres. Multi-fidelity simulation of a turbofan engne with results zoomed into mini-maps for a zero-d cycle simulation. *ASME Turbo Expo 2004: Power for Land, Sea and Air*, 14-17 June 2004.

[61] Joseph P. Veres. Axial and centrifugal compressor mean line flow analysis method. *47th AIAA Aerospace Sciences Meeting including The New Horizon Forum and Aerospace Exposition*, 5-8 January 2009.

[62] Joseph P. Veres and Douglas R. Thurman. Conceptual design of a two spool compressor for the NASA large civil tilt rotor engine. Technical report, NASA, 2010.

[63] Joseph P. Veres, Philip C. E. Jorgenson, William B. Wright, and Peter Struk. A model to assess the risk of ice accretion due to ice crystal ingestion in a turbofan engine and its effects on performance. *4th AIAA Atmospheric and Space Environments Conference*, 25-28 June 2012.

[64] Jeffryes W. Chapman, Thomas M. Lavelle, Ryan D. May, Jonathan S. Litt, and Ten-Huei Guo. Toolbox for the modeling and analysis of thermodynamic systems (t-mats) user's guide. Technical report, NASA, 2014.

[65] Reema Kundu, J. V. R. Prasad, and Yedidia Neumeier. Validation of a 1d transient simulation model of a multistage axial compressor. *Proceedings of the ASME 2015 Gas Turbine India Conference*, 2-3 December 2015.

[66] Lucas Pawsey. *Shaft Failure and Overspeed Modelling.* PhD thesis, Cranfield University, 2018.

[67] R. Crowe, M. Sommerfeld, and Y. Tsuji. *Multiphase Flows with Droplets and Particles.* CRC Press LLC, 1998.

[68] Marco Vito Portincasa. Development of a transient combustion model. Master's thesis, Cranfield University, 2015.

[69] NASA. *CEA NASA. NASA Computer Program for Calculating of the Chemical Equilibrium with Applications.* NASA Glenn Research Center, Cleveland, OH.

[70] John. D. Anderson and John Wendt. *Computational Fluid Dynamics*, volume 206. Springer, 1995.

[71] Robert MacCormack. The effect of viscosity in hypervelocity impact cratering. *AIAA Hypervelocity Impact Conference*, 1969.

[72] World Meteorological Organisation. Guide to meteorological instrument and methods of observation. Technical report, WMO, 2010.

[73] Refrigerating American Society of Heating and Air-Conditioning Engineers. 2001 ashrae fundamentals handbook (si). Technical report, ASHRAE, 2001.

[74] J. R. Welty, G. L. Rorrer, C. E. Wicks, and R. E. Wilson. *Fundmentals of Momentum, Heat and Mass Transfer.* Wiley, 1969.

[75] Kaushik Das. *Numerical Simulations of Icing in Turbomachinery.* PhD thesis, University of Cincinnati, 2006.

[76] D. M. Murpy and T. Koop. Review of the vapour pressures of ice and supercooled water for atmospheric applications. *Quarterly Journal of the Royal Meteorological Society*, December 2006.

[77] International Association for the Properties of Water and Steam. Iapws industial formulation 1997 for the thermodynamic properties of water and steam. Technical report, IAPWS, 1997.

[78] Advisory Group for Aerospace Research & Development. Recommended practices for the assessment of the effects of atmospheric water ingestion on the performance and operability of gas turbine engines, AGARD advisory report no. 332. Technical report, AGARD, 1995.

[79] Chr Mundo, Martin Sommerfeld, and Cameron Tropea. On the modeling of liquid sprays impinging on surfaces. *Atomization and Sprays*, 1998.

[80] Engineering Toolbox. Water vapor - specific heat. *Available at: https://engineeringtoolbox.com/water-vapor-d_979.html (Accessed 21 September 2019)*, 2005.

# Appendix A

# Interpolation Tables

| $\frac{T\varepsilon}{k}$ [-] | $\Omega$ [-] | $\frac{T\varepsilon}{k}$ [-] | $\Omega$ [-] | $\frac{T\varepsilon}{k}$ [-] | $\Omega$ [-] |
|---|---|---|---|---|---|
| 0.30 | 2.6620 | 1.55 | 1.1820 | 3.60 | 0.9058 |
| 0.35 | 2.4760 | 1.60 | 1.1670 | 3.70 | 0.8998 |
| 0.40 | 2.3180 | 1.65 | 1.1530 | 3.80 | 0.8942 |
| 0.45 | 2.1840 | 1.70 | 1.1400 | 3.90 | 0.8888 |
| 0.50 | 2.0660 | 1.75 | 1.1280 | 4.00 | 0.8836 |
| 0.55 | 1.9660 | 1.80 | 1.1160 | 4.50 | 0.8610 |
| 0.60 | 1.8770 | 1.85 | 1.1050 | 5.00 | 0.8422 |
| 0.65 | 1.7980 | 1.90 | 1.0940 | 6.00 | 0.8124 |
| 0.70 | 1.7290 | 1.95 | 1.0840 | 7.00 | 0.7896 |
| 0.75 | 1.6670 | 2.00 | 1.0750 | 8.00 | 0.7712 |
| 0.80 | 1.6120 | 2.10 | 1.0570 | 9.00 | 0.7556 |
| 0.85 | 1.5620 | 2.20 | 1.0410 | 10.00 | 0.7424 |
| 0.90 | 1.5170 | 2.30 | 1.0260 | 20.00 | 0.6640 |
| 0.95 | 1.4760 | 2.40 | 1.0120 | 30.00 | 0.6232 |
| 1.00 | 1.4390 | 2.50 | 0.9996 | 40.00 | 0.5960 |
| 1.05 | 1.4060 | 2.60 | 0.9878 | 50.00 | 0.5756 |
| 1.10 | 1.3750 | 2.70 | 0.9770 | 60.00 | 0.5596 |
| 1.15 | 1.3460 | 2.80 | 0.9672 | 70.00 | 0.5464 |
| 1.20 | 1.3200 | 2.90 | 0.9576 | 80.00 | 0.5352 |
| 1.25 | 1.2960 | 3.00 | 0.9490 | 90.00 | 0.5256 |
| 1.30 | 1.2730 | 3.10 | 0.9406 | 100.00 | 0.5130 |
| 1.35 | 1.2530 | 3.20 | 0.9328 | 200.00 | 0.4644 |
| 1.40 | 1.2330 | 3.30 | 0.9256 | 400.00 | 0.4170 |
| 1.45 | 1.2150 | 3.40 | 0.9186 | | |
| 1.50 | 1.1980 | 3.50 | 0.9120 | | |

Table A.1: Collision diffusivity, $\Omega$, for mass diffusivity based on Lennard-Jones Potential, taken from Welty[74]

| $t\ [degC]$ | $\gamma\ [mm/degC^2]$ | $t\ [degC]$ | $\gamma\ [mm/degC^2]$ |
|---|---|---|---|
| 0.01 | 75.64 | 190.00 | 39.95 |
| 5.00 | 74.95 | 195.00 | 38.82 |
| 10.00 | 74.23 | 200.00 | 37.69 |
| 15.00 | 73.50 | 205.00 | 36.55 |
| 20.00 | 72.75 | 210.00 | 35.41 |
| 25.00 | 71.99 | 215.00 | 34.25 |
| 30.00 | 71.20 | 220.00 | 33.10 |
| 35.00 | 70.41 | 225.00 | 31.93 |
| 40.00 | 69.60 | 230.00 | 30.77 |
| 45.00 | 68.78 | 235.00 | 29.60 |
| 50.00 | 67.94 | 240.00 | 28.42 |
| 55.00 | 67.10 | 245.00 | 27.24 |
| 60.00 | 66.24 | 250.00 | 26.06 |
| 65.00 | 65.36 | 255.00 | 24.87 |
| 70.00 | 64.47 | 260.00 | 23.67 |
| 75.00 | 63.58 | 265.00 | 22.48 |
| 80.00 | 62.67 | 270.00 | 21.30 |
| 85.00 | 61.75 | 275.00 | 20.11 |
| 90.00 | 60.82 | 280.00 | 18.94 |
| 95.00 | 59.87 | 285.00 | 17.77 |
| 100.00 | 58.91 | 290.00 | 16.61 |
| 105.00 | 57.94 | 295.00 | 15.45 |
| 110.00 | 56.96 | 300.00 | 14.30 |
| 115.00 | 55.97 | 305.00 | 13.17 |
| 120.00 | 54.96 | 310.00 | 12.04 |
| 125.00 | 53.95 | 315.00 | 10.92 |
| 130.00 | 52.93 | 320.00 | 9.81 |
| 135.00 | 51.89 | 325.00 | 8.73 |
| 140.00 | 50.85 | 330.00 | 7.66 |
| 145.00 | 49.80 | 335.00 | 6.61 |
| 150.00 | 48.74 | 340.00 | 5.59 |
| 155.00 | 47.67 | 345.00 | 4.60 |
| 160.00 | 46.58 | 350.00 | 3.65 |
| 165.00 | 45.49 | 355.00 | 2.75 |
| 170.00 | 44.40 | 360.00 | 1.90 |
| 175.00 | 43.30 | 365.00 | 1.13 |
| 180.00 | 42.19 | 370.00 | 0.45 |
| 185.00 | 41.07 | 374.00 | 0.00 |

Table A.2: Behaviour of water surface tension with varying temperature[74]

| $T\ [K]$ | $C_p\ [kJ/kgK]$ | $T\ [K]$ | $C_p\ [kJ/kgK]$ |
|---|---|---|---|
| 175 | 1.850 | 1250 | 2.458 |
| 200 | 1.851 | 1300 | 2.490 |
| 225 | 1.852 | 1350 | 2.521 |
| 250 | 1.855 | 1400 | 2.552 |
| 275 | 1.859 | 1500 | 2.069 |
| 300 | 1.864 | 1600 | 2.662 |
| 325 | 1.871 | 1700 | 2.711 |
| 350 | 1.880 | 1800 | 2.756 |
| 375 | 1.890 | 1900 | 2.798 |
| 400 | 1.901 | 2000 | 2.836 |
| 450 | 1.926 | 2100 | 2.872 |
| 500 | 1.954 | 2200 | 2.904 |
| 550 | 1.984 | 2300 | 2.934 |
| 600 | 2.015 | 2400 | 2.962 |
| 650 | 2.047 | 2500 | 2.987 |
| 700 | 2.080 | 2600 | 3.011 |
| 750 | 2.113 | 2700 | 3.033 |
| 800 | 2.147 | 2800 | 3.053 |
| 850 | 2.182 | 2900 | 3.072 |
| 900 | 2.217 | 3000 | 3.090 |
| 950 | 2.252 | 3500 | 3.163 |
| 1000 | 2.288 | 4000 | 3.217 |
| 1050 | 2.323 | 4500 | 3.258 |
| 1100 | 2.358 | 5000 | 3.292 |
| 1150 | 2.392 | 5500 | 3.322 |
| 1200 | 2.425 | 6000 | 3.350 |

Table A.3: Behaviour of water vapour isobaric specific heat with varying temperature[80]

# Appendix B

# Accreted Ice Formulation

This appendix will be focused on the adaptations of the air-particles interaction equations, the particles parameters and the particles source terms to the case of accreted ice.

## B.1 Air-Ice Interaction Equations

Given the static nature of the accreted ice, only thermodynamic phenomena are considered, since the ice is not accelerated by the flow.
The thermodynamic equations that regulate the accreted ice differ from the particles ones only for what concerns the contact area between the ice and the flow, that passes from being a sphere to a ring.
So, the evaporation equation becomes:

$$dmv_{1i} = 2h_{mi}\pi\left(\rho_{is} - RH\rho_{vs}\right)\left(r_{ext} - \delta_i\right)dxdt$$

Where $dmv_{1i}$ is the evaporated mass from the accreted ice, $h_{mi}$ the mass transfer coefficient between the accreted ice and the main flow, and $\rho_{is}$ is the density of the saturated vapour at the accreted ice temperature.
The accreted ice melting equation is:

$$dm_{wi} = \frac{2h_i\pi\left(r_{ext}-\delta\right)\left(T-T_i\right)dxdt - L_{vwi}dmv_{1wi} - L_{vii}dmv_{1ii} - C_{pi}\left(273.15-T_i\right)}{L_m}$$

Where $dm_{wi}$ is the accreted ice melted portion in the time step $dt$, $h_i$ the heat transfer coefficient between the accreted ice and the main flow, $T_i$ the temperature of the accreted ice, $L_{vwi}$ and $L_{vii}$ the latent heat of evaporation respectively for water and ice at the accreted ice temperature, $dmv_{1wi}$ and $dmv_{1ii}$ the water and ice evaporated from the accreted ice, and $C_{pi}$ the specific heat of the accreted ice.
The temperature rise equation is:

$$dT_i = \frac{2h_i\pi\left(r_{ext}-\delta\right)\left(T-T_i\right)dxdt - L_{vwi}dmv_{1ii} - L_m dm_{wi}}{C_{pi}}$$

Finally, the vaporisation equation becomes:

$$dmv_{2i} = \frac{2h\pi\left(r_{ext}-\delta\right)\left(T-T_i\right)dxdt - C_{pi}\left(T_{vap}-T_i\right)}{L_{vwi}}$$

## B.2 Accreted Ice Thermodynamic Parameters

The thermodynamic parameters for the accreted ice have the exact same formulation as the particles parameters.
The only major change that affects all of them is the formulation of the Reynolds number, which for the case at hand is:

$$Re = \frac{\rho u\left[2\left(r_{ext}-r_m\right)-\delta\right]}{\mu}$$

In this formulation the only velocity present is the one of the main flow, since $u_i$ would be 0, and the particles diameter is substituted by the actual compressor annulus width.

## B.3 Ice Source Terms

There are two main differences between the particles and the accreted ice source terms, one is the lack of the momentum source term, and the second the simplification that derives from the fact that the ice is modelled so that it accretes at stations corresponding to the grid elements.
With the ice not being dragged by the flow, and the vapour coming from it not having any initial momentum, the relative source term, even if calculated, would be 0. The ice will in fact produce some drag, since it would protrude from the compressor outer wall, but this effect, with the ice thickness not growing past a few centimeters, is considered to be a local effect, neglibible in a 1-D formulation.
On the other side, the fact that the ice accretion points correspond to the grid elements introduces a great simplification in the source terms calculation process, since it is possible to calculate them directly.
So the mass source term will be:

$$S_{im} = \frac{dmv_{1i} + dmv_{2i}}{dxdt}$$

And the energy source term:

$$S_{ie} = \frac{(dmv_{1i} + dmv_{2i})\, h_{pi} - dQ_i}{dxdt}$$

With $h_{pi}$ being the specific enthalpy of the vapour being released by the accreted ice, and $dQ_i$ the amount of heat that the ice absorbed in the time step $dt$.